

Modelling of Timber-Concrete Composite Structures Subjected to Short-Term Monotonic Loading

by

Cong Liu

A thesis submitted in conformity with the requirements

for the degree of Master of Applied Science

Civil Engineering

University of Toronto

© Copyright by Cong Liu (2016)

Modelling of Timber-Concrete Composite Structures Subjected to Short-Term Monotonic Loading

Cong Liu

Master of Applied Science

Civil and Environmental Engineering

University of Toronto

2016

Abstract

Timber-concrete composite (TCC) is an innovative and efficient construction material which exploits the best properties of timber and concrete. The presence of shear connectors enables the two dissimilar materials to act together as a whole, resulting in an increase in global stiffness as well as load-carrying capacity. As this composite material is becoming increasingly more popular in the construction industry, there is a need to develop an analysis tool which has general applicability to timber-concrete composite systems with variations in loading schemes, specimen configurations, materials, and types of shear connectors.

A generic 2D nonlinear finite element model is proposed in this thesis, and is verified through extensive numerical simulations of six experiment series carried out by researchers around the globe. Good agreement between experimentally observed behaviour and numerical simulations were generally obtained.

Acknowledgements

I would like to express my deepest gratitude to Professor Frank Vecchio for his guidance and support over the course of my research studies. Without his boundless patience, continual support and encouragement, I could not have achieved my goals. I would also like to thank Professor Paul Gauvreau for his invaluable comments while reviewing my thesis.

I would like to thank my colleagues and friends Anca Jurcut, Benard Isojeh, Stamatina Chasioti, Mark Hunter, Andac Lulec, Vahid Sadeghian, Saif Shaban, Siavash Habibi, Raymond Ma, Giorgio Proestos, Allan Kuan, Edvard Bruun, and Dr. Min Sun for their friendship and advice throughout the course of this project.

I would like to acknowledge the generous financial support that I received from: the Natural Sciences and Engineering Research Council of Canada (NSERC), Read Jones Christoffersen Consulting Engineers (RJC), the University of Toronto, and Professor Frank Vecchio.

Last but not least, I would like to thank my parents for their unconditional love, encouragement, and patience.

Table of Contents

Chapter 1 Introduction	1
1.1 Background	1
1.2 Organization of Thesis.....	3
Chapter 2 LITERATURE REVIEW	4
2.1 Introduction	4
2.2 Mechanical Properties	4
2.3 Constitutive Relations	6
2.4 Failure Criteria of Wood.....	9
2.5 Structural Behaviour of TCC Beams	10
2.6 Connection Systems.....	12
2.7 Analytical Methods for TCC.....	13
2.8 Numerical Modelling of TCC	13
Chapter 3 VecTor2 Methodology.....	16
3.1 Introduction	16
3.2 Stiffness Matrix Formulation	16
3.3 Modelling of Shear Connectors.....	21
3.4 Failure Criteria Formulation.....	24
Chapter 4 Modelling of Plain Timber Specimens.....	27
4.1 Introduction	27
4.2 Gentile (2000)	27
4.3 Conclusion.....	36
Chapter 5 Modelling of Timber-Concrete Composite Beams.....	50
5.1 Introduction	50
5.2 Model Description.....	50
5.3 Model Inputs.....	52
5.4 Validation	57
5.5 Sensitivity Analysis	93
5.6 Conclusion.....	97
Chapter 6 Conclusions and Recommendations	99

6.1 Conclusions	99
6.2 Recommendations	100
References	101
Appendix Modelling Guideline.....	105

List of Figures

Figure 1-1 Typical forms of TCC (Frangi and Fontana, 2003)	1
Figure 2-1 Typical stress-strain curves for wood (Holmberg et al.,1998)	6
Figure 2-2 Proposed stress-strain curves in compression (Lau, 2000)	8
Figure 2-3 Failure modes and failure planes (Hashin, 1980)	10
Figure 2-4 Definition of composite action (Lukaszewka, 2009)	11
Figure 2-5 Typical load-deflection response of TCC.....	12
Figure 2-6 Comparison of different connection systems (Dias, 2005)	12
Figure 2-7 FE model (van der Linden, 1999)	14
Figure 2-8 1D FE model (Fragiacomo, 2005).....	15
Figure 2-9 FE model in ABAQUS (Persaud and Symons, 2006).....	15
Figure 3-1 VecTor2 coordinate reference systems (Vecchio, 1990)	16
Figure 3-2 Typical stress-strain curve for wood (grain direction).....	20
Figure 3-3 Typical stress-strain curve for wood (transverse direction)	21
Figure 3-4 The link element (Wong et el., 2004)	22
Figure 3-5 The contact element (Wong et el., 2004).....	22
Figure 3-6 Multi-linear approximation (Persaud and Synmons, 2006).....	24
Figure 3-7 Bond definition user-interface.....	24
Figure 4-1 Test configuration for half-scale beams (Gentile, 2000)	28
Figure 4-2 Cross-sections of half-scale reinforced beams (Gentile, 2000)	28
Figure 4-3 Test configuration for full-scale beams (Gentile, 2000)	29
Figure 4-4 Configuration of full-scale reinforced beams (Gentile, 2000)	29
Figure 4-5 Stress-strain relationships for GFRP (Gentile, 2000)	30
Figure 4-6 Half-scale plain timber beams	32
Figure 4-7 Half-scale beams with GFRP reinforcement.....	32
Figure 4-8 Full-scale beams with GFRP reinforcement at the bottom (FS1 and FS2).....	32
Figure 4-9 Full-scale beam with GFRP reinforcement at the sides (FS3).....	32
Figure 4-10 Full-scale plain timber beam (FS4).....	32
Figure 4-11 VecTor2 load-deflection responses	38
Figure 5-1 Sample model with smeared shear connectors	51

Figure 5-2 Sample model with discrete shear connectors	52
Figure 5-3 Concrete definition interface.....	53
Figure 5-4 Wood definition interface	56
Figure 5-5 Contact element definition interface	57
Figure 5-6 Details of the proposed system (Persaud and Symons, 2006)	58
Figure 5-7 Push-out test specimen (Persaud and Symons, 2006)	60
Figure 5-8 VecTor2 model.....	60
Figure 5-9 Load-deflection plot.....	61
Figure 5-10 Load-slip plot	61
Figure 5-11 Deflected shape at collapse.....	62
Figure 5-12 Variations of connections with and without coach screws: (a) rectangular; (b) triangular; and (c) toothed plate connection (Yeoh, 2010).....	63
Figure 5-13 Typical four-point bending test setup (dimensions in mm) (Yeoh, 2010)	63
Figure 5-14 Typical cross-sections of the bending specimens (Yeoh, 2010)	63
Figure 5-15 FE model for specimens A1 and A2	64
Figure 5-16 Load-slip curves (Yeoh, 2010)	65
Figure 5-17 Load-deflection plots	67
Figure 5-18 Arrangement of Specimen F1 (Yeoh, 2010).....	70
Figure 5-19 Specimen details and result (Cecotti et al., 2006)	70
Figure 5-20 Cross sections of (a) CS1 and (b) CS3 (Deam et al., 2008)	72
Figure 5-21 Test setup (Deam et al., 2008).....	72
Figure 5-22 Connector layout for Specimen CS3 (Deam et al., 2008)	73
Figure 5-23 Adopted and adjusted load-slip curve (Deam et al., 2008)	73
Figure 5-24 FE model for Specimen CS3 (Deam et al., 2008)	74
Figure 5-25 Definition of bond between tendon and timber (Deam et al., 2008)	74
Figure 5-26 Load-deflection plots for Specimen CS1 and CS3	75
Figure 5-27 Experimental setup for Gerber Specimen	77
Figure 5-28 FE model for Series 2	78
Figure 5-29 Load-deflection plots	78
Figure 5-30 Close-up of sudden force drops.....	83
Figure 5-31 Experimental setup (van der Linden, 1999).....	85
Figure 5-32 Connector Types (van der Linden, 1999).....	85

Figure 5-33 Load-deflection response	86
Figure 5-34 Crack pattern at 14 kN per jack	90
Figure 5-35 Crack pattern at 30 kN per jack	90
Figure 5-36 Specimen cross section (Lukaszewska, 2009).....	90
Figure 5-37 Connector types (a) SP+N; (b) SST + S (Lukaszewska, 2009)	91
Figure 5-38 Connector Layout (a) Top: Specimen 1 and 5 (SP + N); (b) Middle: Specimen 2 and 4 (SST + S); (c) Bottom: Specimen 3 (SST + S) (Lukaszewska, 2009)	91
Figure 5-39 Load-deflection response continued (Lukaszewska, 2009)	93
Figure 5-40 FE models with different mesh size	94
Figure 5-41 Comparison of predicted load-deflection responses of different mesh size	94
Figure 5-42 Load-deflection responses of Specimen CS1 with linear and nonlinear material constitutive models.....	96
Figure 5-43 Load-deflection responses of Specimen S7 with linear and nonlinear material constitutive models.....	96

List of Tables

Table 4-1 Summary of the models	33
Table 4-2 Summary of input parameters	33
Table 4-3 Reinforcement details	34
Table 4-4 Summary of ultimate loads	49
Table 5-1 Default concrete models	53
Table 5-2 Concrete properties	54
Table 5-3 Input Parameters	60
Table 5-4 Summary of the FE model	60
Table 5-5 Summary of the Yeoh specimens	64
Table 5-6 Summary of results	67
Table 5-7 Characteristics of specimens	71
Table 5-8 Specimen characteristics	76
Table 5-9 Timber specification	76

Chapter 1 Introduction

1.1 Background

Timber-concrete composite (TCC) is a construction material which was first introduced to the construction industry in Europe, as an alternative to reinforced concrete, due to the steel shortage after World War II. This construction technique has seen rapid development in the past two decades and found extensive structural applications, including renovation and upgrading of existing timber structures, new construction of mid- to low-rise buildings, and construction of mid- to short-span bridges. The composite material comprises two materials, concrete and timber; the composite system typically takes the forms of a concrete slab supported by one or multiple timber beams, or by a timber panel, as demonstrated in Figure 1-1, respectively. The synergy or, in other words, the degree of composite action between the two dissimilar materials arises from the shear connectors, which provide resistance to interlayer slip after the composite material is loaded in flexure. Ideally, shear connectors need to be sufficiently stiff under service loads to ensure a high degree of composite action, yet sufficiently soft to provide global ductility to the composite system in the ultimate limit state. As such, a well-designed TCC system is expected to remain linear-elastic under serviceability limit state, and to undergo nonlinear plastic deformation as the shear connectors start to yield.

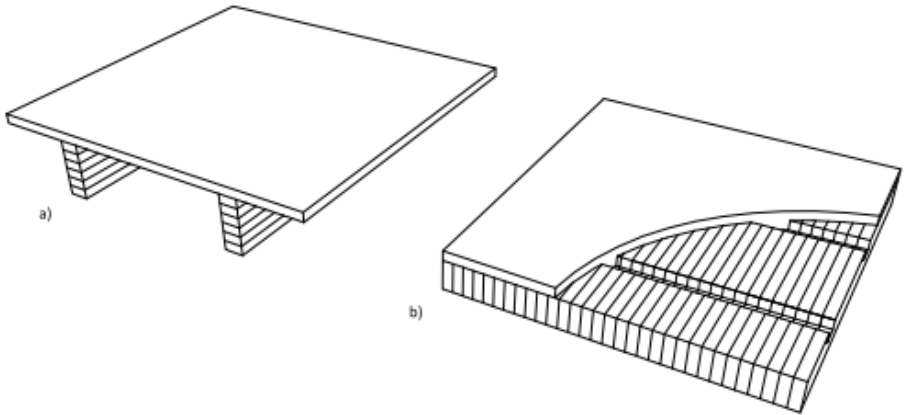


Figure 1-1 Typical forms of TCC (Frangi and Fontana, 2003)

Although several analytical methods have been proposed to cope with the design and analysis of TCC structures, each analytical method has its own underlying assumptions and limited scope of application. As such, none of the methods are universally agreed upon and adopted in the mainstream design codes. The Gamma Method, for instance, is currently adopted in Eurocode 5. This method is suitable for linear-elastic analysis of TCC beams under serviceability limit state, yet it neglects the plastic deformation of the shear connectors which, ultimately, results in an overestimation of the post-yielding global stiffness. In addition, the Gamma Method was developed based on the analytical solution of a composite beam subjected to uniformly-distributed load; therefore, the method does not apply to situations where a TCC beam is subjected to point loads or non-uniformly-distributed loads.

Various finite element models have been developed by several researchers (van der Linden, 1999; Fragiaco, 2005; Persaud and Symons, 2006). While these models can predict the load-deflection response with reasonable accuracy, they are limited to the analysis at a global level due to the nature of 1D FE analysis and the limitations of frame elements used in these models. Moreover, 1D frame FE models are not applicable to complex experimental setups, such as the prestressed specimens or the specimens built with cross-laminated timber (CLT) tested by Deam et al (2008) and Gerber (2016), respectively.

In light of the current development of FE analysis in this field, this research programme aims to develop a generic 2D finite element model which takes material nonlinearity and yielding of shear connectors into account. The model will also need to be flexible and be easily adapted to deal with the variations of TCC experimental setups.

VecTor2, originally developed at the University of Toronto for the nonlinear analysis of reinforced or prestressed concrete structures, is a powerful 2D nonlinear finite element analysis program. The program employs a total load, iterative secant stiffness algorithm which has been proven to be successful in the nonlinear analysis of reinforced concrete structures. It has the potential to analyze plain timber or TCC structures provided that appropriate material constitutive models are implemented.

1.2 Organization of Thesis

This thesis presents the work undertaken to expand VecTor2's capabilities to analyze plain timber and timber-concrete composite structures. A brief overview of the current developments of TCC technology, along with the research objectives of this thesis, are presented in Chapter 1.

Chapter 2 provides a literature survey that covers the key aspects related to this research project. The topics reviewed in his chapter include the mechanical properties of wood, wood constitutive models, failure criteria, structural behaviour of TCC, connection systems, and analytical models of TCC, as well as numerical methods.

Chapter 3 explains the details of the stiffness matrix formulation for membrane elements and bond-slip elements, implementation of wood constitutive models, and implementation of existing failure criteria applicable to wood.

Chapter 4 validates the work reported in Chapter 3, through comparison of the experimental results and the numerical results of the specimens tested by Gentile (2000). The specimens investigated included plain timber beams and timber beams reinforced with GFRP bars, all of which were subjected to short-term monotonic loadings.

Chapter 5 proposes a generic 2D model, and examines the model's accuracy and general applicability through numerical corroborations of six experiment series carried out by researchers around the globe. The specimens investigated have variations in terms of experimental setups, materials, and types of shear connectors.

Chapter 6 presents conclusions drawn from the numerical corroborations of this study, and provides recommendations for future work.

Chapter 2 LITERATURE REVIEW

2.1 Introduction

This chapter presents a literature survey that covers the different aspects related to this research study, including the mechanical properties and the constitutive relationships of timber, failure criteria of wood, structural behaviour of TCC, and numerical modelling of TCC structures subjected to short-term loadings.

Although the material in this field is very broad, the information provided in this chapter is not intended to be exhaustive; instead, it provides an overview of the subject matter, and serves as a stepping stone to the subsequent work of this research study.

2.2 Mechanical Properties

Contrary to concrete, wood is characterized as an anisotropic material with three axes of symmetry; namely, longitudinal, radial, and tangential, denoted as **L**, **R**, **T**, respectively. The mechanical properties along these axes are unique and independent of others.

The elastic properties of timber can be described by twelve elastic constants, including three elastic moduli (E_L, E_R, E_T), three shear moduli (G_{RT}, G_{LT}, G_{LR}), and six Poisson's ratios ($\mu_{LR}, \mu_{RL}, \mu_{LT}, \mu_{TL}, \mu_{RT}, \mu_{TR}$). The shear moduli are specific to the planes as indicated by the subscripts, while for the Poisson's ratios, the first letter of the subscripts refers to the direction of applied stress and the second letter to the direction of lateral deformation. The six Poisson's ratio can be reduced to three according to the following relationship.

$$\frac{\mu_{ij}}{E_j} = \frac{\mu_{ji}}{E_i}$$

where $i \neq j$; $i, j = L, R, T$.

While in the elastic region, timber can be described by Hooke's law as follows:

$$\begin{pmatrix} \varepsilon_{LL} \\ \varepsilon_{RR} \\ \varepsilon_{TT} \\ \gamma_{RT} \\ \gamma_{LT} \\ \gamma_{LR} \end{pmatrix} = \begin{bmatrix} \frac{1}{E_L} & -\frac{\mu_{LR}}{E_R} & -\frac{\mu_{LT}}{E_T} & & & \\ -\frac{\mu_{RL}}{E_L} & \frac{1}{E_R} & -\frac{\mu_{RT}}{E_T} & & & \\ -\frac{\mu_{TL}}{E_L} & -\frac{\mu_{TR}}{E_R} & \frac{1}{E_T} & & & \\ & & & \frac{1}{G_{RT}} & 0 & 0 \\ & & & 0 & \frac{1}{G_{LT}} & 0 \\ & 0 & & 0 & 0 & \frac{1}{G_{LR}} \end{bmatrix} \begin{pmatrix} \sigma_{LL} \\ \sigma_{RR} \\ \sigma_{TT} \\ \sigma_{RT} \\ \sigma_{LT} \\ \sigma_{LR} \end{pmatrix}$$

Or simply

$$\boldsymbol{\varepsilon} = \mathbf{C}\boldsymbol{\sigma}$$

$$\boldsymbol{\sigma} = \mathbf{D}\boldsymbol{\varepsilon}$$

$$\mathbf{D} = \mathbf{C}^{-1}$$

where $\boldsymbol{\varepsilon}$ is the strain vector, $\boldsymbol{\sigma}$ is the stress vector, \mathbf{D} is the material stiffness matrix, and \mathbf{C} is the compliance matrix.

Although the mechanical properties of wood differ with respect to species, moisture content, and temperature, as well as density, the following relations (Bodig 1982) can be used to roughly relate one another:

$$E_L : E_R : E_T \approx 20 : 1.6 : 1$$

$$G_{LR} : G_{LT} : G_{RT} \approx 10 : 9.4 : 1$$

$$E_L : G_{LR} \approx 14 : 1$$

2.3 Constitutive Relations

Similar to the mechanical properties, the constitutive relations of wood vary by axes of symmetry. Figure 2-1 (Holmberg et al.,1998) demonstrates typical stress-strain curves for wood along different axes of symmetry.

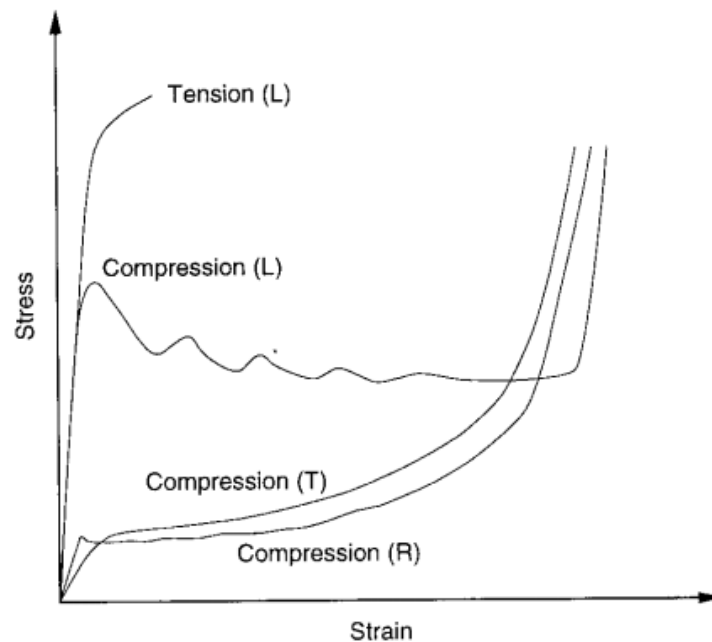


Figure 2-1 Typical stress-strain curves for wood (Holmberg et al.,1998)

As can be seen, wood, when subjected to axial tension along the longitudinal direction, behaves in a linear-elastic manner up to the proportional limit, followed by a negligible amount of plastic deformation. Such plasticity is often ignored by researchers in the field. By contrast, significant plasticity can be found when wood is subjected to axial compression in the longitudinal direction. Similar stress-strain behaviours can be found in both radial and tangential directions. For this reason, wood is sometimes regarded as transversely isotropic material.

It should be noted that these stress-strain curves are typically obtained from small wood specimens which are straight-grained and are clear of visible defects. In structural applications, the size of a wood member is often much greater, resulting in a reduced tensile strength. Such reduction in tensile strength arises from the presence of defects such as knots, finger joints, or

stress concentration due to grain discontinuity. Nevertheless, the stress-strain curves in compression agree fairly well with those shown in Figure 2-1.

Many researchers have dealt with the nonlinear stress-strain behaviour of timber in compression. Neely (1898) proposed a simple model which assumes an elasto-plastic stress-strain relationship in compression with the material remaining linear-elastic in tension (Figure 2-2a). A slight modification was suggested by Bazan (1980) (Figure 2-2b), in which the stress-strain relationship remains linear elastic up to the proportional limit, followed by a linear decline in stress with increasing strain. The limitation of Bazan's model is that the model will not work for large strain since it may produce negative stress.

Malotra and Mazur (1970) suggested a nonlinear stress-strain relation (Figure 2-2c) which was first introduced by Ylinen (1956), and is given by:

$$\varepsilon = \frac{1}{E} \left[c \cdot \sigma - (1 - c) \cdot f_c \cdot \ln\left(1 - \frac{\sigma}{f_c}\right) \right]$$

where ε is strain, σ is stress, f_c is maximum compression stress, E is Young's modulus and c is the shape parameter.

A detailed study of the stress-strain relationship of timber was carried out by Glos (1978) using specimens subjected to longitudinal axial compression. Based on experimental data, a nonlinear curve with polynomials up to the 7th order was obtained (Figure 2-2d). The stress-strain relationship proposed by Glos is as follows:

$$\sigma = \frac{\varepsilon/\varepsilon_1 + G_1 \cdot (\varepsilon/\varepsilon_1)^7}{G_2 + G_3 \cdot (\varepsilon/\varepsilon_1) + G_4 \cdot (\varepsilon/\varepsilon_1)^7}$$

$$G_1 = \frac{100 \cdot f_s}{6E \cdot (1 - f_s/f_c)}$$

$$G_2 = 1/E$$

$$G_3 = 1/f_c - 7/6E$$

$$G_4 = G_1/f_s$$

where ε is strain, σ is stress, E is the Young's modulus, f_c is the maximum compression stress, f_s is the residual stress, and ε_1 is the strain corresponds to maximum stress.

The four parameters (G_1 to G_4) that define the shape of the stress-strain curve were determined using curvilinear regression techniques. The regression accounts for multiple wood properties measured from the specimens, including density, moisture content, knot area ratio, and percentage of compression wood.

The advantages of the Glos model include: (1) the model will not produce negative stress even at large strain; (2) the model is in better agreement with the true shape of the stress-strain curve compared to other models. Conversely, the drawback of this model is that the four parameters are determined based on specific material properties and need to be calibrated for each data set. In addition, most experiments are typically terminated once the peak compression stress has been reached and thus the full stress-strain curves may not be readily available.

The Glos model can be simplified based on the following relations:

$$f_s = 0.8f_c$$

$$\varepsilon_1 = 0.008 \sim 0.012$$

$$\varepsilon_u \approx 3\varepsilon_1$$

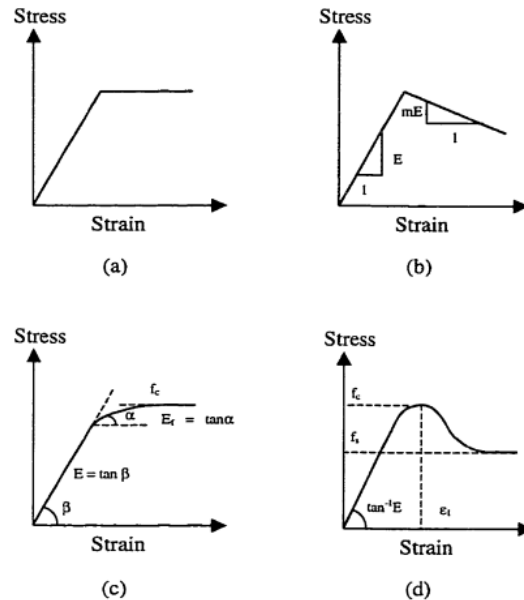


Figure 2-2 Proposed stress-strain curves in compression (Lau, 2000)

2.4 Failure Criteria of Wood

The failure modes of wood can be extremely complex as they can be induced by one or more mechanical stimuli. Failure of a timber beam, for instance, may be caused by rupture of the tension fibres, delamination of fibres due to horizontal shear, buckling of the compression fibres, or a mix of all three. This section reviews some of the failure criteria applicable to wood. These criteria were either developed for wood, or apply to orthotropic composite material in general, such as wood.

The Hankinson formula (1921) is the first well-known one-dimensional empirical formula developed and it provides adequate results for compression and tension in general.

Hill (1950) proposed a failure criterion that is adapted from the von Mises criterion and has the ability to deal with the anisotropic effects of wood. A modification to the Hill criterion was suggested by Azzi and Tsai (1965), known as Tsai-Hill criterion. The Tsai-Hill criterion is applicable to composite materials that have identical mechanical properties in the plane perpendicular to the fibre orientation.

The Norris criterion (1950), originally developed for application to glued laminated timber, has been extensively applied for modelling of strength in solid wood. Several researchers (Van der Put 2005, Kasal and Leichti 2005; de Ruvo et al. 1980), however, have reported that it underpredicts when biaxial loading is combined with shear.

Hoffman (1967) proposed a model that accounts for the difference between tensile strength and compressive strength. It may be seen as an extension of the Hill criterion. This criterion has been widely used for the analysis of brittle composite materials such as wood subjected to tension.

The Hashin failure criterion (1980) was initially developed to account for the failure modes of unidirectional fibre composite. This model assumes no stress interaction between axes of symmetry. According to Hashin, fibre composite materials can have two primary failure modes as shown in Figure 2-3, including fibre failure mode and matrix failure mode. With the fibre mode the failure plane is approximately perpendicular to fibre direction; with the matrix mode, planar fracture takes place in the fibre direction.

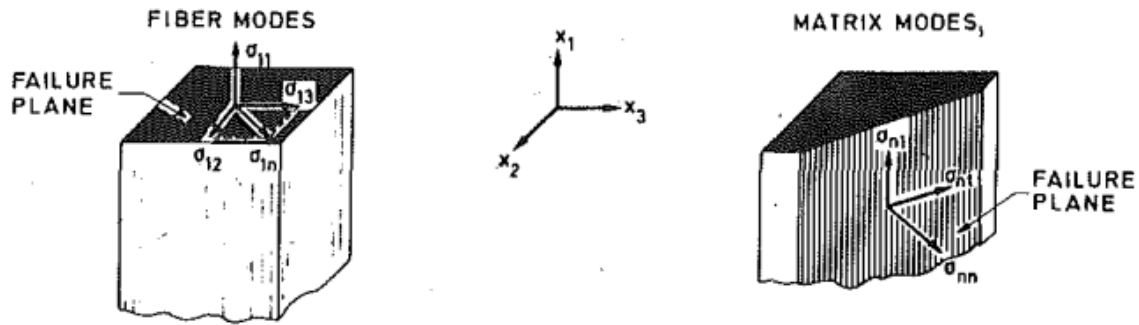


Figure 2-3 Failure modes and failure planes (Hashin, 1980)

Both compression and tension can give rise to the two failure mechanisms. Therefore, there are four failure modes, namely tensile fibre mode, compressive fibre mode, tensile matrix mode, and compressive matrix mode. Similar to Tsai-Hill criterion, Hashin's model is applicable to transversely isotropic materials.

2.5 Structural Behaviour of TCC Beams

Timber-concrete composite (TCC) material, as the name suggests, involves two dissimilar materials acting together as one. The synergy between timber and concrete arises from the presence of shear connectors positioned at the interface. The degree of composite action, a term commonly used to quantify the effectiveness of the synergy, depends heavily on the interlayer stiffness. There are three case scenarios as presented in Figure 2-4 (Lukaszewka, 2009), including full composite action, partial composite action, and no composite action. In the case of full composite action, the interlayer is considered to be infinitely rigid and therefore slip cannot occur, whereas in the case of no composite action, the interlayer stiffness is assumed to be zero, allowing slip to occur freely. The actual degree of composite action of TCC systems generally lies between the two extremes. To quantify the degree of composite action, the following equation may be used:

$$efficiency = \frac{\delta - \delta_N}{\delta_F - \delta_N}$$

where δ is the actual deflection, δ_N is the theoretical deflection assuming no composite action, and δ_F is the theoretical deflection assuming full composite action.

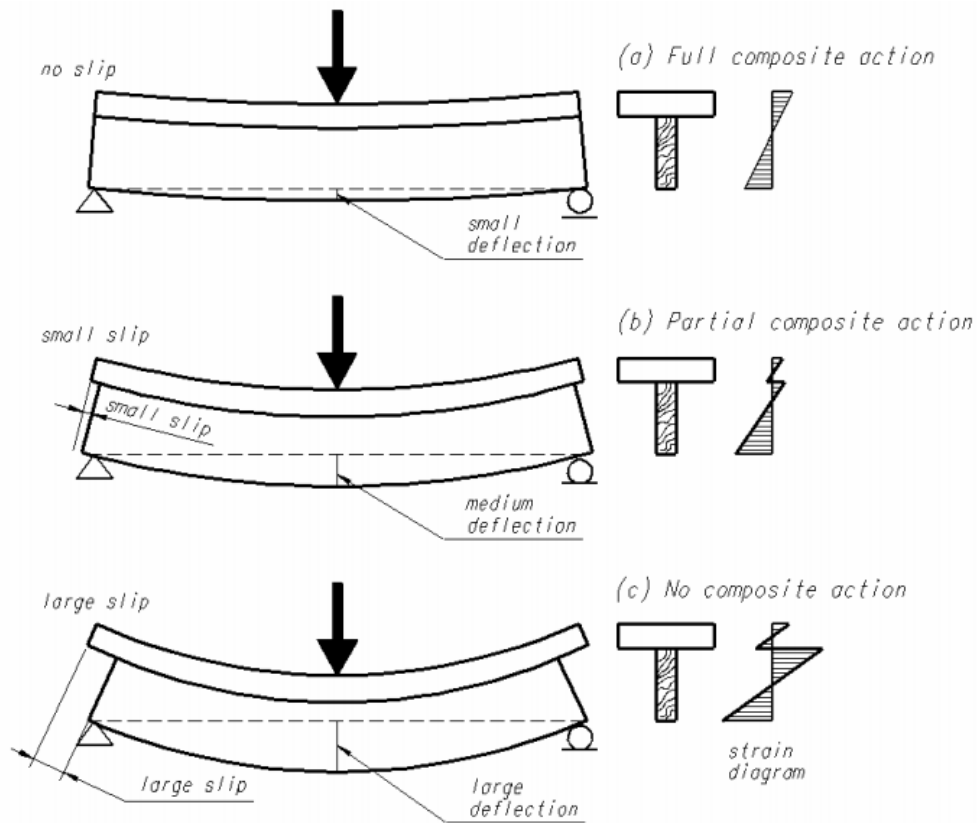


Figure 2-4 Definition of composite action (Lukaszewka, 2009)

For any TCC system to be efficient, three design criteria must be satisfied: (1) the timber member must be strong enough to resist both bending and tension induced by gravity loads applied on the beam; (2) the connection system must be sufficiently strong to transfer the design shear force and be sufficiently stiff to provide a high degree of composite action; and (3) the connection system must be sufficiently ductile to provide overall ductility to the entire composite system.

Figure 2-5 presents a typical load-deflection curve for TCC beams subjected to short-term bending. The curve starts with a linear-elastic branch followed by a nonlinear softening portion. Such nonlinearity is likely caused by cracking of concrete, buckling of wood fibres under compression, or progressive yielding of shear connectors. The ultimate failure of TCC beams normally arises from rupturing of wood fibres in the tension zone, particularly near knots or finger joints.

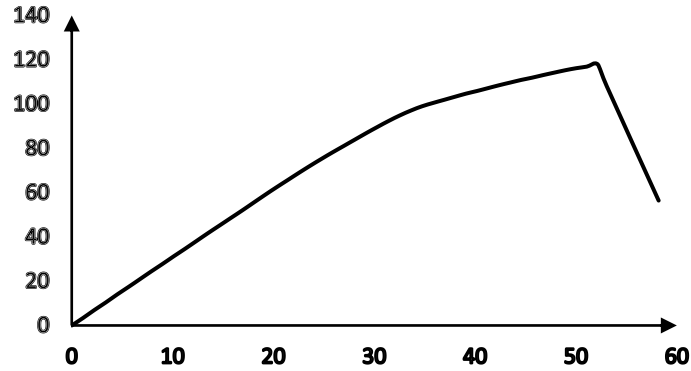


Figure 2-5 Typical load-deflection response of TCC

2.6 Connection Systems

A wide range of connection systems has been developed over the past decades, from simple nails to concrete notches reinforced with steel bars. These connection systems have unique load-slip responses determined through push-out tests. In general, connection systems are evaluated in three aspects, including stiffness, strength, and ductility. Ideally, connection systems should be: 1) strong enough to resist the horizontal shear force along the interface; 2) sufficiently stiff prior to yielding, resulting in a high degree of composite action; and 3) sufficiently ductile after yielding, providing overall ductility to the global TCC system. Figure 2-6 presents typical load-slip relationships for a number of connection systems.

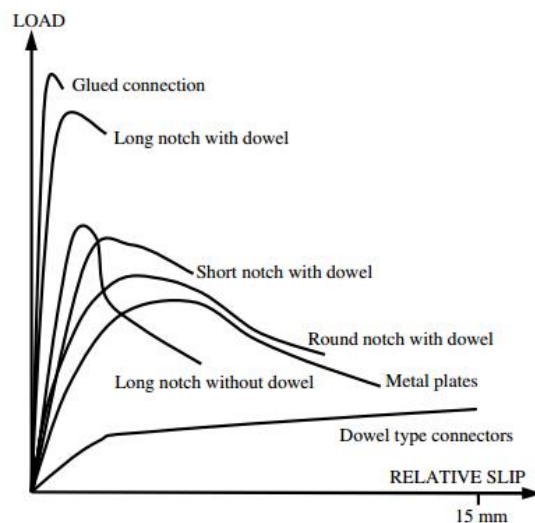


Figure 2-6 Comparison of different connection systems (Dias, 2005)

2.7 Analytical Methods for TCC

There are a number of nonlinear analytical methods developed to date that address the yielding of shear connectors. The Gamma (γ) Method, prescribed by Eurocode 5, neglects the plastic deformations of shear connectors upon yielding. This assumption automatically leads to an overestimation of the post-yielding load-carrying capacity of TCC systems. The Frozen Shear Force model (van der Linden, 1999), on the other hand, accounts for both the elastic and plastic deformations of shear connectors. However, the method assumes simultaneous yielding of all shear connectors, resulting in an underestimation of the post-yielding global structural stiffness. Zhang (2013) proposed an analytical solution that combines the strengths of the Gamma Method and the Frozen Shear Force model together, producing a more accurate post-yielding load-deflection response over the predecessors. In Zhang's method, shear connectors are assumed to be elasto-plastic and are allowed to yield progressively.

2.8 Numerical Modelling of TCC

A number of researchers have used the finite-element method (FEM) to obtain the global load-deflection response of TCC structures subjected to short-term bending.

A one-dimensional FE model (Figure 2-7) was presented by van der Linden (1999) using the DIANA finite-element program (DIANA, 1992). In his model, shell elements were used to model the concrete slab while frame elements were used for the timber joist. The shear connectors were modelled as distinct spring elements. Only half of the beam was modelled due to symmetry. The Tresca criterion (DIANA, 1992) and Hoffman criterion (1967) were implemented for concrete and timber, respectively. The nonlinear load-slip response of shear connectors was approximated as multi-linear curve. Unfortunately, van der Linden did not provide any direct comparison of the numerical results against experimental data. Instead, the FE model was used in conjunction with a Monte Carlo simulation to obtain a mean load-deflection response.

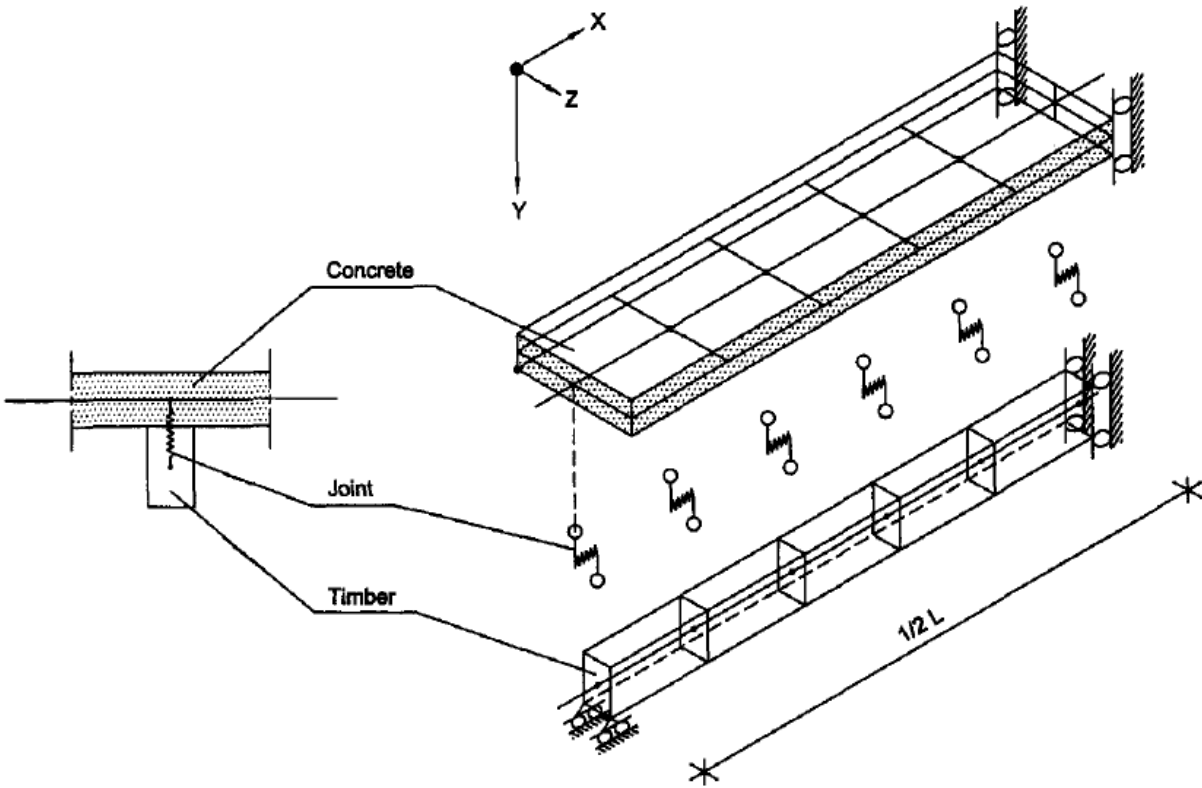


Figure 2-7 FE model (van der Linden, 1999)

Fragiacomo (2005) presented a different version of one-dimensional FE model (Figure 2-8) that consisted of two parallel beam elements, the concrete slab and the timber joist, connected with smeared spring elements that represented the shear connectors. A nonlinear uniaxial stress-strain relationship with a softening branch was used for concrete in compression and tension, while an elasto-brittle relationship in tension and elasto-plastic with limited ductility stress-strain relationship in compression were used for timber. This model was validated against actual TCC specimens tested by Lukaszewska (2009) and by Fragiaco (2012), providing good agreement.

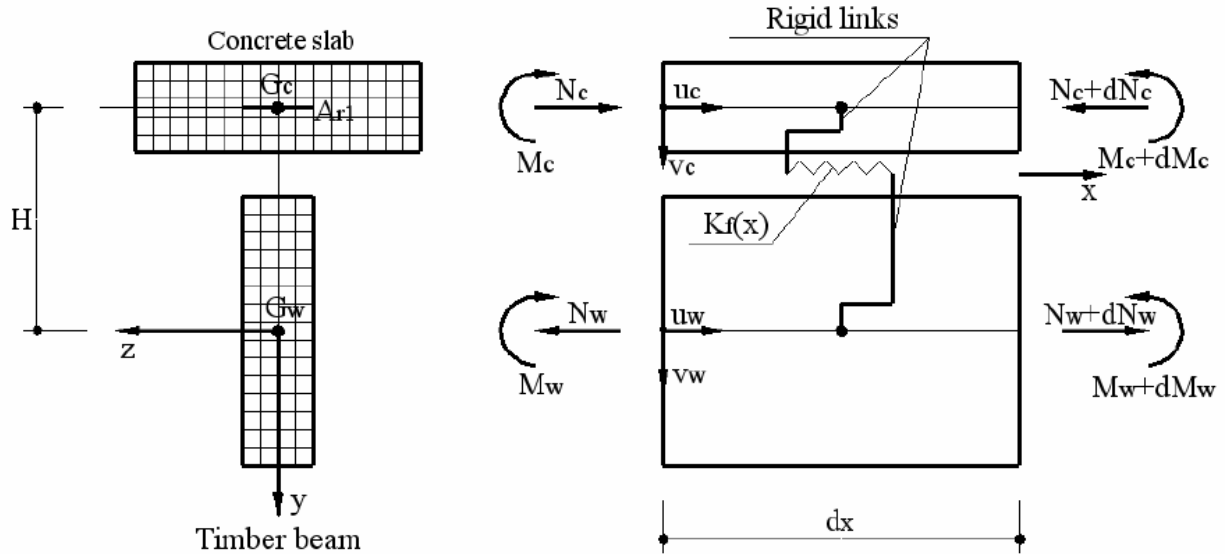


Figure 2-8 1D FE model (Fragiacomo, 2005)

Persaud and Symons (2006) developed a FE model (Figure 2-9) in ABAQUS to model their TCC specimen. Beam elements were used to model the concrete slab and the timber joist. Both timber and concrete were modelled as linear-elastic materials with no cracking in concrete. The shear connectors were modelled as discrete spring elements.

Overall, the numerical result was in good agreement with the experimental data, particularly for the early load stages up to fifty percent of the collapse load. However, the model underpredicted the deflection in the final load stages. The authors suggested the discrepancy was likely due to cracking of concrete which was not considered in the material models.

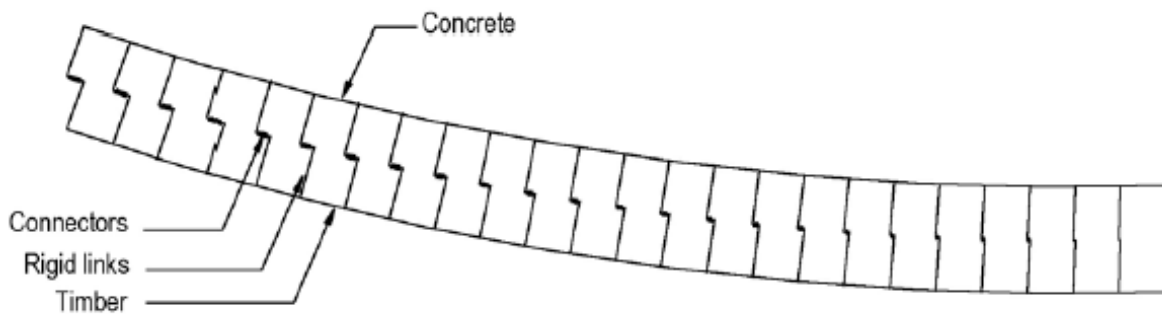


Figure 2-9 FE model in ABAQUS (Persaud and Symons, 2006)

Chapter 3 VecTor2 Methodology

3.1 Introduction

This chapter discusses the numerical modelling of timber-concrete composite (TCC) structures using VecTor2, a two-dimensional finite element program specifically developed for the analysis of reinforced concrete membrane structures subjected to static and dynamic loading. VecTor2 employs a total load algorithm with an iterative secant stiffness formulation, using the Modified Compression Field Theory (MCFT) (Vecchio and Collins, 1986) and the Disturbed Stress Field Model (DSFM) (Vecchio, 2000) as the governing behavioural models. These behavioural models consider cracked reinforced concrete as an orthotropic material, with rotating cracks smeared through the concrete elements. To date, VecTor2 has found extensive application in research studies and forensic analysis of existing reinforced concrete structures. It has the potential to be extended to analyse timber or TCC structures provided that adequate timber models and failure criteria are implemented.

3.2 Stiffness Matrix Formulation

3.2.1 Material Stiffness Matrix Formulation

Figure 3-1 demonstrates the global coordinate reference system used in VecTor2.

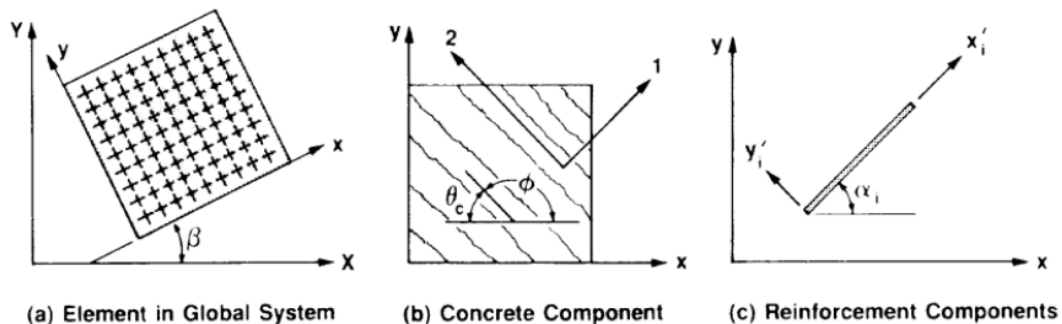


Figure 3-1 VecTor2 coordinate reference systems (Vecchio, 1990)

For any elements in VecTor2, the total strains $[\varepsilon]$ are related to element stresses $[\sigma]$ by the material stiffness matrix $[D]$, as follows:

$$[\sigma] = [D][\varepsilon] \quad (3-1)$$

The material stiffness matrix formulation in VecTor2 varies by materials and element types. The material stiffness matrix for concrete is evaluated as a composite stiffness matrix, as such:

$$[D] = [D_c] + \sum_{i=1}^n [D_s]_i \quad (3-2)$$

where $[D_c]$ is the concrete material stiffness matrix, and $[D_s]_i$ is reinforcement component stiffness matrix in the i^{th} direction.

As the MCFT and DSFM treat the reinforced concrete as an orthotropic material in the principal stress directions, it is necessary to formulate the concrete material stiffness matrix, $[D_c]'$, with respect to these directions. If it is assumed that the post-cracking Poisson's effect is negligible, then $[D_c]'$ can be expressed as follows:

$$[D_c]' = \begin{bmatrix} \overline{E_{c1}} & 0 & 0 \\ 0 & \overline{E_{c2}} & 0 \\ 0 & 0 & \overline{G_c} \end{bmatrix} \quad (3-3)$$

The secant moduli $\overline{E_{c1}}$, $\overline{E_{c2}}$, $\overline{G_c}$ are computed from the current values of the principal stresses, f_{c1} and f_{c2} , and the corresponding principal net concrete strains, ε_{c1} and ε_{c2} , as follows:

$$\overline{E_{c1}} = \frac{f_{c1}}{\varepsilon_{c1}}, \quad \overline{E_{c2}} = \frac{f_{c2}}{\varepsilon_{c2}}, \quad \overline{G_c} = \frac{\overline{E_{c1}} \cdot \overline{E_{c2}}}{\overline{E_{c1}} + \overline{E_{c2}}} \quad (3-4)$$

Similarly, the reinforcement component stiffness matrices, $[D_s]'_i$ must be first evaluated with respect to their longitudinal axes. The reinforcement is assumed only to resist uniaxial stress, and be evenly distributed through the element. Thus, $[D_s]'_i$ is given as:

$$[D_s]'_i = \begin{bmatrix} \rho_i \overline{E_{si}} & 0 & 0 \\ 0 & 0 & 0 \\ 0 & 0 & 0 \end{bmatrix} \quad (3-5)$$

where ρ_i is the reinforcement ratio for the reinforcement component and the secant modulus $\overline{E_{si}}$ is computed based on the current stress f_{si} and strain ε_{si} , as follows.

$$\overline{E_{si}} = \frac{f_{si}}{\varepsilon_{si}} \quad (3-6)$$

In VecTor2, wood can be approximated as a fixed orthotropic material with two axes of symmetry: parallel to the grain and perpendicular to the grain. This represents a significant deviation to how cracked concrete is modelled in VecTor2, where the axes of orthotropy typically rotate. The Poisson's effect may not be neglected and the material stiffness matrix for wood, $[D_w]$, subjected to plane stress condition, is taken as:

$$[D_w]' = \begin{bmatrix} \frac{1}{\overline{E_L}} & -\frac{\nu_{TL}}{\overline{E_T}} & 0 \\ -\frac{\nu_{LT}}{\overline{E_L}} & \frac{1}{\overline{E_T}} & 0 \\ 0 & 0 & \frac{1}{\overline{G_{LT}}} \end{bmatrix}^{-1} \quad (3-7)$$

The secant moduli $\overline{E_L}$, $\overline{E_T}$, and $\overline{G_{LT}}$ can be computed in a similar fashion as done for concrete.

The material stiffness matrices, $[D_c]'$, $[D_s]'_i$, and $[D_w]'$ are transformed from their respective local coordinate systems to the global coordinate reference system by means of the transformation matrix, $[T]$, as follows:

$$[D_c] = [T_c]^T [D_c]' [T_c] \quad (3-8)$$

$$[D_s]_i = [T_{si}]^T [D_s]'_i [T_{si}] \quad (3-9)$$

$$[D_w] = [T_w]^T [D_w]' [T_w] \quad (3-10)$$

$$[T] = \begin{bmatrix} \cos^2\psi & \sin^2\psi & \cos\psi \cdot \sin\psi \\ \sin^2\psi & \cos^2\psi & -\cos\psi \cdot \sin\psi \\ -2\cos\psi \cdot \sin\psi & 2\cos\psi \cdot \sin\psi & \cos^2\psi - \sin^2\psi \end{bmatrix} \quad (3-11)$$

For concrete, the angle ψ is the inclination of the principal tensile axis with respect to the positive x-axis, while for reinforcement, ψ is the angle between the orientation of the reinforcement and the positive x-axis. For wood, ψ is the angle between the grain orientation and the positive x-axis (counterclockwise positive).

3.2.2 Element Stiffness Matrix Formulation

Once the material stiffness matrix is determined, the element stiffness matrix $[k]$ can be determined as follows:

$$[k] = \int_{vol} [B]^T [D]' [B] dV \quad (3-12)$$

where $[B]$ is the strain-displacement matrix with its form dependent on the element type, which may be triangular, rectangular, and quadrilateral.

Further details of VecTor2 can be found in “VecTor2 and FormWorks User’s Manual” (Wong et al., 2013).

3.2.3 Constitutive Model for Wood

The accuracy of the constitutive model is critical as it heavily influences the material stiffness matrix. In order to model timber and TCC structures, a nonlinear constitutive model for wood has been implemented in VecTor2. The constitutive model adopted for wood consists of both linear and nonlinear portions. The Glos model (1978) has been chosen for wood in compression, while a linear-elastic behaviour is assumed for wood in tension up to peak tensile stress, followed by a linear softening branch. The linear softening branch is intentionally included for the modelling of

timber structures reinforced with fibre-reinforced polymers (FRP); more details will be given in Chapter 4. A typical stress-strain curve for wood in the grain orientation is shown in Figure 3-2.

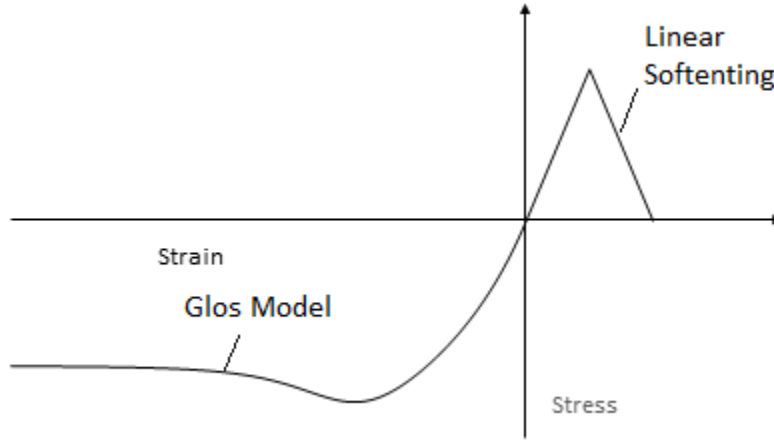


Figure 3-2 Typical stress-strain curve for wood (grain direction)

The formulation of the Glos model is given as:

$$\sigma = \frac{\varepsilon/\varepsilon_1 + G_1 \cdot (\varepsilon/\varepsilon_1)^7}{G_2 + G_3 \cdot (\varepsilon/\varepsilon_1) + G_4 \cdot (\varepsilon/\varepsilon_1)^7} \quad (3-13)$$

$$G_1 = \frac{100 \cdot f_s}{6E \cdot (1 - f_s/f_c)} \quad (3-14)$$

$$G_2 = 1/E \quad (3-15)$$

$$G_3 = 1/f_c - 7/6E \quad (3-16)$$

$$G_4 = G_1/f_s \quad (3-16)$$

where ε is the net strain, σ is the stress, E is the Young's modulus, f_c is the maximum compression stress, f_s is the residual stress, and ε_1 is the strain corresponding to maximum stress.

The Glos model can be simplified based on the following relations (Glos, 1978):

$$f_s = 0.8f_c$$

$$\varepsilon_1 = 0.008 \sim 0.012 \text{ (0.010)}$$

$$\varepsilon_u \approx 3\varepsilon_1$$

The stress-strain behaviour in the transverse direction is approximated as linear elastic-plastic for both compression and tension. The elastic modulus is typically taken as 5% of that in the longitudinal direction. A typical stress-strain curve for wood in transverse orientation is presented in Figure 3-3.

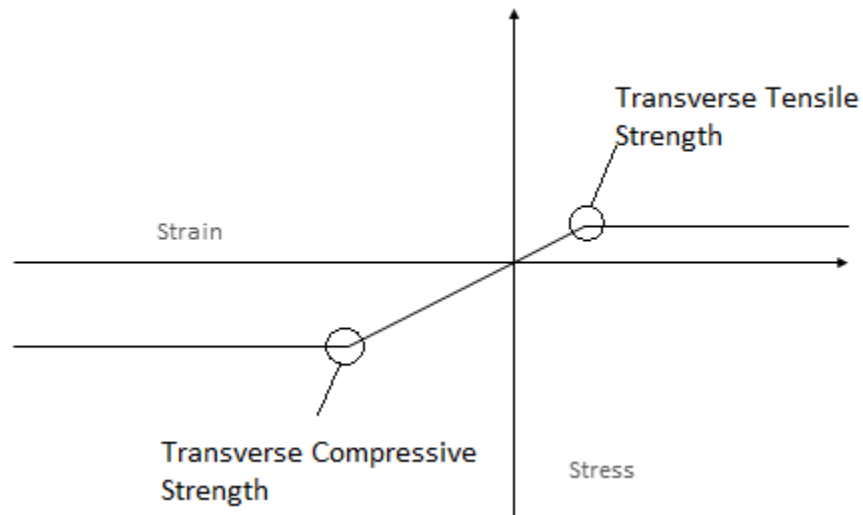


Figure 3-3 Typical stress-strain curve for wood (transverse direction)

3.3 Modelling of Shear Connectors

3.3.1 Bond-Slip Elements

The shear connectors connecting the timber and the concrete components can be modelled by bond-slip elements. VecTor2 has two built-in bond-slip elements: link elements and contact elements.

The link element is a non-dimensional element defined by two different nodes sharing the same coordinates prior to slippage. It may be idealized as two springs orthogonal to one another. One spring deforms tangentially to the connected elements while the other spring deforms perpendicular to the connected elements. A graphical representation of the link element is presented in Figure 3-4.

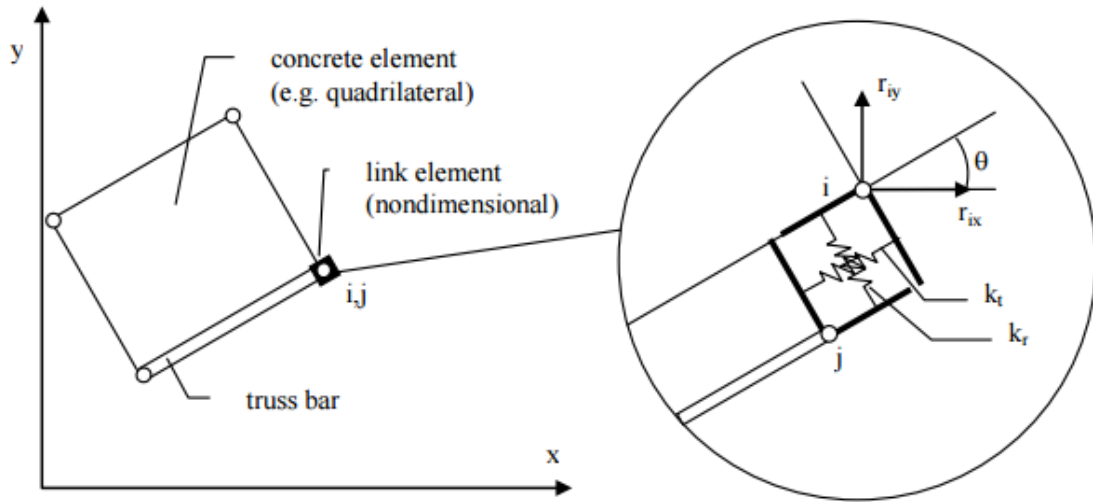


Figure 3-4 The link element (Wong et al., 2004)

The contact element, shown in Figure 3-5, is a four-noded element with linear dimension, defined as the distance between node i (j) and node m (n). The four nodes (i, j, m, n) defining the element are divided into two node pairs. Similar to the link element, the nodes within each node pair share the identical coordinates prior to slippage.

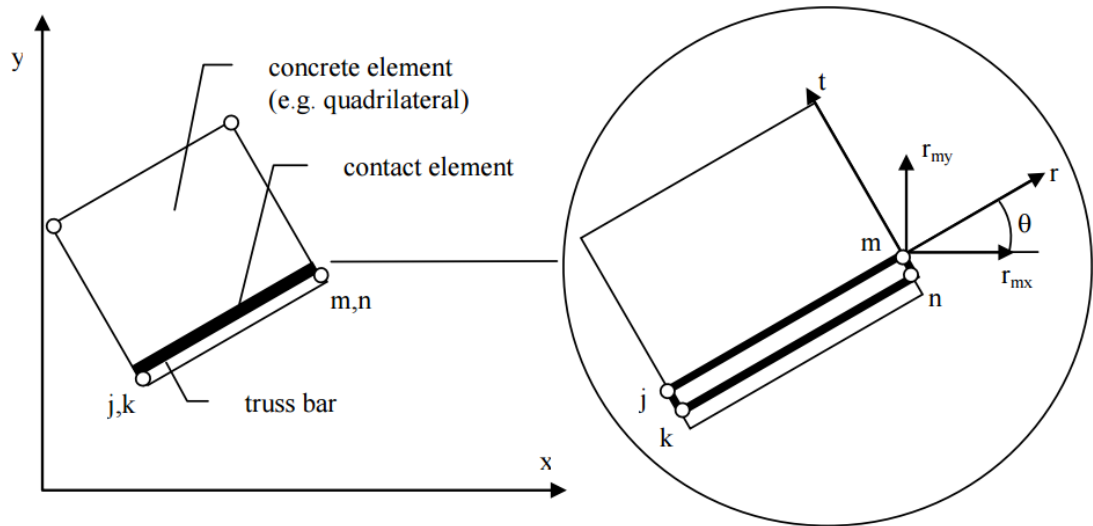


Figure 3-5 The contact element (Wong et al., 2004)

The contact element represents a continuous interface along the shared edge of the connected elements. With two node pairs defining the contact interface, the displacement of any point

along the contact element is linearly interpolated from the nodal displacements to ensure compatibility of the connected elements.

Since the link element is dimensionless, it is suitable for situations where the shear connectors are concentrated at distinct locations, such as screw or dowel type fasteners. By contrast, the contact element may be considered as a more flexible and realistic representation of the shear connectors. The contact element may be used to model concentrated connectors, as well as those connectors that are large in size such as notched concrete connections, or those that are continuous along the span, such as continuous metal plate connections. However, as a trade-off, the stiffness formulation for the contact element is inherently more complex and requires more computation effort than that for the link element. Additional details regarding stiffness formulations of the bond-slip elements may be found in “VecTor2 and FormWorks User’s Manual” (Wong et al., 2013).

3.3.2 Load-Slip Relations

In VecTor2, the load-slip behaviour of the connectors is approximated by a piece-wise linear curve. An example of this approximation is shown in Figure 3-6, in which the real load-slip behaviour of screw connectors tested by Persaud and Synmons (2006) was approximated by three line segments. The piece-wise curve is defined by four reference points connected with straight lines. By default, VecTor2 treats the origin (0,0) as one of the reference points and the remaining three points are manually input by users. It should be noted that the load-slip relation must be first converted to the stress-slip domain simply by dividing the force by the tributary area of the contact element. The user-interface for defining the stress-slip behaviour of the contact element is presented in Figure 3-7.

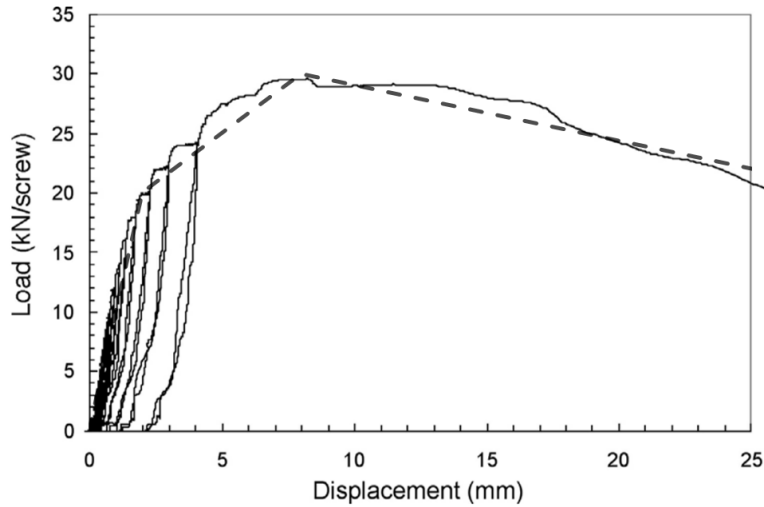


Figure 3-6 Multi-linear approximation (Persaud and Symons, 2006)

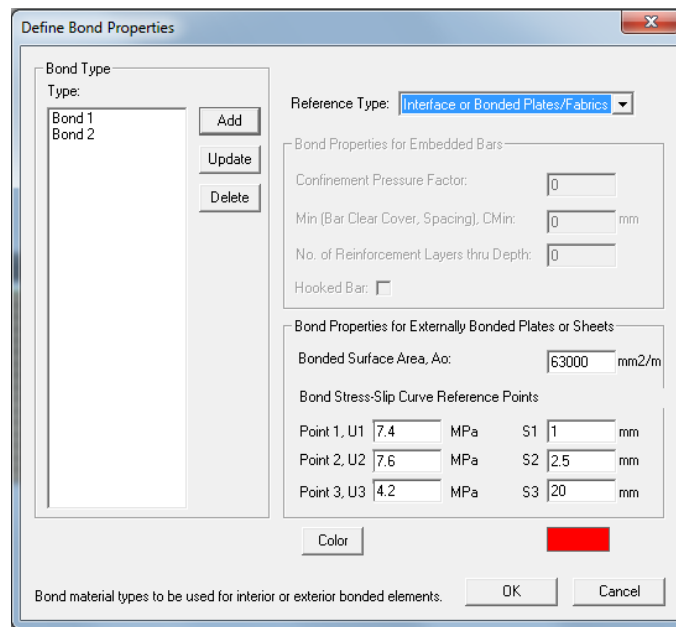


Figure 3-7 Bond definition user-interface

3.4 Failure Criteria Formulation

Since wood elements in VecTor2 are modelled as a fixed-orthotropic material subjected to bi-axial stress, three failure criteria may be applicable to the scenario, including the Tsai-Azzi criterion (1966), the Norris criterion (1962), and the Hashin criterion (1980).

The Tsai-Azzi criterion takes into account the difference in uniaxial tensile and compressive strengths, and is as follows:

$$\frac{\sigma_L^2}{f_L^2} - \frac{\sigma_L \sigma_T}{f_L^2} + \frac{\sigma_T^2}{f_T^2} + \frac{\tau_{LT}^2}{f_{LT}^2} = 1 \quad (3-14)$$

where f_T , f_L , and f_{LT} are the uniaxial and shearing strengths relative to the corresponding directions.

The Norris criterion is similar to the Tsai-Azzi criterion except that the interaction term is nonbiased towards directions. The Norris criterion is given as:

$$\frac{\sigma_L^2}{f_L^2} - \frac{\sigma_L \sigma_T}{f_L f_T} + \frac{\sigma_T^2}{f_T^2} + \frac{\tau_{LT}^2}{f_{LT}^2} = 1 \quad (3-15)$$

The Hashin criterion characterizes wood failure by four scenarios, including:

Fibre tension mode:

$$\frac{\sigma_L^2}{f_{L,t}^2} + \frac{\tau_{LT}^2}{f_{L,v}^2} = 1 \quad (3-16)$$

Fibre compression mode:

$$\frac{\sigma_L}{f_{L,c}} = 1 \quad (3-17)$$

Matrix tension mode:

$$\frac{\sigma_T^2}{f_{T,t}^2} + \frac{\tau_{LT}^2}{f_{L,v}^2} = 1 \quad (3-18)$$

Matrix compression mode:

$$\frac{\sigma_T^2}{4f_{T,v}^2} + \left[\left(\frac{f_{T,c}}{2f_{T,v}} \right)^2 - 1 \right] \frac{\sigma_T^2}{f_{T,c}^2} + \frac{\tau_{LT}^2}{f_{L,v}^2} = 1 \quad (3-19)$$

where $f_{L,t}$, $f_{L,c}$, $f_{T,t}$, $f_{T,c}$, $f_{L,v}$, and $f_{T,v}$ are, respectively, the strengths related to longitudinal tension and compression, transverse tension and compression, and longitudinal and transverse shear.

The Hashin criterion has been adopted into VecTor2 to account for different types of failure modes. For flexure-critical timber beams, failures typically occur at the bottom of the beam, where the wood fibre is essentially subjected to uniaxial tensile stress. In that scenario, both Equation 3-18 and Equation 3-19 will be equal to zero on the left side, and the matrix failure mode will never govern the ultimate failure. Moreover, the second term of Equation 3-16 is zero, and therefore the Hashin criterion is reduced to uniaxial failure criterion which is the same as the Rankine Criterion.

For shear-critical conditions, failures are more likely governed by a combination of shear stress and axial stress, and the matrix failure modes become more prominent. However, it should also be pointed out that the transverse tensile strength and the transverse shear strength are the less commonly known mechanical properties of wood; their values are typically not available in the literature.

Chapter 4 Modelling of Plain Timber Specimens

4.1 Introduction

The objective of this chapter is to verify the adequacy of the constitutive models and the failure criteria implemented for timber. The verification study was carried out by modelling in VecTor2 the timber beams tested by Gentile (2000), followed by a detailed comparison between the analytical and the experimental results.

4.2 Gentile (2000)

4.2.1 Specimen Details

The experiment series conducted by Gentile (2000), chosen for the verification study, consisted of twenty-two half-scale timber beams and four full-scale timber beams tested to failure. All specimens were simply supported and tested under four-point bending. Among the specimens, fifteen of the half-scale specimens and three of the full-scale specimens were reinforced with glass fibre-reinforced polymer (GFRP) bars, with the remaining plain timber beams serving as control specimens. Epoxy resin was used to bond the GFRP bars to the timber, creating a perfect bond condition.

For all the half-scale specimens, the cross sections were 100 x 300 mm with a load span of 600 mm and a support span of 4000 mm. Lateral bracing was provided in the middle of each shear span to prevent lateral-torsional instability. The GFRP bars were installed in the grooves that were cut 30 mm above the bottom fibres into the sides of the specimens. The grooves had a constant depth of 25 mm, and varying width to accommodate different numbers of GFRP bars. A schematic of the test setup and the cross sections of the half-scale specimens are shown in Figure 4-1 and 4-2, respectively.

For the four full-scale specimens, the cross sections were 200 x 600 mm with a load span of 1,200 mm, and a support span of 10 metres. Lateral bracing was provided at the loading points to

prevent lateral-torsional instability. Two of the beams had grooves cut into the bottom face of the beams and one of the beams had grooves cut into the sides of the beam. The grooves had a depth and width of 20 x 20 mm, 15 x 15 mm, and 40 x 20 mm for Beam FS-1, FS-2, and FS-3, respectively. Due to the available lengths of the GFRP bars used, only the central 6.0 m was reinforced. A schematic of the test setup and the configuration of the half-scale specimens are shown in Figure 4-3 and 4-4, respectively.

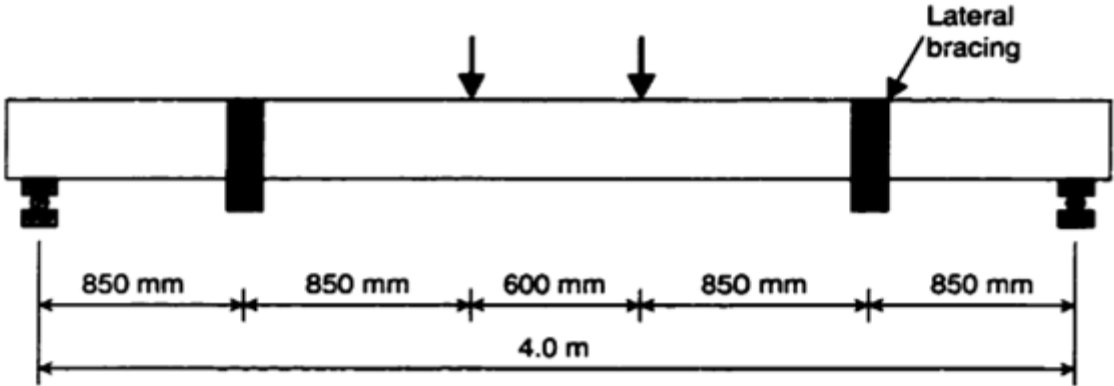


Figure 4-1 Test configuration for half-scale beams (Gentile, 2000)

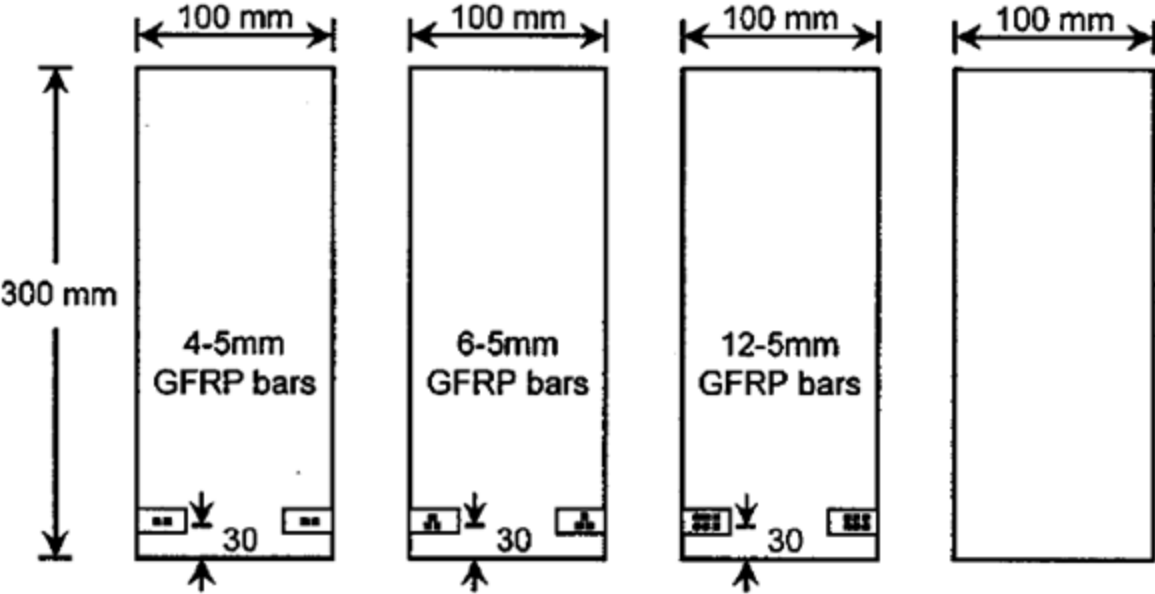


Figure 4-2 Cross sections of half-scale reinforced beams (Gentile, 2000)

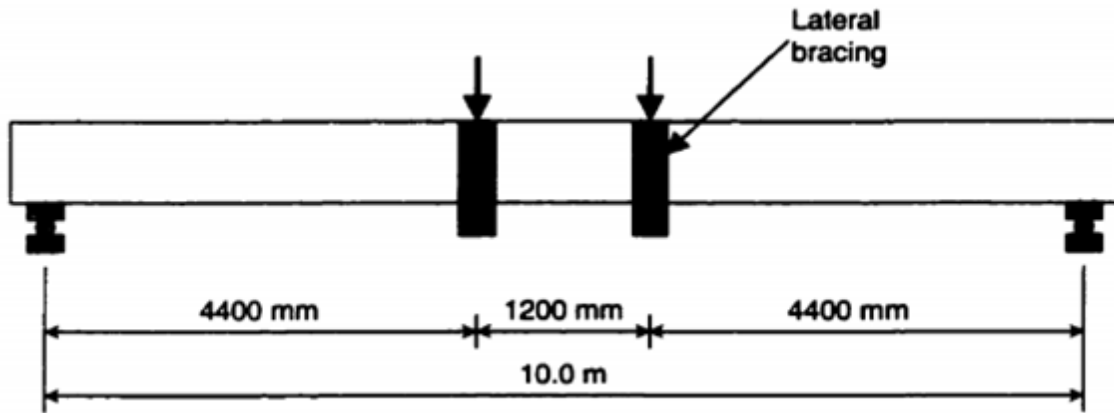


Figure 4-3 Test configuration for full-scale beams (Gentile, 2000)

Figure 4-3

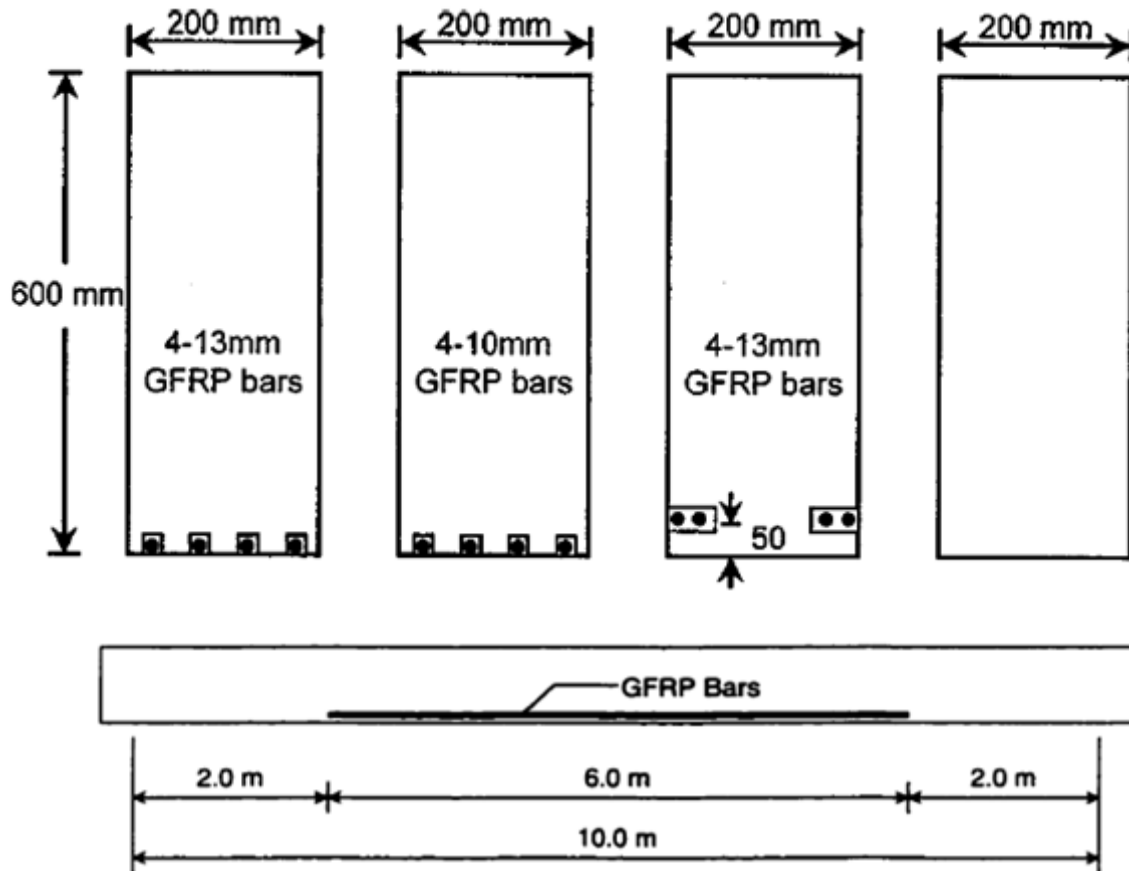


Figure 4-4 Configuration of full-scale reinforced beams (Gentile, 2000)

4.2.2 Materials

The timber used in the experiments was structural grade Douglas Fir with an allowable bending stress of 11 MPa (1600 psi) as specified by AASHTO (1996). New timber was used to prepare the half-scale beams, while the full-scale beams were taken from an existing timber bridge in Manitoba, which had been in service for 40 years at the time of the experiments.

Two types of GFRP bars were used for flexural strengthening of the test beams. The half-scale beams were reinforced by Rotaflex rods, produced by Rotafix Ltd, UK, while C-Bar, produced by Marshall Industries Composites Inc, USA, was used to reinforce the full-scale beams. The Rotaflex rods had a 5 mm diameter, a nominal tensile strength of 1800 MPa, and a modulus of elasticity of 56 GPa. The C-Bar used had diameters of 10 mm and 13 mm, a nominal tensile strength of 700 MPa, and a modulus of elasticity of 42 GPa. The stress-strain relationships for the two GFRP bars are presented in Figure 4-5.

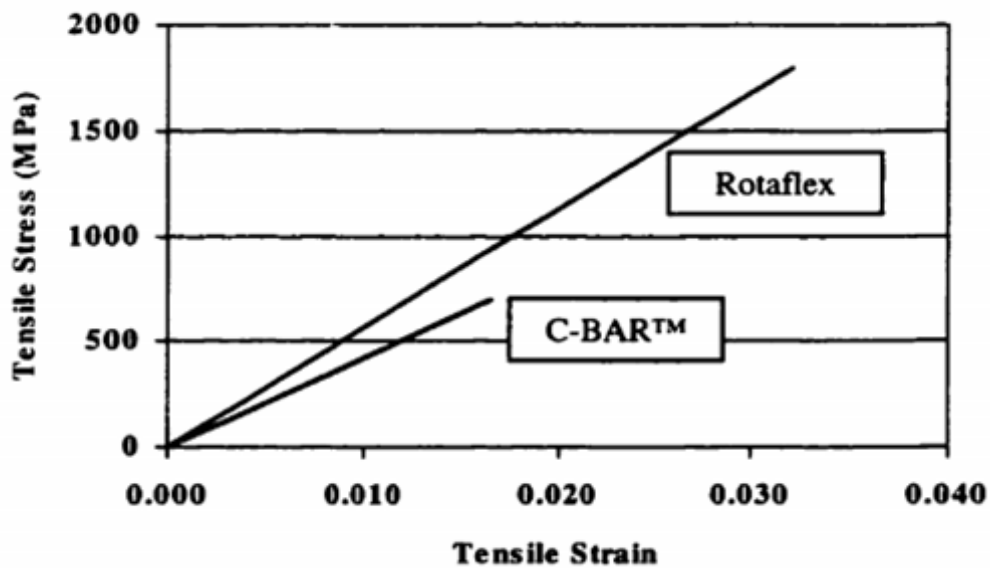


Figure 4-5 Stress-strain relationships for GFRP (Gentile, 2000)

4.2.3 Modelling Details

Both the plain timber specimens and the reinforced timber specimens were modelled in VecTor2 using the auto-meshing function, with only half of the span modelled due to symmetry. Rectangular membrane elements were used to model the timber, while truss elements were used to model the GFRP bars. Perfect bonding was assumed between the GFRP bars and the timber. The finite-element models created for both the half-scale beams and the full-scale beams are presented in Figure 4-6 through Figure 4-12. A summary of the finite element models is given in Table 4-1.

The modulus of elasticity (MOE) and the modulus of rupture (MOR) in the longitudinal direction were reported by Gentile (2000); these values were used as the input mechanical properties of timber. The modulus of rupture may be used as the tensile strength parallel to the grain, although it is not a true stress because the formula by which it is calculated is valid only within the elastic range.

It was impossible to perform FE analysis for the timber beams with only the MOE and the MOR available, since there were other inputs required by VecTor2, namely the tensile strength perpendicular to the grain, the compressive strength parallel to the grain, the compressive strength perpendicular to the grain, and the shear strength. Representative values may be found in Chapter 4 of the US Wood Handbook. However, these values were obtained from small defect-free samples which may not be appropriate to use for full-scale structural grade timber.

To make the subsequent FE analysis possible, reasonable assumptions were made as follows: The magnitude of the longitudinal compressive strength was taken as equal to that of the longitudinal tensile strength. The tensile strength perpendicular to the grain and the shear strength were assumed to be one-tenth of the tensile strength parallel to the grain, while the transverse compressive strength was assumed to be 20% of that of the longitudinal counterpart. The full explanation for the assumptions made here is given in Section 5.3.2 of this thesis. Lastly, the elastic modulus perpendicular to the grain orientation was calculated as per the relations discussed in Chapter 2 (Bodig 1982). A summary of the input parameters and the reinforcement details is shown in Table 4-2 and Table 4-3, respectively.

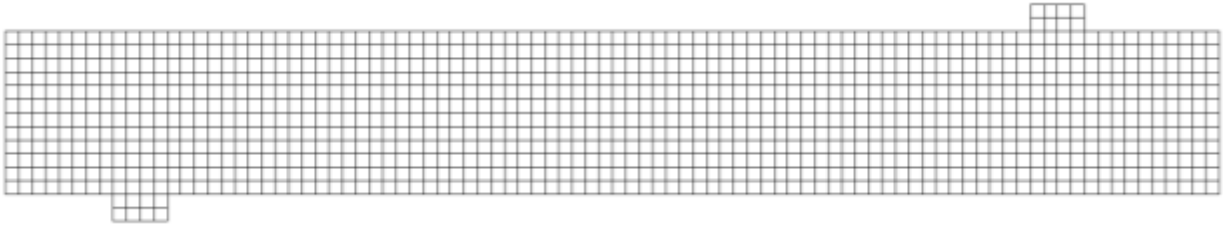


Figure 4-6 Half-scale plain timber beams

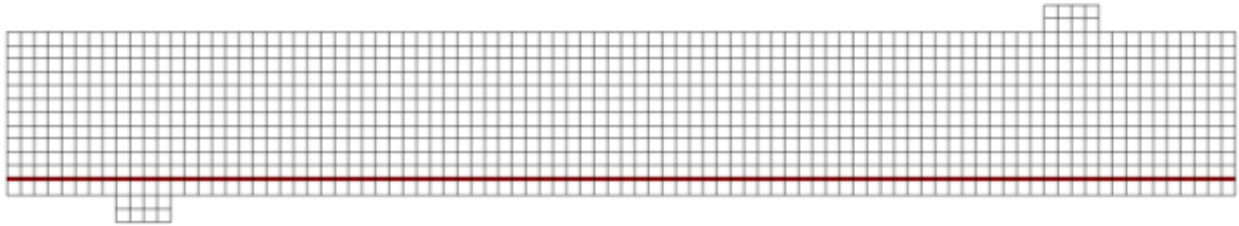


Figure 4-7 Half-scale beams with GFRP reinforcement

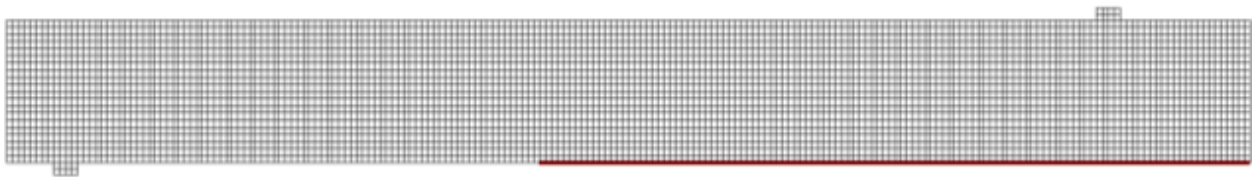


Figure 4-8 Full-scale beams with GFRP reinforcement at the bottom (FS1 and FS2)

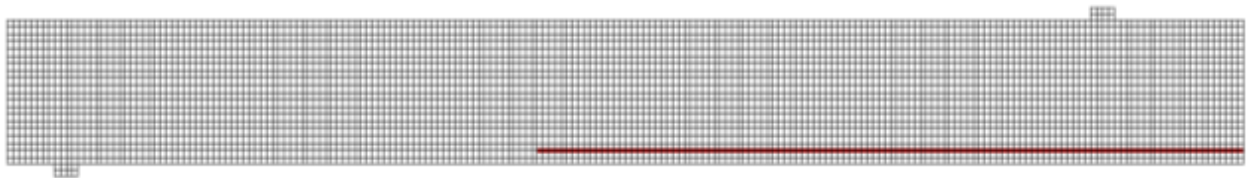


Figure 4-9 Full-scale beam with GFRP reinforcement at the sides (FS3)



Figure 4-10 Full-scale plain timber beam (FS4)

Table 4-1 Summary of the models

Scale	Half	Full
Mesh Size (width x height)	25 x 25 mm	25 x 30 mm
Nodes	1203	4451
Rectangles	1096	4216
Truss	NA / 90	NA / 120

Table 4-2 Summary of input parameters

Beam ID	MOE Para. to Grain (MPa)	Tensile Para. to Grain (MPa)	Compressive Para. to Grain (MPa)	Tensile Perp. to Grain (MPa)	Compressive Perp. to Grain (MPa)	Shear Long. to Tran. (MPa)
A1	10257	21.2	21.2	2.1	4.2	2.1
A2	10855	43.3	43.3	4.3	8.7	4.3
B1	8568	21.6	21.6	2.2	4.3	2.2
C1	10197	37.0	37.0	3.7	7.4	3.7
D1	12491	52.8	52.8	5.3	10.6	5.3
D2*	11189	36.0	36.0	3.6	7.2	3.6
F1	6999	18.8	18.8	1.9	3.8	1.9
F2	6039	23.0	23.0	2.3	4.6	2.3
G1	14662	43.7	43.7	4.4	8.7	4.4
G2	10969	44.2	44.2	4.4	8.8	4.4
H1	9654	25.0	25.0	2.5	5.0	2.5
H2	9327	32.0	32.0	3.2	6.4	3.2
I1	14724	61.3	61.3	6.1	12.3	6.1
I2	13140	58.7	58.7	5.9	11.7	5.9
J1	7602	19.8	19.8	2.0	4.0	2.0
K1	7450	37.2	37.2	3.7	7.4	3.7
L1	7274	27.1	27.1	2.7	5.4	2.7
L2	7598	34.1	34.1	3.4	6.8	3.4
FS-1	10506	44.3	44.3	4.4	8.9	4.4
FS-2	13276	55.3	55.3	5.5	11.1	5.5
FS-3	8445	36.1	36.1	3.6	7.2	3.6
FS-4	11870	24.8	24.8	2.5	5.0	2.5

Table 4-3 Reinforcement details

Beam ID	Scale	Diam. of GFRP (mm)	# of GFRP	Area of GFRP (mm ²)	% of GFRP	Fy (MPa)	Fu (MPa)	E (MPa)
A1	Half	-	-	-	-	-	-	-
A2	Half	5	12	246	0.82	1800	1800	56000
B1	Half	-	-	-	-	-	-	-
C1	Half	-	-	-	-	-	-	-
D1	Half	5	4	82	0.27	1800	1800	56000
D2	Half	5	4	82	0.27	1800	1800	56000
F1	Half	-	-	-	-	-	-	-
F2	Half	5	4	82	0.27	1800	1800	56000
G1	Half	-	-	-	-	-	-	-
G2	Half	5	12	246	0.82	1800	1800	56000
H1	Half	-	-	-	-	-	-	-
H2	Half	5	6	123	0.41	1800	1800	56000
I1	Half	5	6	123	0.41	1800	1800	56000
I2	Half	5	12	246	0.82	1800	1800	56000
J1	Half	-	-	-	-	-	-	-
K1	Half	5	6	123	0.41	1800	1800	56000
L1	Half	5	6	123	0.41	1800	1800	56000
L2	Half	5	12	246	0.82	1800	1800	56000
FS-1	Full	13	4	504	0.42	700	700	42000
FS-2	Full	10	4	312	0.26	700	700	42000
FS-3	Full	13	4	504	0.42	700	700	42000
FS-4	Full	-	-	-	-	-	-	-

4.2.4 Modelling Results

Shown in Figure 4-13 are the comparisons between the VecTor2 simulation results and the experimental results, presented as the red dotted line and black solid line, respectively. In general, VecTor2 was capable of predicting the pre-peak global load-deflection responses and the global stiffness with sufficient accuracy.

The post-peak load-deflection response of the reinforced specimens was also reasonably well captured by VecTor2. In general, the reinforced specimens exhibited more post-peak displacement than those without reinforcement. Specimen F2, with a modulus of elasticity (MOE) of 6039 MPa and a modulus of rupture (MOR) of 23 MPa, exhibited a smooth and progressive post-peak response with only 0.27% reinforcement. On the contrary, Specimen D1, while having the same amount of reinforcement and being approximately two times stronger and stiffer than Specimen F2, experienced a brittle failure as the applied load and the stiffness dropped rapidly once the maximum force was reached. Specimen I2 had a reinforcement ratio of 0.82%, and demonstrated an improved post-peak response than that of Specimen D1. Based on the above observations, it may be concluded that the amount of post-peak response depended not only on the reinforcement ratio, but also the quality of the timber.

Regarding the failure modes, tension failure was predicted by VecTor2 in the constant moment region for all specimens; whereas, as per Gentile (2000), the failure modes of the specimens included tension failure, compression failure, and flexural-shear failure which was only found in three of the reinforced specimens. Due to the lack of information, the specimens that had flexural-shear failures were excluded from the analysis. All plain timber beams failed in brittle tension with no signs of crushing in compression zone, which was in agreement with the VecTor2 predictions. While all the reinforced specimens initially developed tensile cracks in the constant moment region, half of those experienced ductile compression failure due to crushing of wood fibre in the top face. Unfortunately, Gentile (2000) did not identify the failure modes of individual specimen and therefore it was impossible to proceed any further with the analysis of failure modes. Nevertheless, it was believed that VecTor2 was unable to predict the ductile compression failures for two possible reasons as follows: 1. The true compressive strength of timber was not

reported in the original literature and was assumed to have the same magnitude as the tensile strength; 2. The presence of GFRP bars hindered the propagation of tension-initiated cracks, leading to a much more improved post-cracking tensile response of timber. Although the currently adopted constitutive model included a simple linear softening branch in tension, the appropriateness of it was not validated experimentally.

Although the perfect bonding assumption agreed fairly well with the experimental observations, there were some localized debonding of GFRP bars adjacent to tensile cracks. None of the failures were caused by debonding or delamination of the reinforcement; in the case of timber beams externally reinforced with FRP sheets or strips, as has been reported by other researchers (Dorey and Cheng 1996, Hernandez et al. 1997, and Bakoss et al. 1999), debonding or delamination of the reinforcement was found to be crucial to the ultimate failures.

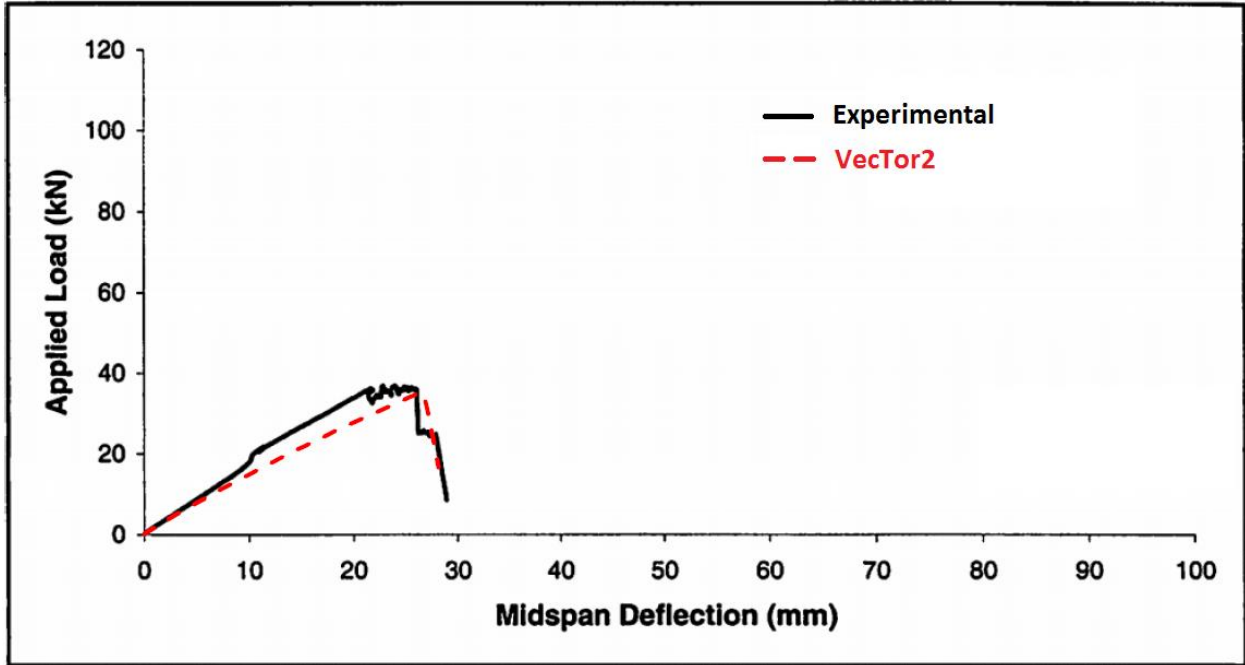
Table 4-4 presented the ultimate loads predicted by VecTor2, which agreed well with the experimental measurements. The only exception was Specimen D2, in which the failure occurred outside of the constant moment region, causing an underestimation of the modulus of elasticity (MOE).

4.3 Conclusions

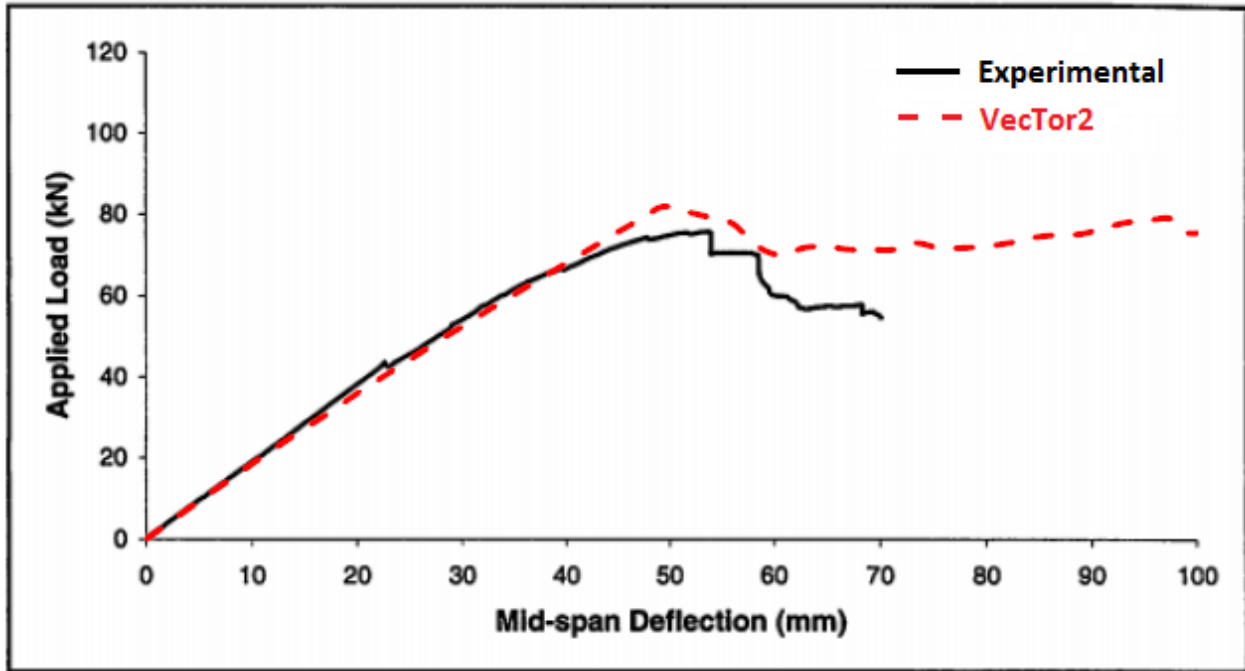
Based on the verification studies performed in this chapter, it was found that the constitutive models adopted, and the assumptions made for the unknown mechanical properties of wood, were appropriate in general for flexure-critical conditions. Due to the lack of information on specimen material properties, VecTor2 was unable to capture the compression failures observed in some of the reinforced specimens. Nevertheless, VecTor2 was able to predict the global stiffness, the failure loads, and the initial cracks initiated by tension with sufficient accuracy.

Timber beams, when sufficiently reinforced, can have a higher tensile strength and improved post-peak response than plain timber beams. Further research effort should be undertaken to better understand the interaction between timber and FRP reinforcement, and to quantify the influence of reinforcement on the post-peak tensile response of wood. There is also merit in

developing a more realistic constitutive model which can ultimately improve the post-peak FE predictions.

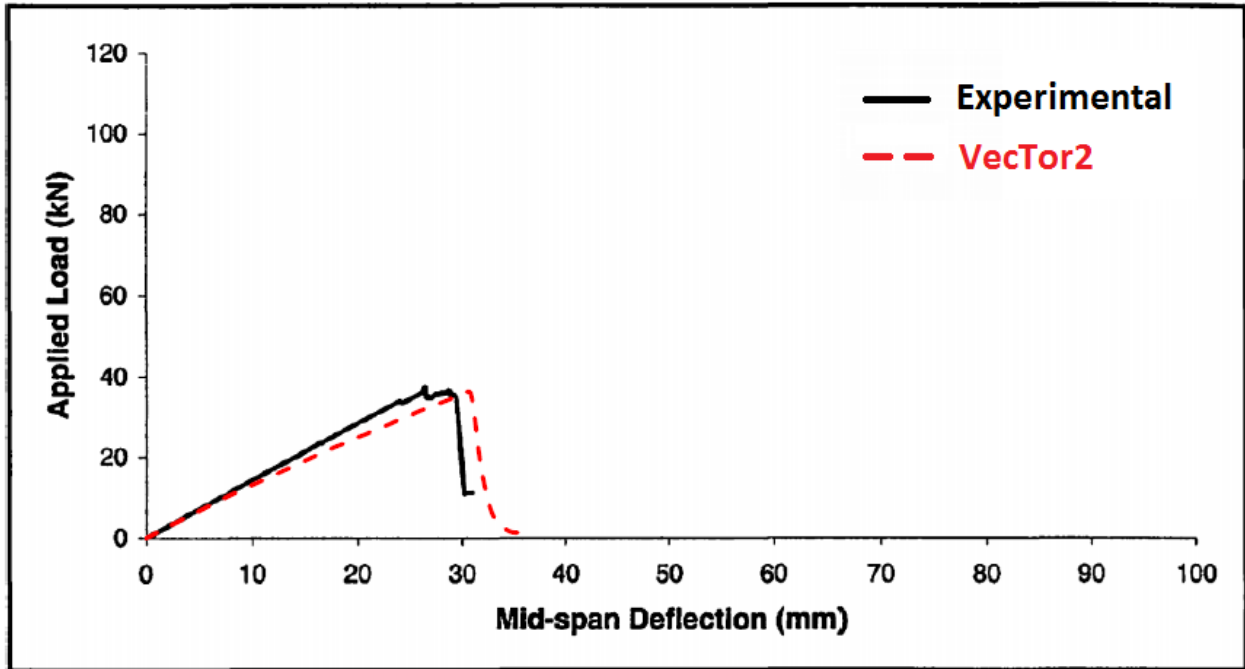


(a) Specimen A1

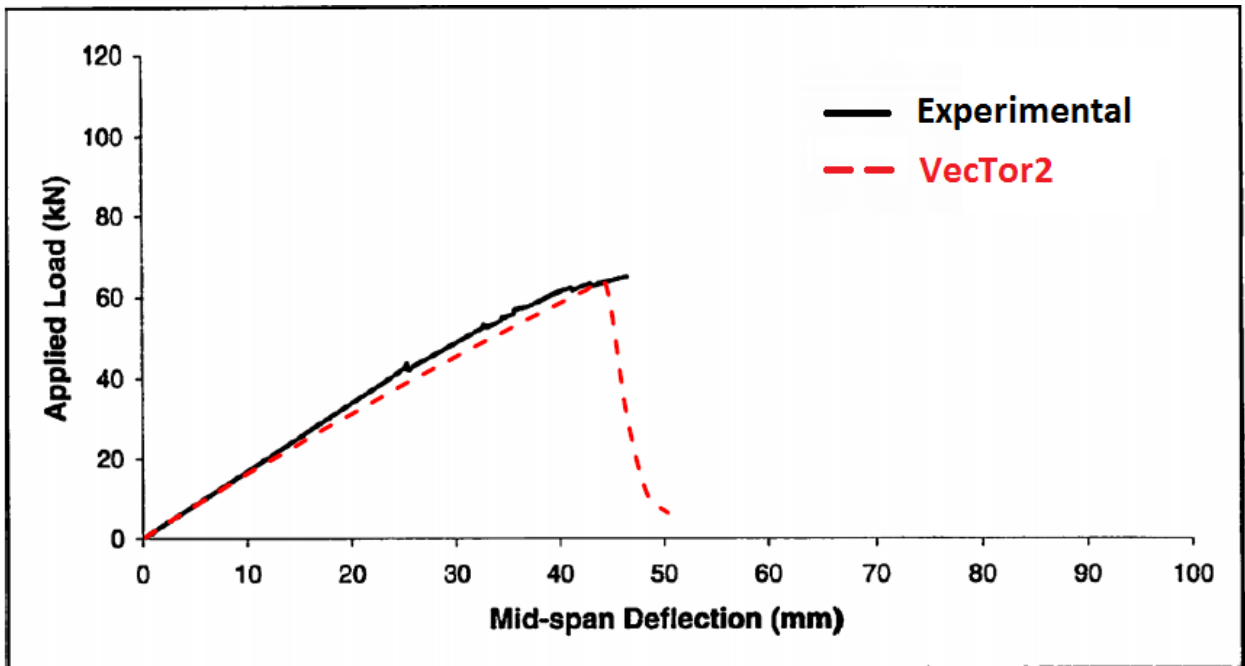


(b) Specimen A2

Figure 4-11 VecTor2 load-deflection responses

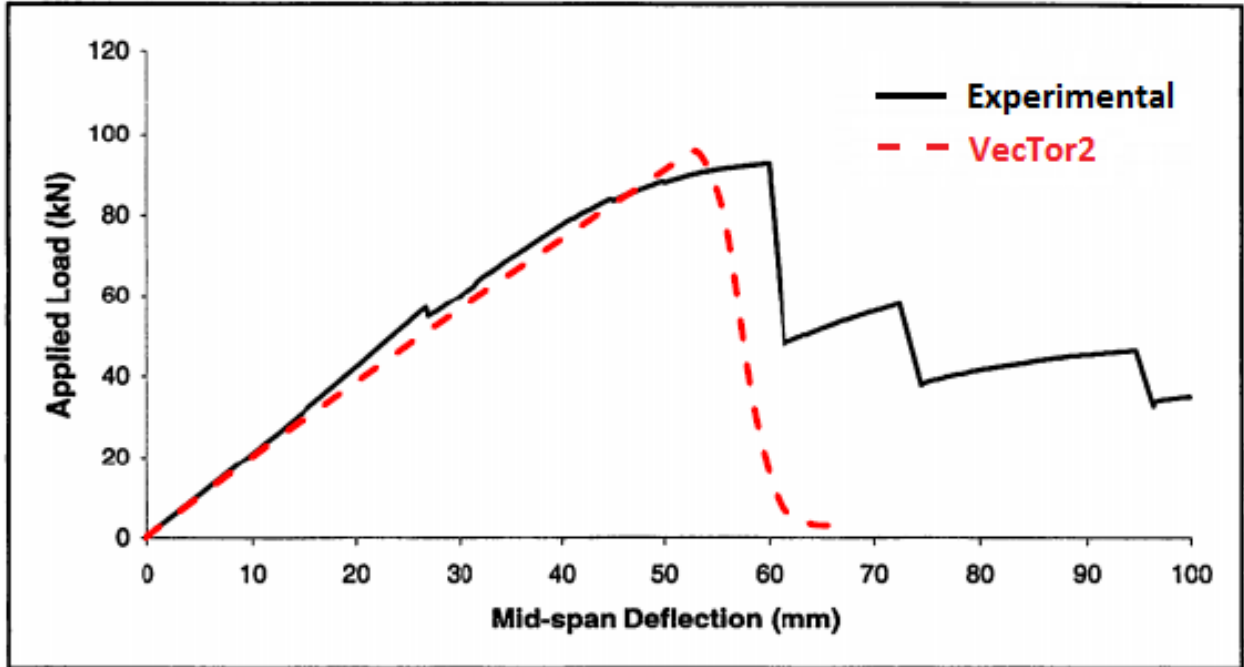


(c) Specimen B1

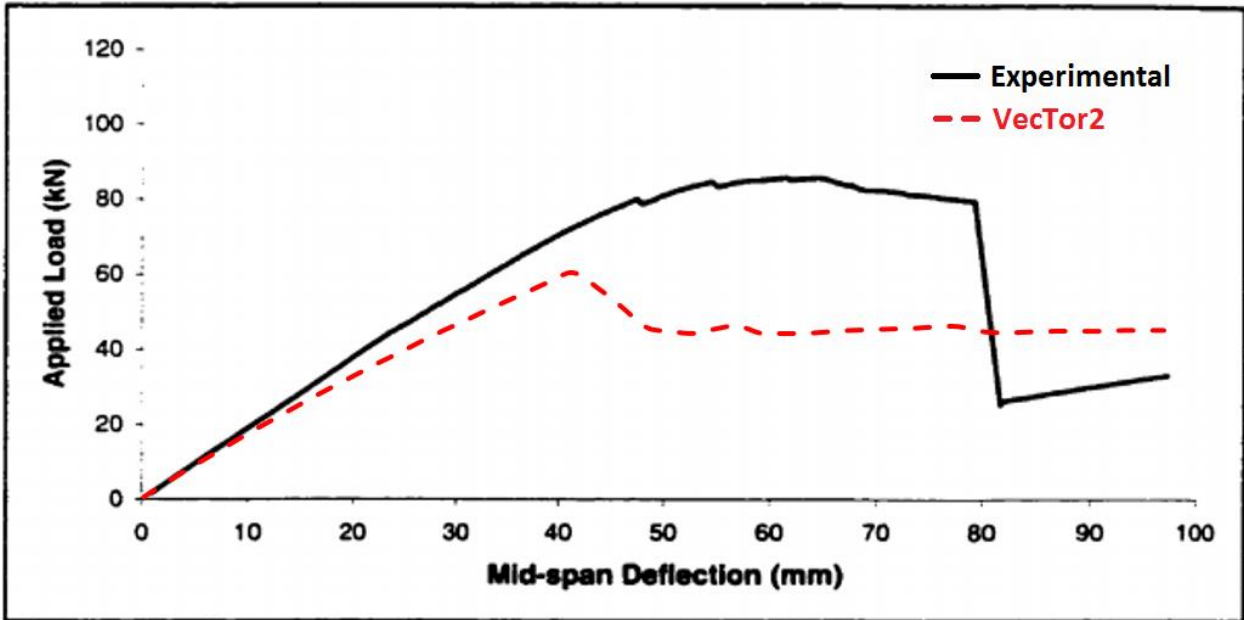


(d) Specimen C1

Figure 4-11 VecTor2 load-deflection responses (continued)

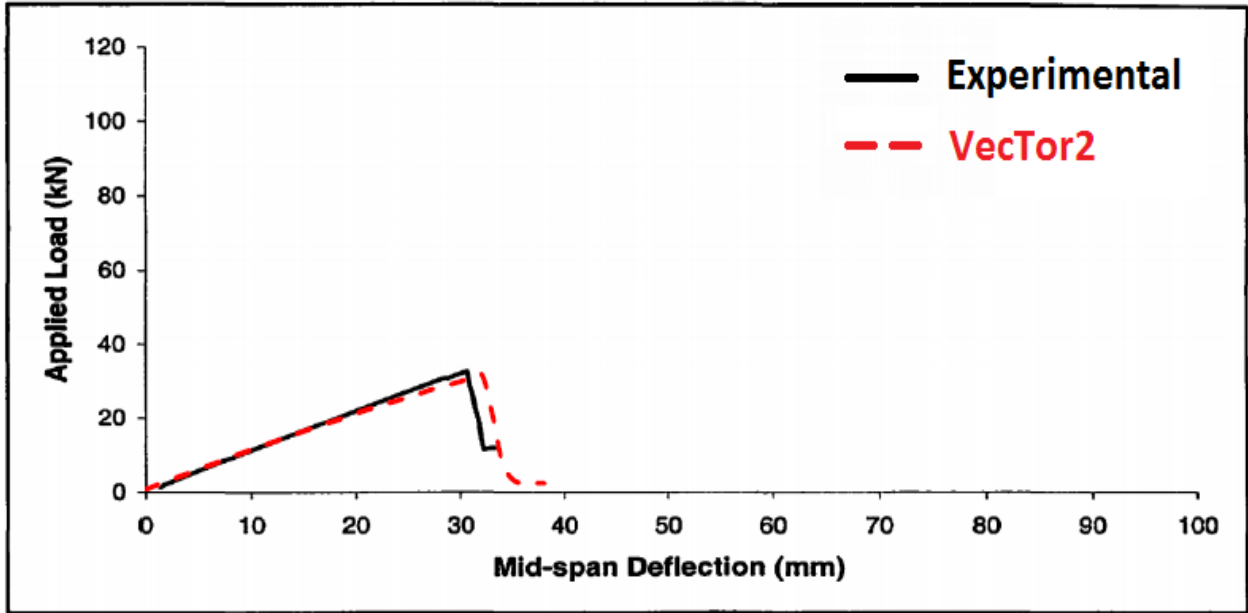


(e) Specimen D1

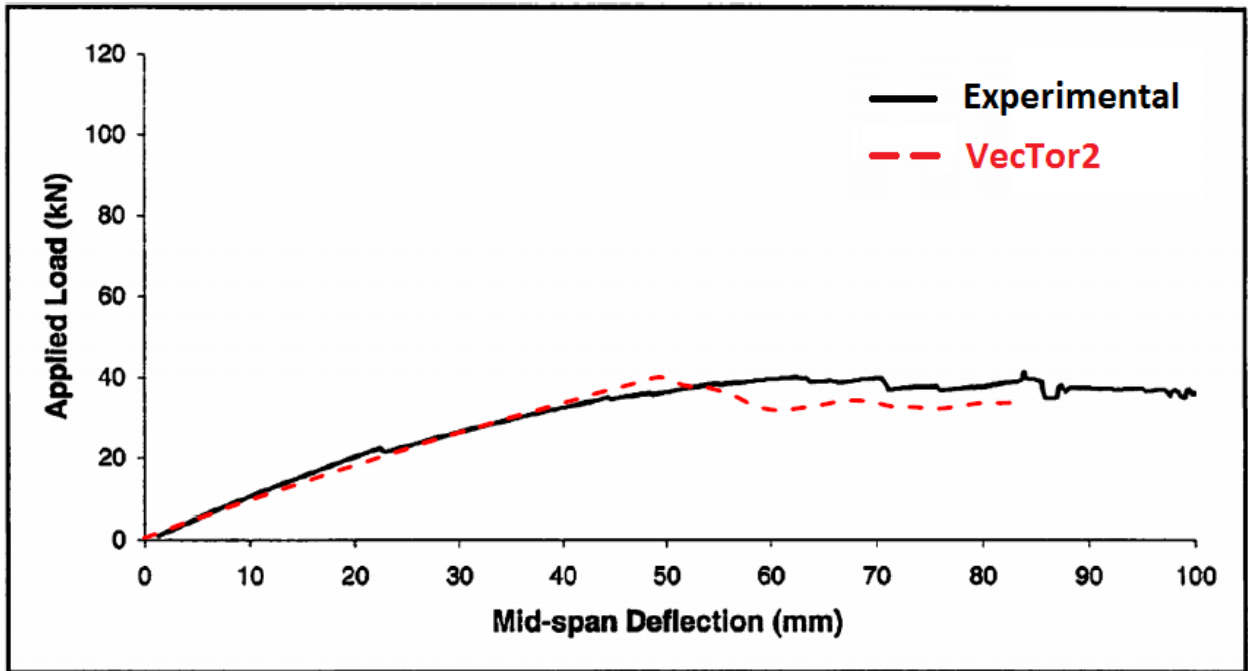


(f) Specimen D2

Figure 4-11 VecTor2 load-deflection responses (continued)

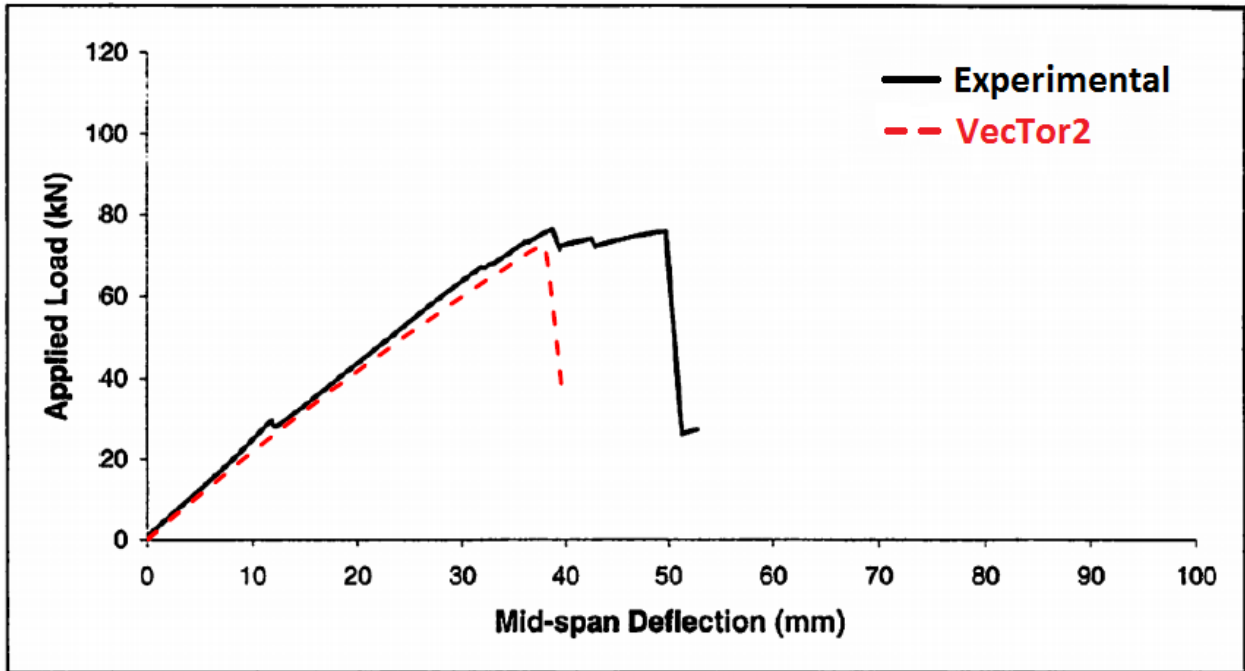


(g) Specimen F1

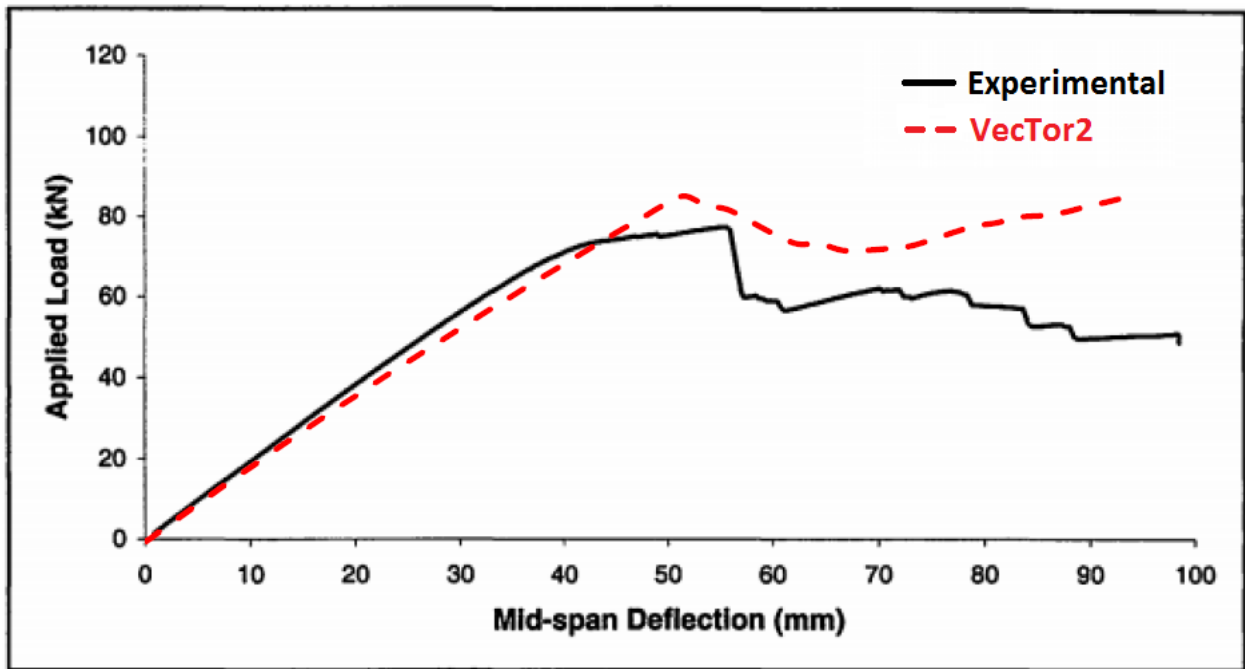


(h) Specimen F2

Figure 4-11 VecTor2 load-deflection responses (continued)

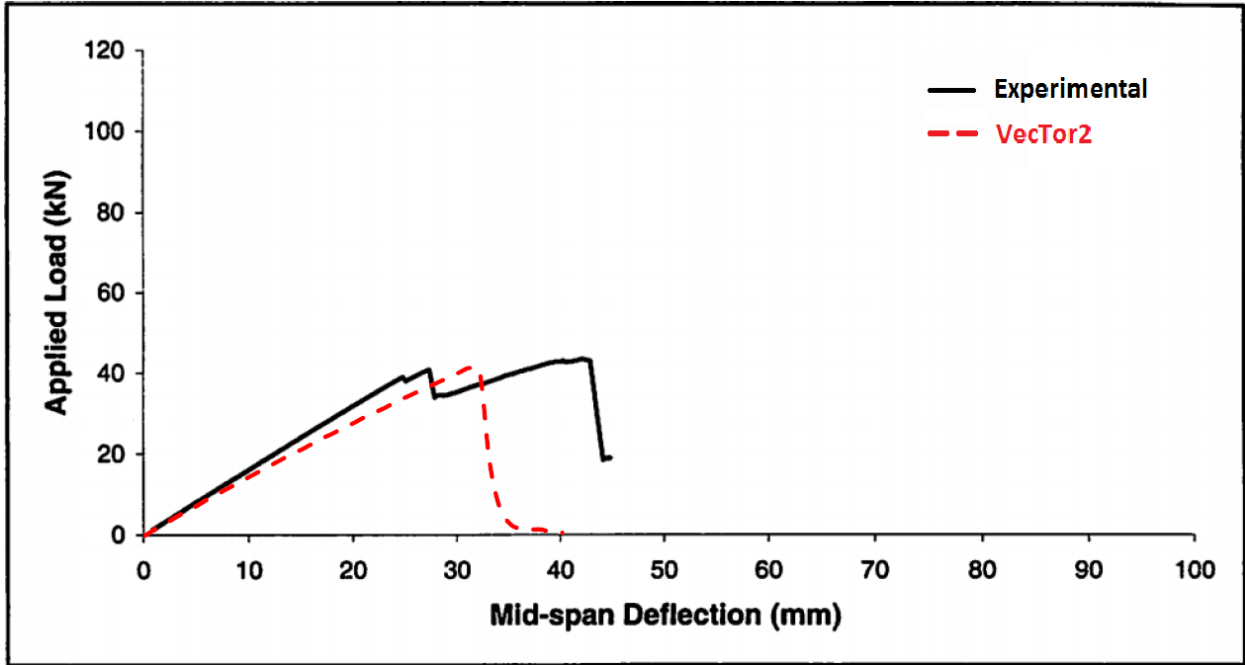


(i) Specimen G1

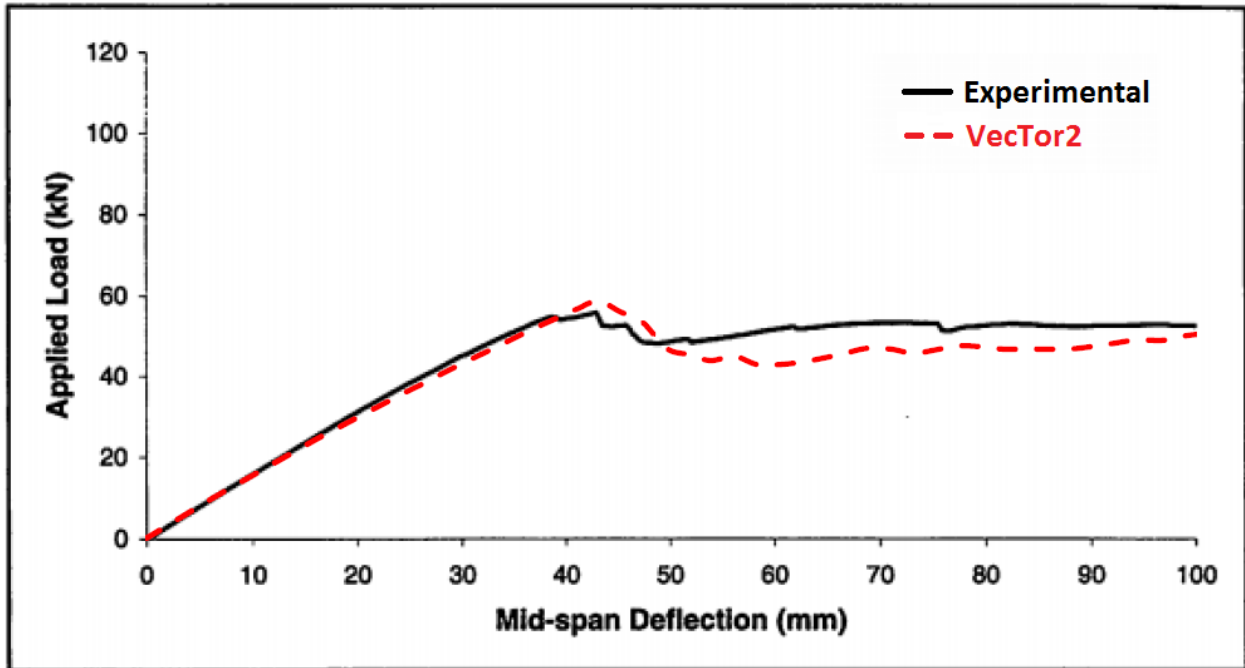


(j) Specimen G2

Figure 4-11 VecTor2 load-deflection responses (continued)

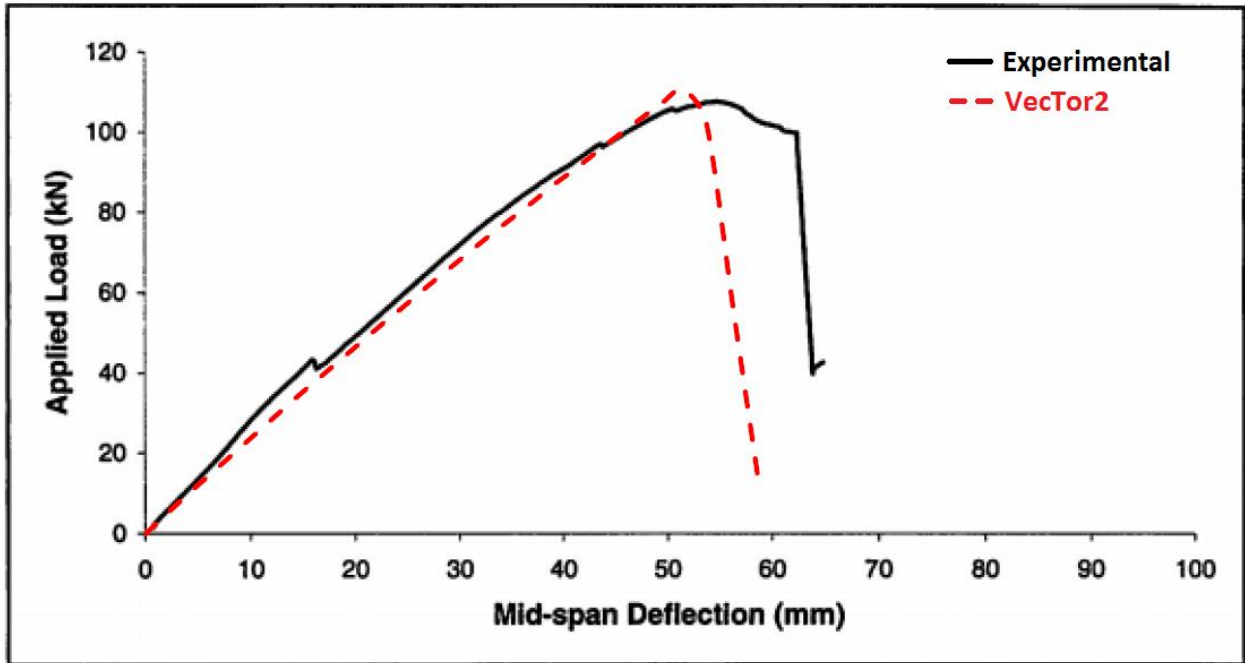


(k) Specimen H1

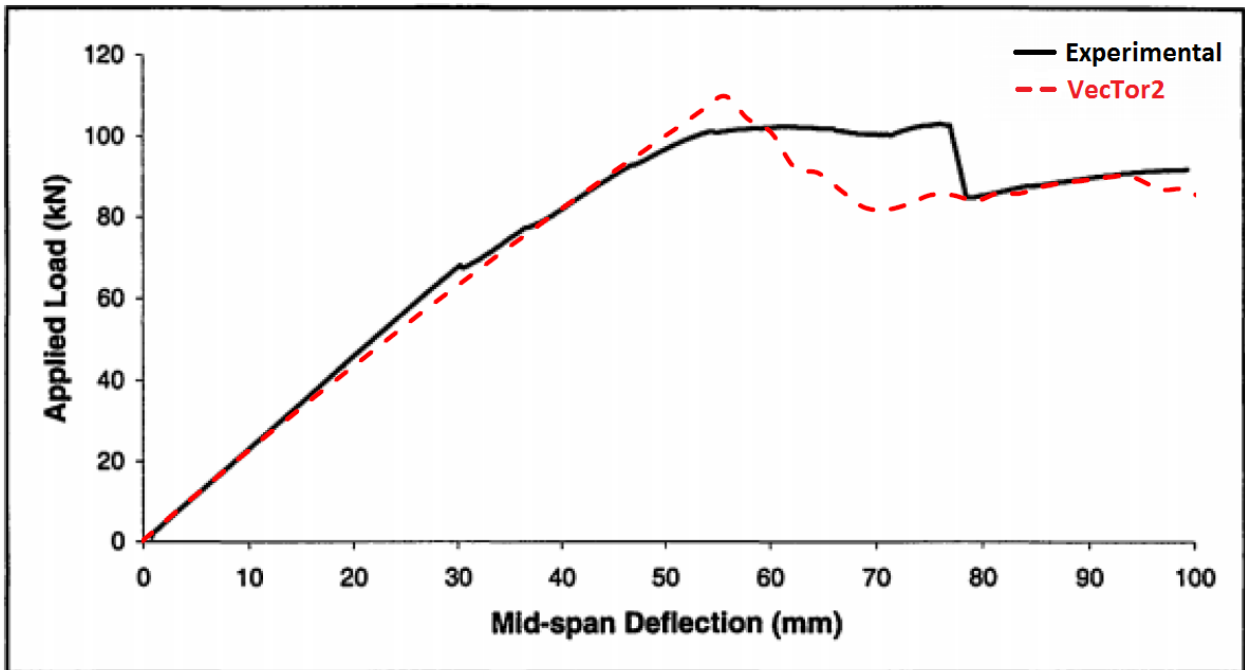


(l) Specimen H2

Figure 4-11 VecTor2 load-deflection responses (continued)

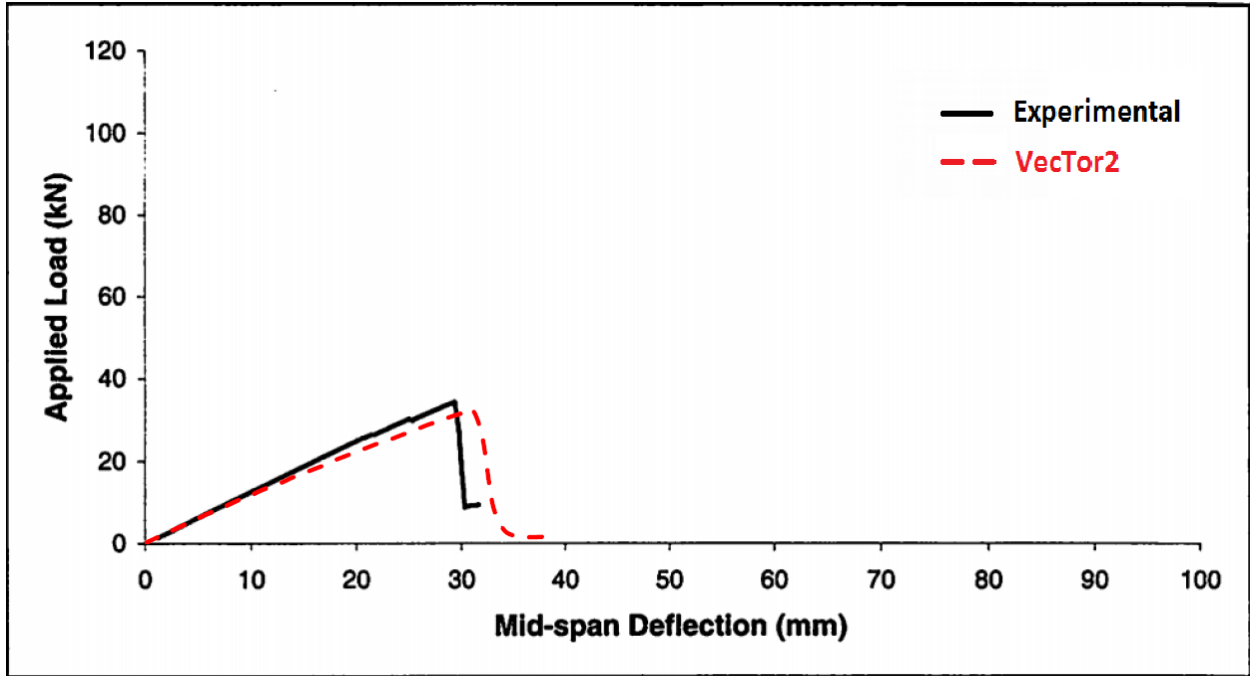


(m) Specimen I1

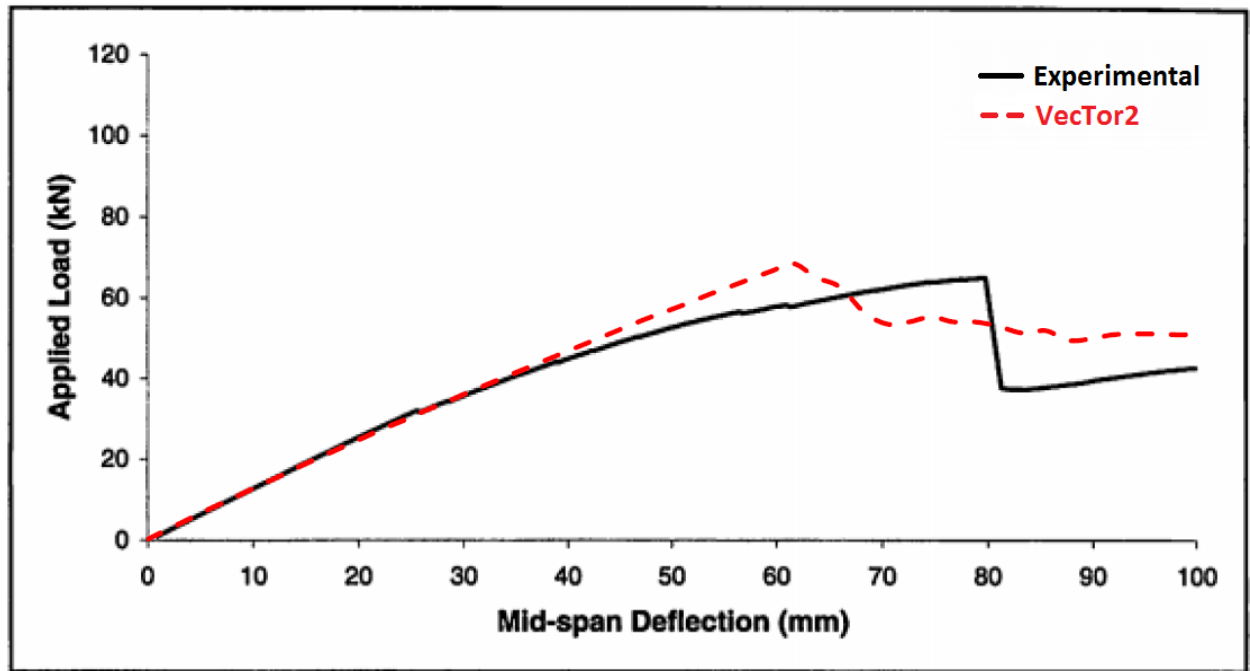


(n) Specimen I2

Figure 4-11 VecTor2 load-deflection responses (continued)

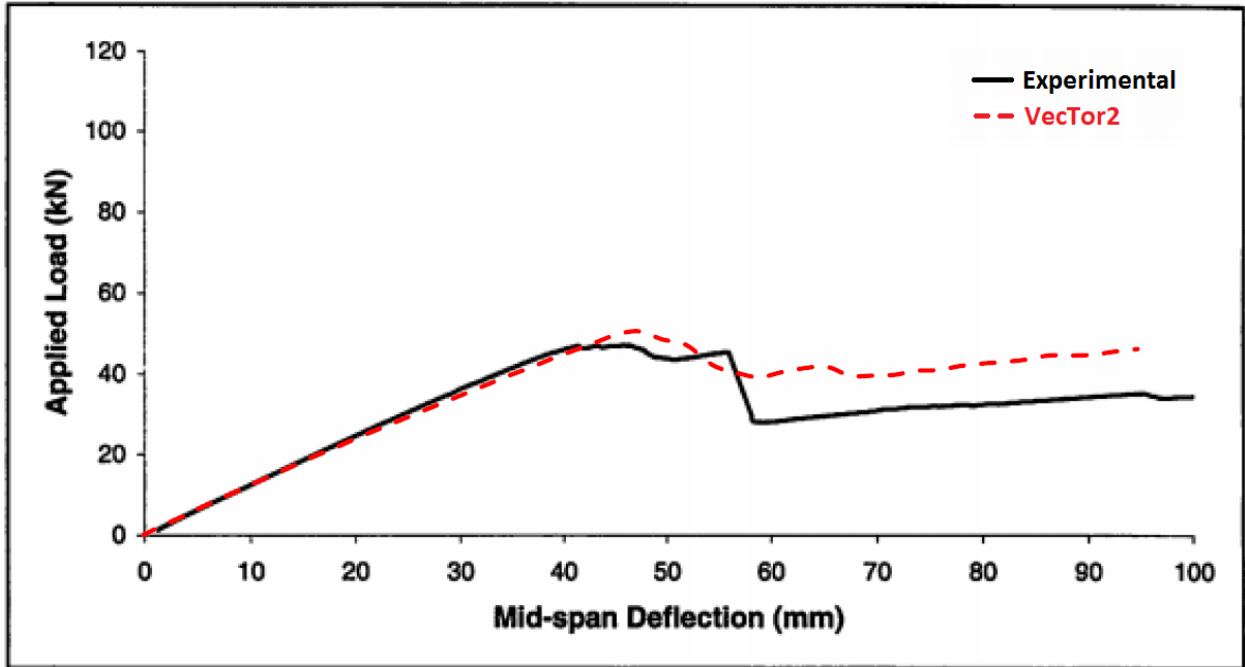


(o) Specimen J1

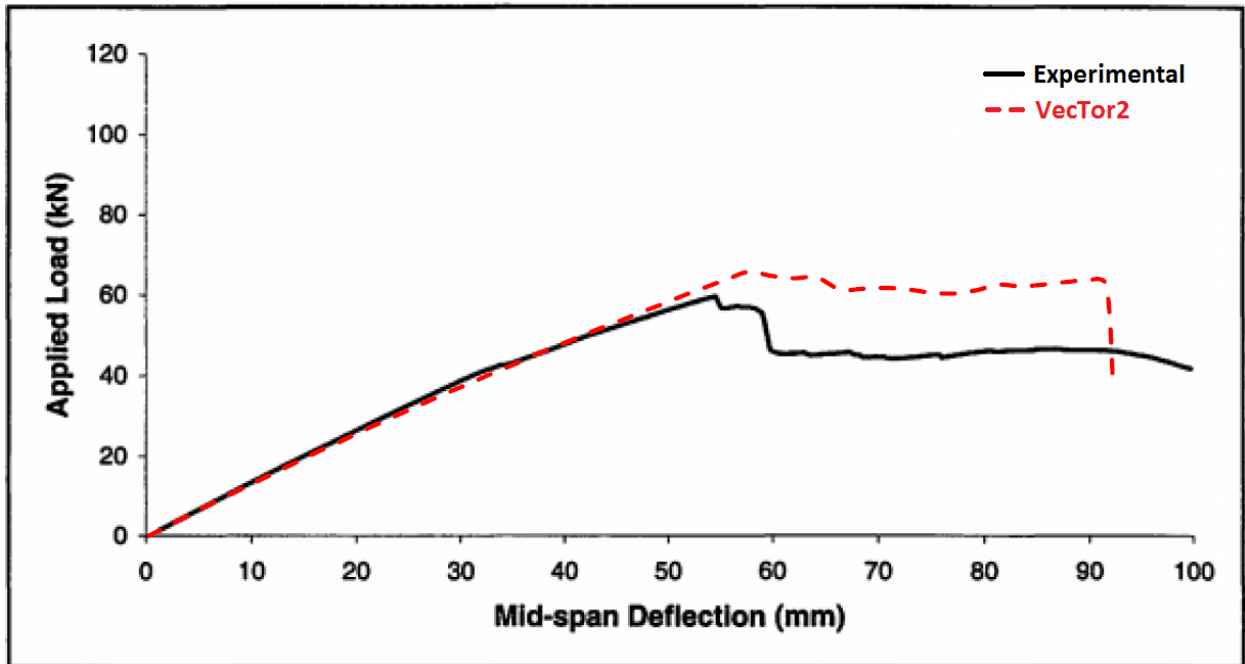


(p) Specimen K1

Figure 4-11 VecTor2 load-deflection responses (continued)

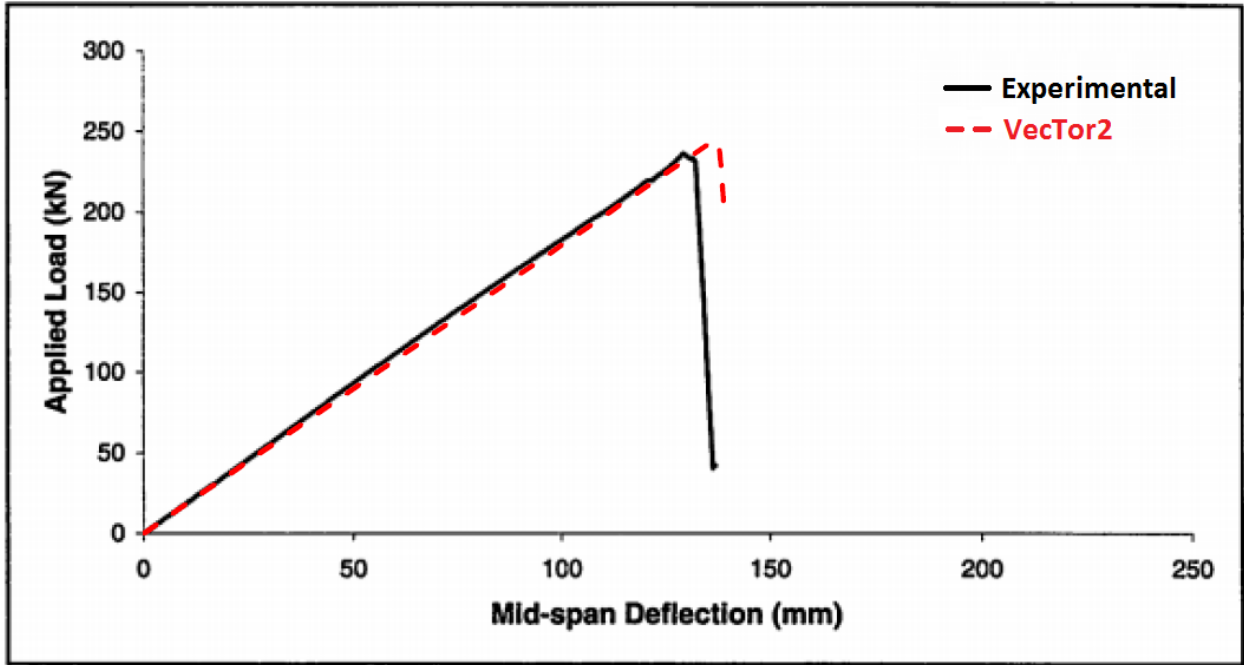


(q) Specimen L1

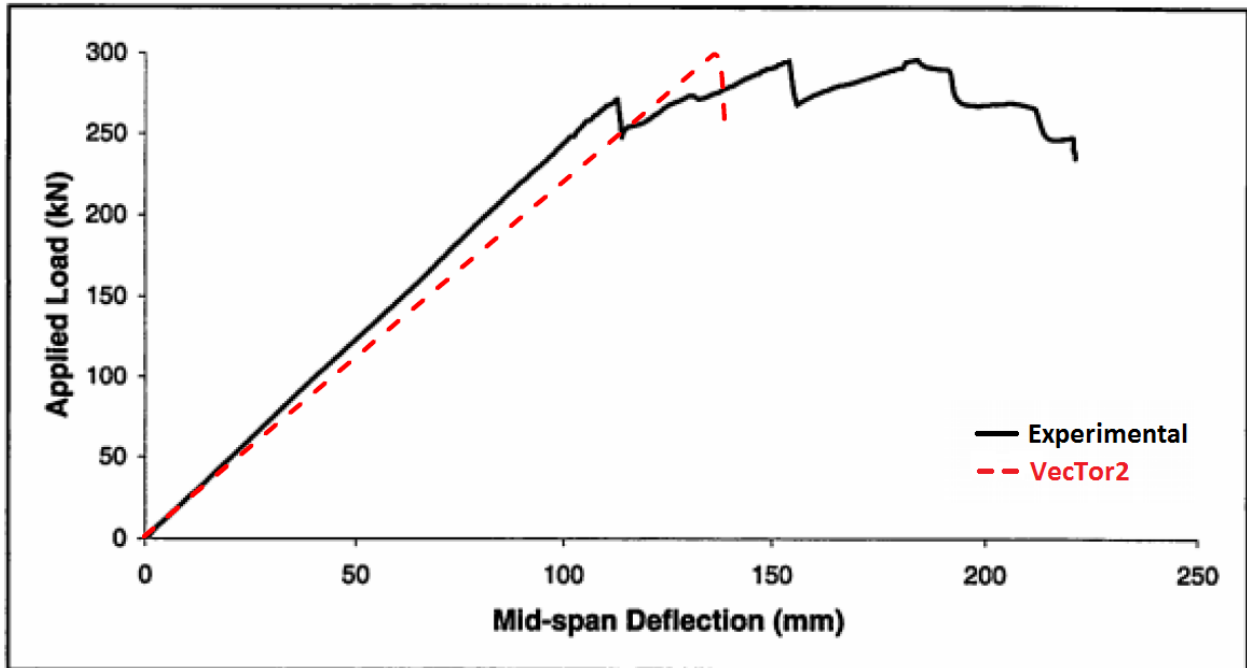


(r) Specimen L2

Figure 4-11 VecTor2 load-deflection responses (continued)

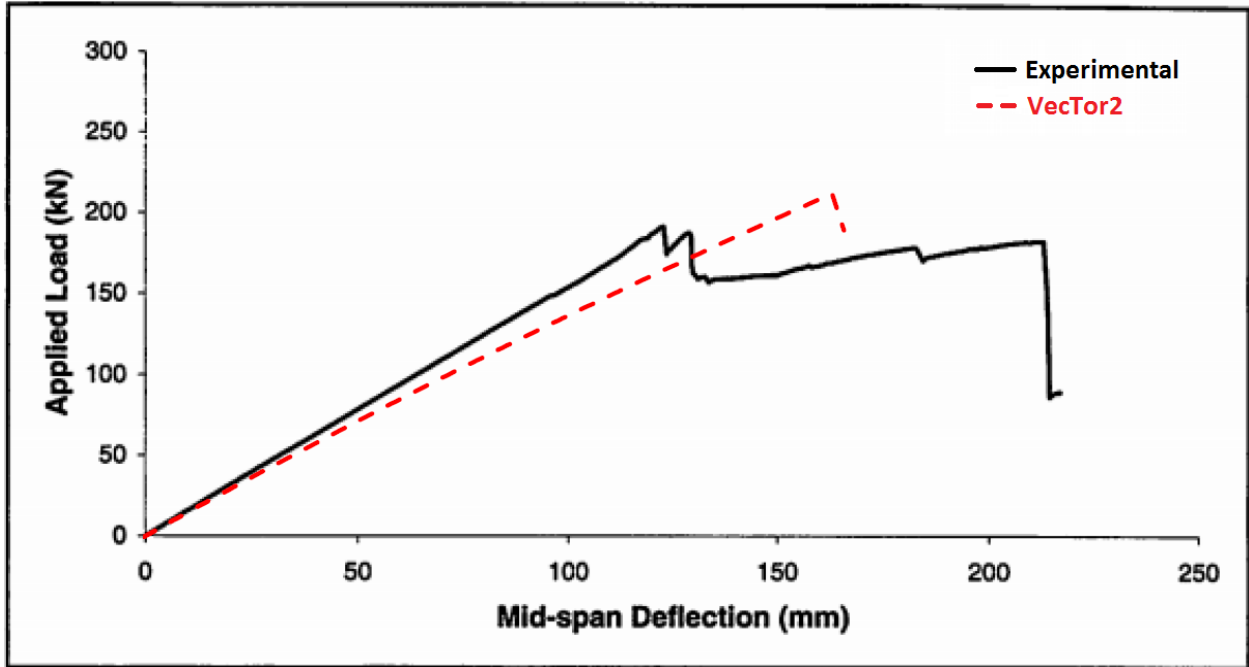


(s) Specimen FS-1

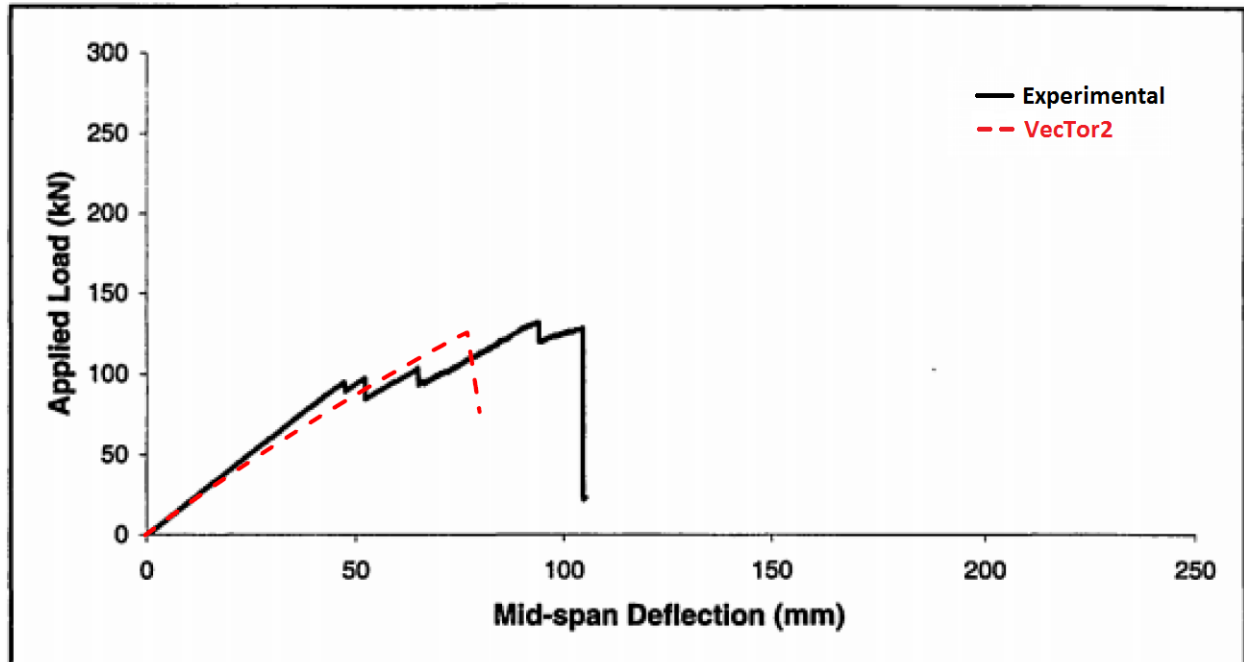


(t) Specimen FS-2

Figure 4-11 VecTor2 load-deflection responses (continued)



(u) Specimen FS-3



(v) Specimen FS-4

Figure 4-11 VecTor2 load-deflection responses (continued)

Table 4-4 Summary of ultimate loads

Beam ID	Pu (Exp.) (kN)	Pu (VT2) (kN)	Pu (VT2)/ Pu (Exp.)
A1	36.9	34.6	0.94
A2	75.8	82.0	1.08
B1	37.5	35.8	0.95
C1	64.7	63.0	0.97
D1	92.6	95.2	1.03
D2	85.7	60.0	0.70
F1	32.5	31.0	0.95
F2	40.0	40.0	1.00
G1	76.5	72.2	0.94
G2	77.4	85.4	1.10
H1	43.5	41.6	0.96
H2	55.9	58.4	1.04
I1	107.5	111.0	1.03
I2	103.0	90.0	0.87
J1	34.4	32.6	0.95
K1	65.1	68.2	1.05
L1	47.2	50.6	1.07
L2	59.6	69.0	1.16
FS-1	236.0	243.0	1.03
FS-2	296.0	298.6	1.01
FS-3	191.0	212.4	1.11
FS-4	132.0	126.4	0.96
		Mean	1.00
		Stand. Deviation	0.10
		COV	9.57%

Chapter 5 Modelling of Timber-Concrete Composite Beams

5.1 Introduction

In Chapter 4, VecTor2's capability of modelling the behaviour of plain timber beams was examined. This chapter builds on the successful modelling results from Chapter 4, and is devoted to the numerical modelling of timber-concrete composite (TCC) beams subjected to short-term monotonic loadings. A series of experimental and numerical corroborations were performed and the results are discussed.

The experiments selected for the verification studies are briefly described while additional details may be found in the original literature as referenced in this thesis. In what follows, the description of the finite element models created for the corresponding specimens are given, along with a detailed comparison between the experimental and the numerical results.

5.2 Model Description

Despite the fact that the experiments performed by different researchers varied considerably in terms of dimensions, load configurations, mechanical properties, materials, and the types of shear connectors, all the finite element models created in this verification studies share the following similarities:

1. All models consist of two basic elements: the membrane elements and the contact elements. The membrane elements were used to model the timber and the concrete components while the contact elements were used to represent the shear connectors.
2. Bearing plates were introduced to all the models to mitigate high local stress for the elements directly in contact with the supports and the loading jacks. The bearing plates were also modelled with membrane elements.
3. A number of the specimens had interlayers (e.g. particle board) between the concrete and the timber members. Such interlayers were treated as an integral part of the underlying timber members, and were assumed to have the same mechanical properties.

It is possible that this simplification can result in an overestimation of the global stiffness as the interlayers are likely softer than the timber member. Moreover, the presence of interlayer reduces the penetration depth of the shear connectors into the timber members, which can cause a reduction in the stiffness and load-carrying capacity of the shear connectors.

A sample FE model with an exaggerated span-to-depth ratio is presented in Figure 5-1. This general model represents a TCC beam subjected to four-point bending. Due to symmetry, only half of the beam is modelled. For the purpose of illustration, the model has a coarse mesh and includes all the possible components as discussed, with the concrete, the timber, and the interlayer components shaded in grey, brown, and yellow, respectively. The green and blue elements represent the bearing plates. The red line between the concrete and the interlayer depicts the smeared contact elements, representing continuous shear connectors. Alternatively, the shear connectors may be modelled as discrete as shown in Figure 5-2.

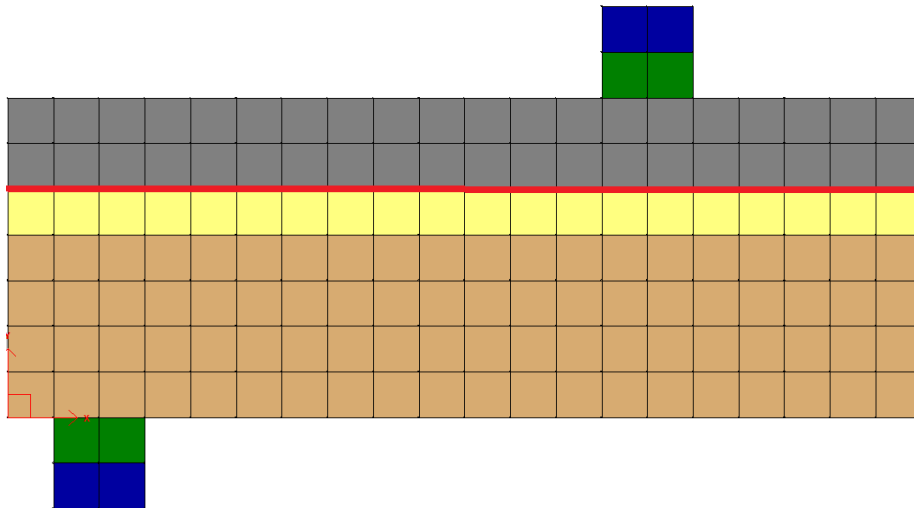


Figure 5-1 Sample model with smeared shear connectors

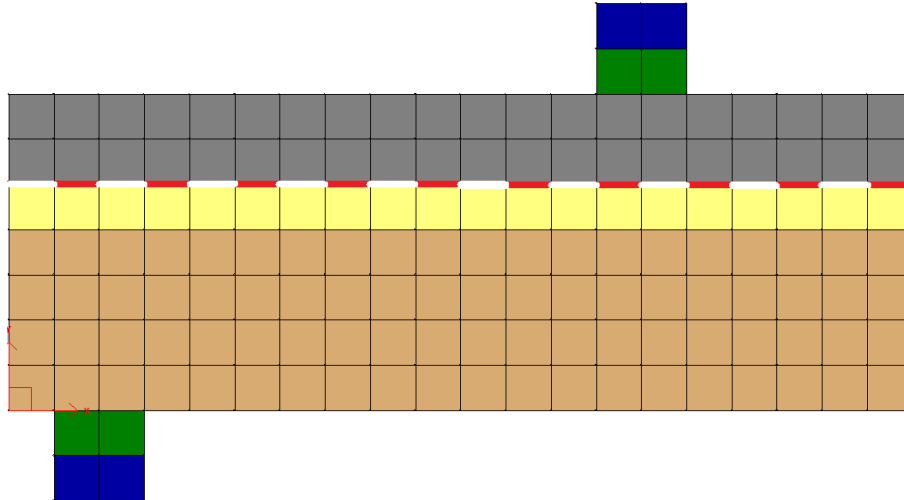


Figure 5-2 Sample model with discrete shear connectors

5.3 Model Inputs

5.3.1 Concrete

While VecTor2 has a number of built-in advanced material and behavioural models implemented for concrete, only the default models were used for the verification studies. As per the published literature, the global failure of timber-concrete composite beams was rarely governed by the concrete component; therefore, there was no need to use the advanced models which were implemented for specific case scenarios. The default concrete models in VecTor2 are tabulated in Table 5-1.

A screenshot of the VecTor2 concrete material definition interface is shown in Figure 5-3. Two input parameters are required as a minimum for concrete, including thickness (mm) and concrete cylinder compressive strength f'_c (MPa). Unless otherwise specified, all other material properties set to zero by default are computed as per Table 5-2.

Table 5-1 Default concrete models

Concrete Models			
Compression Pre-Peak	Hognestad (Parabola)	Dilation	Variable-Kupfer
Compression Post-Peak	Modified Park-Kent	Cracking Criterion	Mohr-Coulomb (Stress)
Compression Softening	Vecchio 1992-A	Crack Stress Calculation	Basic (DSFM/MCFT)
Tension Stiffening	Modified Bentz 2003	Crack Width Check	Agg/2.5 Max Crack Width
Tension Softening	Bilinear	Crack Slip Calculation	Walraven
FRC Tension	SDEM-Monotonic	Creep and Relaxation	Not Considered
Confined Strength	Kupfer / Richart	Hysteretic Response	Nonlinear w/ Plastic offsets

Material types to be used for rectangular, quadrilateral and triangular elements only. * Enter '0' for VT2 default value.

Figure 5-3 Concrete definition interface

Table 5-2 Concrete properties

Concrete Properties			
Thickness (mm)	user input	C_c (/°C)	10×10^{-6}
f'_c (MPa)	user input	Max. agg. size (mm)	20
f'_t (MPa)	$0.33\sqrt{f'_c}$	Density	2400
E_c (MPa)	$3320\sqrt{f'_c} + 6900$	Kc (mm²/s)	1.2
ϵ_o (MPa)	$1.8 + 0.0075 \cdot f'_c$	Sx (mm)	1000
ν_o	0.15	Sy (mm)	1000

5.3.2 Timber

Owing to the orthotropic nature of wood, the required input parameters for timber are quite extensive. A screenshot of the VecTor2 timber material definition interface is presented in Figure 5-4. The majority of these required inputs were not available from the original literature, including the longitudinal compressive strength, the transverse compressive and tensile strength, and the shear strength, as well as the Poisson’s ratios. Representative values may be found in Chapter 4 of the US Wood handbook titled “Wood handbook – Wood as an engineering material” which was published by Green et al. (1999). However, as pointed out by the authors, values reported in the handbook were obtained from small defect-free wood pieces. Therefore, the appropriateness of these properties to represent full-scale structural timber is questionable.

The longitudinal tensile strength of the specimens, on the other hand, was reported by most of the authors. The source of these values was typically from the manufacturers’ specifications or, occasionally, from regional design guidelines such as the Eurocode. These values are inherently conservative as they are intended for practical use by design engineers; use of these values in the FE models likely results in an early termination of the analysis once the longitudinal tensile strength of wood is reached.

Based on the aforementioned circumstances and the limited availability of data, a number of assumptions and simplifications were adopted to make the subsequent validations possible, including the following:

1. The published longitudinal tensile strength was used as a starting point for all the FE models. However, in case of early termination of the analysis, the longitudinal tensile strength was progressively increased to ensure that a complete global load-deflection response was replicated.
2. Based on the experimental observation as discussed in Chapter 4 of this thesis, the predominant failure mode of plain timber beams is through tensile failure of the bottom fibre, typically initiated near knots or finger-joints. The implication of this experimental observation is that the longitudinal compressive strength is likely as strong as the longitudinal tensile strength, if not stronger. Therefore, unless explicitly stated in the literature, the magnitude of the longitudinal compressive strength was taken as equal to that of the longitudinal tensile strength.
3. The transverse tensile strength was assumed to be 10% of the longitudinal tensile strength while the transverse compressive strength was taken as 20% of the longitudinal compressive strength. These assumption are largely consistent with the values published in the US Wood handbook.
4. Although the US Wood handbook suggests that the shear strength parallel to the grain may be taken as 20 to 25% of the longitudinal compressive strength, 10% was adopted in the FE models to account for the fact that the timber used in the experiments were engineered wood products such as laminated-veneer lumber (LVL), glued-laminated timber (glulam), and cross-laminated timber (CLT). These engineered wood products contain not only natural defects but also artificial defects such as finger-joints or inadequate glue between the layers. In fact, rolling shear failure is a common type of failure found in CLT.
5. As density and Poisson's ratios hardly influence the numerical results, these values were taken directly from the US Wood handbook.
6. The transverse Young's modulus was taken as one twentieth of the longitudinal Young's modulus as per the relations proposed by Bodig (1982). Refer to Section 2.2 of this thesis for additional information.

By adopting these assumptions and simplifications, the minimum required input parameters for timber were reduced to three: the thickness (mm), the longitudinal tensile strength (MPa), and the Young's modulus parallel to the grain.

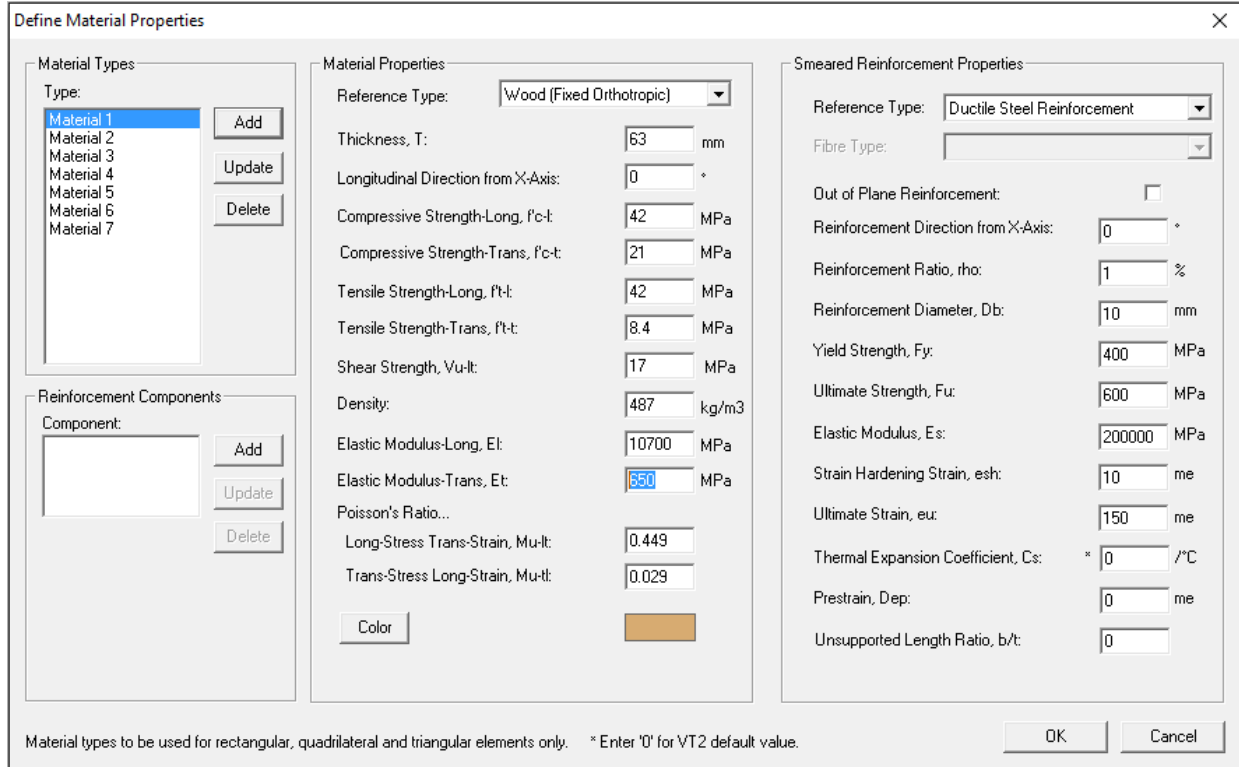


Figure 5-4 Wood definition interface

5.3.3 Shear Connectors

The load-slip relationship of the shear connectors is used as an input in VecTor2. The load-slip relationship is approximated by a piece-wise curve as discussed in Section 3.3.2 of this thesis, and must be converted to stress-slip format by converting the force to an equivalent stress as per Equation 5-1. A screenshot of the VecTor2 contact element definition interface is given in Figure 5-5. Note that the “Bonded Surface Area, A_o ” is the total contact area per meter length, and is taken as the thickness of timber (mm) multiplied by 1000 (mm/m).

$$\sigma = F/A \quad (5-1)$$

where F (N) is the force per shear connector and A (mm²) is the area of the contact element(s) associated with each shear connector.

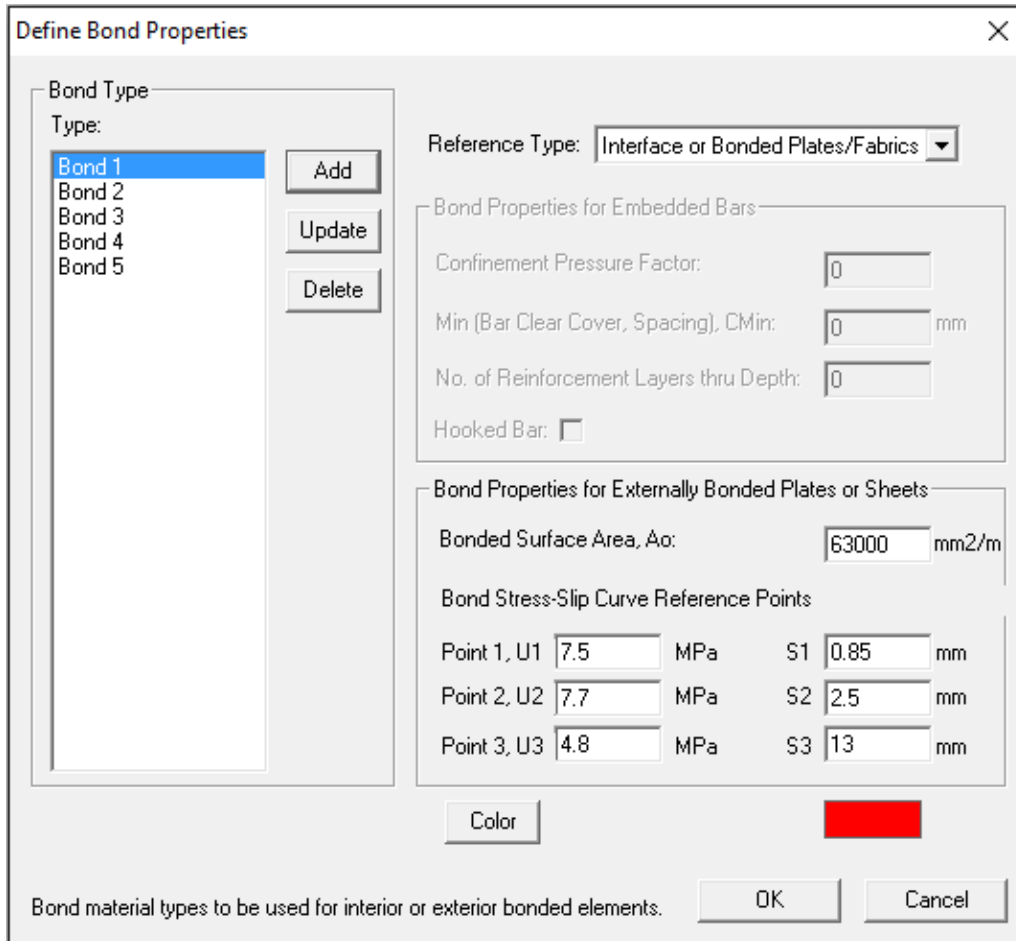


Figure 5-5 Contact element definition interface

5.4 Validation

A total of six experiment series was included in this verification study. These series were intentionally selected to investigate VecTor2's applicability under various conditions. Nevertheless, the modelling approach was similar among these experiments and the general FE model introduced in Section 5.2 was applied consistently.

5.4.1 Persaud and Symons (2006)

A full-scale timber-concrete composite (TCC) floor slab was constructed and tested under three-point bending to failure at the University of Cambridge (Persaud and Symons, 2006). The objective of this experiment was to propose a practical system that could be quickly constructed on site with readily available components. The proposed system used ordinary zinc plated steel coach screws as the shear connectors and a thin ribbed steel decking system to act as a permanent formwork for the cast-in-place concrete floor slab. Details of the proposed system are presented in Figure 5-6. As can be observed, the spacing of the shear connectors was dictated by spacing of the ribs. The out-of-plane thicknesses of the concrete slab and the timber beam were 2000 mm and 100 mm, respectively.

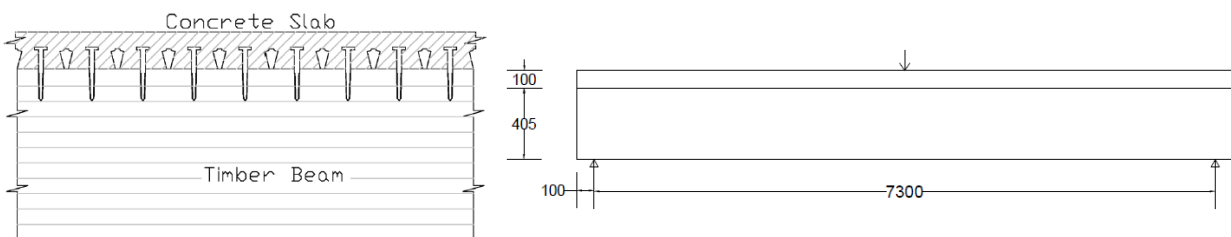


Figure 5-6 Details of the proposed system (Persaud and Symons, 2006)

The push-out test specimen had a similar configuration as the proposed full-scale specimen and is shown in Figure 5-6. The concrete slab was cast on Holorib S280 0.9 mm decking on either side of the timber beam and was 1000 mm long and 600 mm wide, while the sandwiched glulam beam was 1000 mm long and 140 mm wide. The depth of the concrete slab and the timber beam were 100 mm and 630 mm, respectively. The results of the push-out test are shown in Figure 5-7, together with the adopted load-slip curve.

As reported by the authors, the concrete slab had an initial tangent stiffness of 36200 MPa and a cube compressive strength of 47.7 MPa. Since VecTor2 requires the cylinder compressive strength as an input parameter, the 47.7 MPa cube compressive strength was converted to the equivalent cylinder compressive strength as per Neville (1975), and is equal to 43.4 MPa. The timber beam had a measured Young's modulus of 12085 MPa and a mean bending strength of 28 MPa as per the Eurocode. However, the authors estimated the actual failure stress to be as

high as 41.7 MPa. A summary of the input parameters is tabulated in Table 5-3. All other required inputs for timber were calculated as per Section 5.3.2 of this chapter.

A TCC beam was created in VecTor2 based on the aforementioned information and the FE model is demonstrated in Figure 5-8. Smear contact elements were used in the model because the spacing of the connectors in the full-scale specimen was consistent with that of the push-out test specimens. Although the concrete slab did not have a uniform thickness over the depth due to the decking profile, a uniform thickness was assumed in the FE model. This simplification is reasonable because the loss of concrete area may be compensated by the steel decking. In addition, the steel decking can act as confinement and add stiffness to the concrete slab. A summary of the FE model is presented in Table 5-4.

Shown in Figure 5-9 is the experimental load-deflection response versus the predicted load-deflection response; Figure 5-10 compares the predicted and the experimental load-slip curves measured at the beam end. Notice that the dotted lines included in both plots were the analytical result predicted by a 2D Abaqus model created by Persaud and Symons, 2006. Further details of the Abaqus model can be found in their original paper.

Overall, the complete load-deflection response was well captured by VecTor2, better than was done with Abaqus. A mid-span deflection of 75.6 mm and a failure load of 173.6 kN was predicted by VecTor2 while the actual mid-span deflection and the failure load were 74.9 mm and 173 kN, respectively. Moreover, VecTor2 predicted tension failure at mid-span, which was consistent with the experimental observation that the final collapse of the specimen was initiated in the region of a knot in the bottom laminates. An exaggerated deflected shape (5X magnification) of the TCC specimen is depicted in Figure 5-11. One major discrepancy between the experimental result and the VecTor2 prediction was that VecTor2 predicted concrete cracking near the mid span directly under the loading jack, whereas in the experiment, no cracking was observed. Such discrepancy may be attributed to the confining effect of the steel decking which may have prevented the concrete slab from cracking.

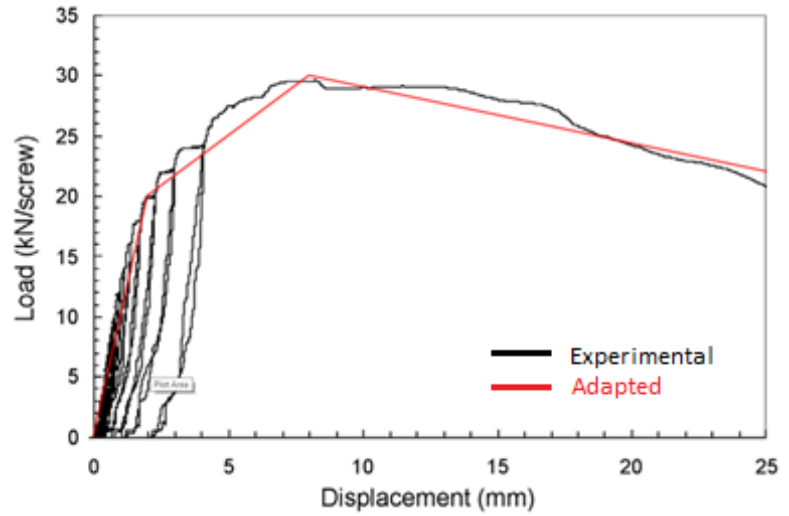


Figure 5-7 Push-out test specimen (Persaud and Symons, 2006)

Table 5-3 Input Parameters

Concrete		Timber	
f'c (MPa)	43.4	ft (MPa)	42
Ec (MPa)	36200	Et (MPa)	12085
t (mm)	2000	G (MPa)	755
		t (mm)	160

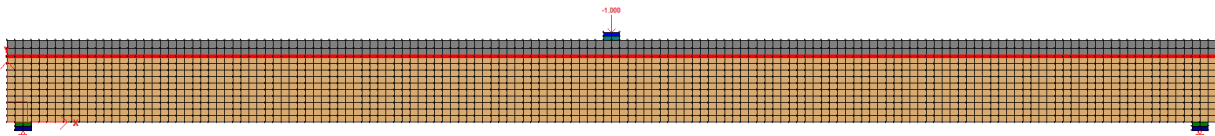


Figure 5-8 VecTor2 model

Table 5-4 Summary of the FE model

Type	Timber	Concrete	Connector
No. of Elements	1500	300	150
Mesh Size (width X height) (mm)	50 X 40	50 X 50	50 X 0

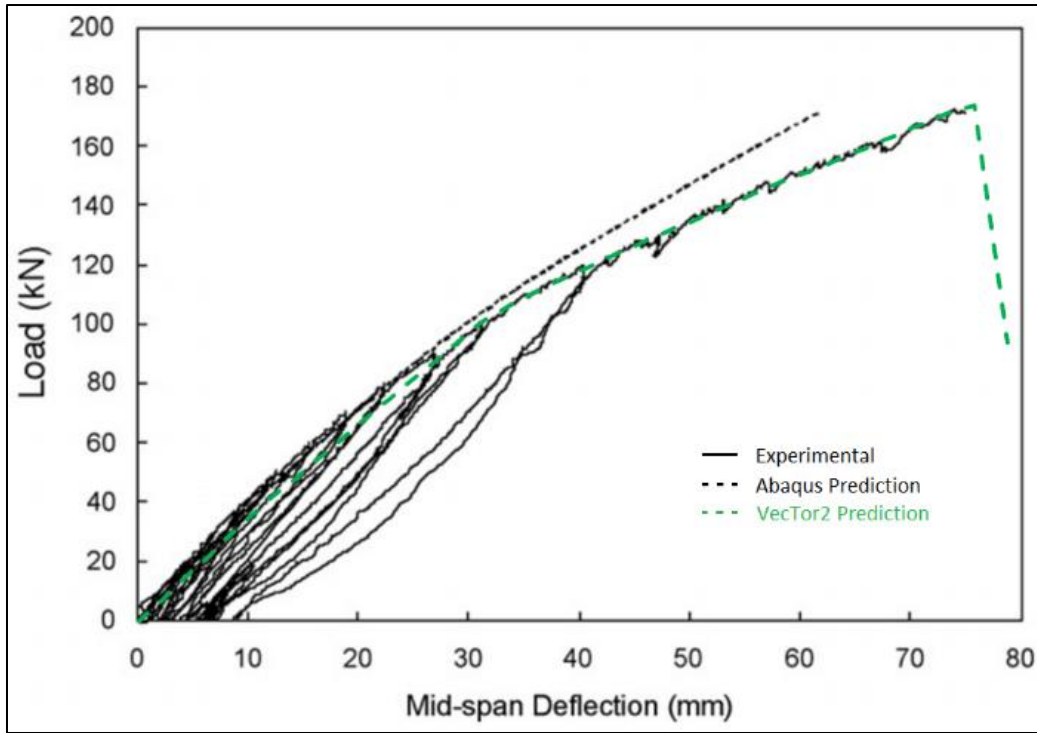


Figure 5-9 Load-deflection plot

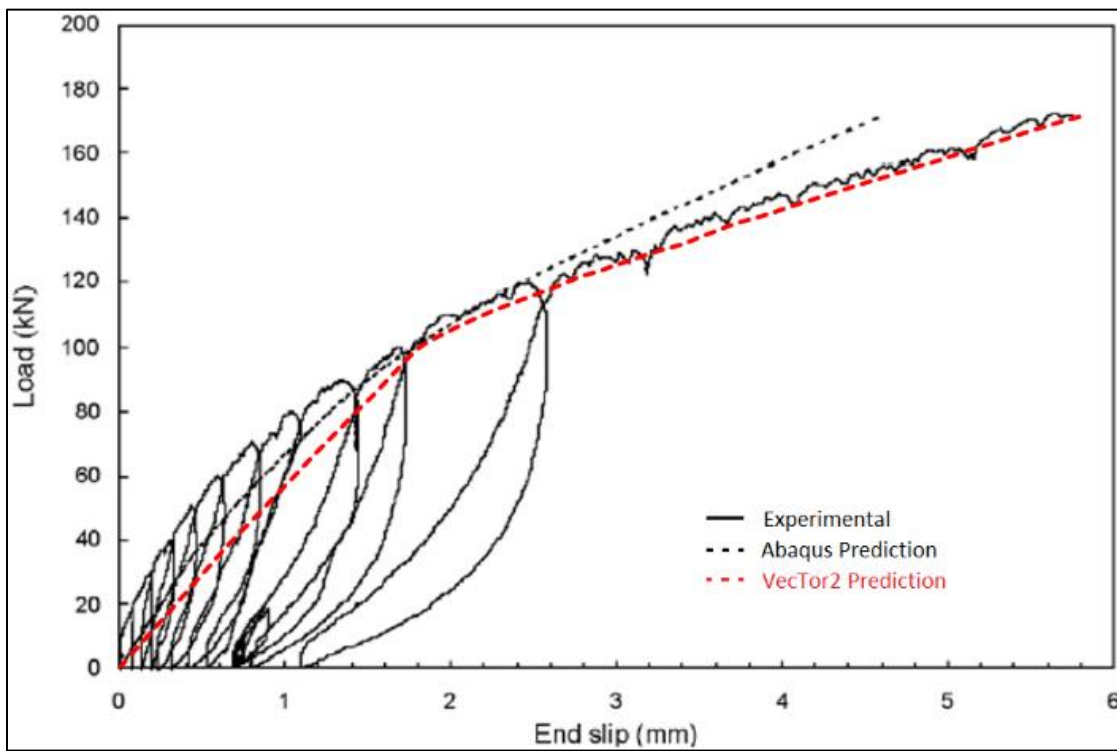


Figure 5-10 Load-slip plot

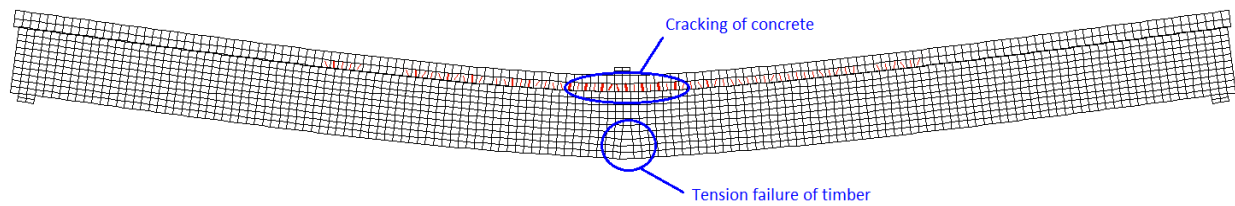


Figure 5-11 Deflected shape at collapse

5.4.2 Yeoh (2010)

Eleven full-scale timber-concrete composite beams were tested at the University of Canterbury in New Zealand by Yeoh (2010) as part of his doctoral work. These semi-prefabricated specimens, while not as easy to construct as the one tested by Persaud and Symons (2006), utilized innovative connection systems. Four connection types were used in these specimens, including metal plates pressed onto the timber beams, triangular notches, and small and large rectangular notches cut from the timber beams. These connection systems, as presented in Figure 5-12, were found to be significantly stiffer and stronger than the plain coach screw connection system. As such, a high degree of composite action can be attained with a significantly less amount of shear connectors.

All specimens were loaded in four-point bending as shown in Figure 5-13 and a summary of the 11 specimens is given in Table 5-5. Note that the values of the modulus of elasticity (MOE) and the modulus of rupture (MOR) were taken as 11300 MPa and 33.4 MPa for all specimens; The actual MOE of each specimen was not measured by the author, and the MOR was the mean as per the manufacturer's specification. An interlayer of 17 mm thick plywood was installed in specimens to act as a permanent formwork for the concrete slab. The cross sections of the bending specimens are illustrated in Figure 5-14.

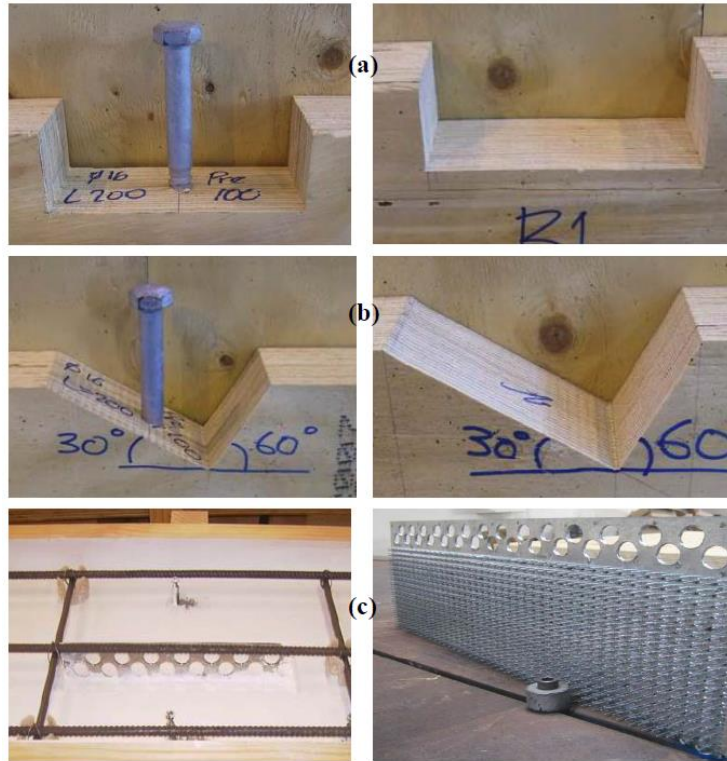


Figure 5-12 Variations of connections with and without coach screws: (a) rectangular; (b) triangular; and (c) toothed plate connection (Yeoh, 2010)

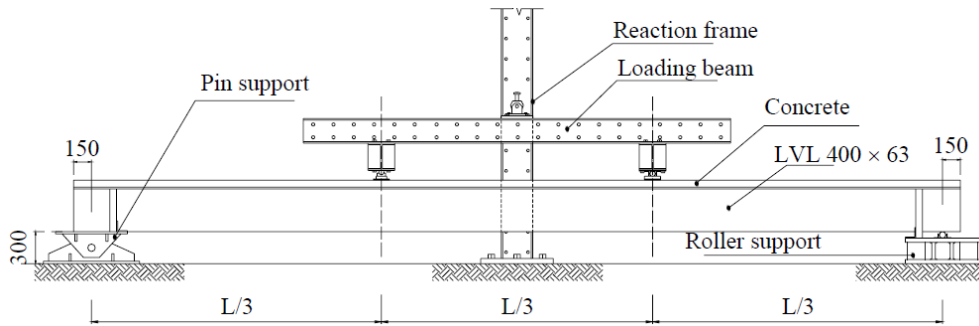


Figure 5-13 Typical four-point bending test setup (dimensions in mm) (Yeoh, 2010)

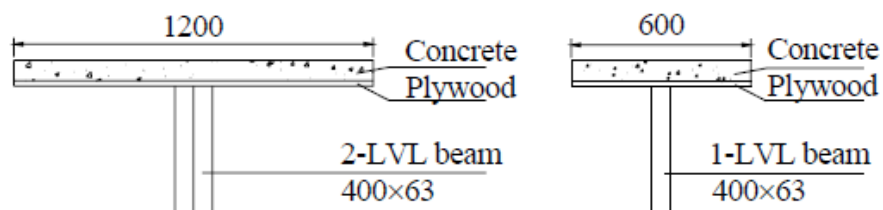


Figure 5-14 Typical cross sections of the bending specimens (Yeoh, 2010)

Table 5-5 Summary of the Yeoh specimens

Beam ID	Span (m)	Dimensions (mm)		Connection		Material Properties		
		Concrete	Timber	No.	Type	f'c (MPa)	MOE (MPa)	MOR (MPa)
A1	8.0	600x65	400x63	6	R150	58.0	11300	33.4
A2	8.0	600x65	400x63	6	R150	58.0	11300	33.4
B1	8.0	600x65	400x63	10	R150	58.0	11300	33.4
B2	8.0	600x65	400x63	10	R150	38.8	11300	33.4
C1	8.0	600x65	400x63	10	T	54.4	11300	33.4
C2	8.0	600x65	400x63	10	T	58.0	11300	33.4
D1	8.0	600x65	400x63	6	R300	54.4	11300	33.4
E1	10.0	600x65	400x63	6	R300	48.2	11300	33.4
E2	10.0	600x65	400x63	6	R300	31.0	11300	33.4
F1	8.0	1200x65	400x126	8	P	54.4	11300	33.4
G1	8.0	1200x65	400x126	10	R150	48.2	11300	33.4

Note: R150 denotes 150 mm rectangular notch connection
R300 denotes 300 mm rectangular notch connection
T denotes triangular notch connection
P denotes toothed plate connection

All the push-out specimens consisted of two shear connectors, one on each side. As such, discrete contact elements were used to model the shear connectors. Figure 5-15 depicts the FE model created for Specimens A1 and A2, with only half of the specimen modelled due to symmetry and the fine mesh. Note that the locations and the dimensions of the contact elements were consistent with the actual specimens. The adopted load-slip relationships for the four connection systems are presented in Figure 5-16.

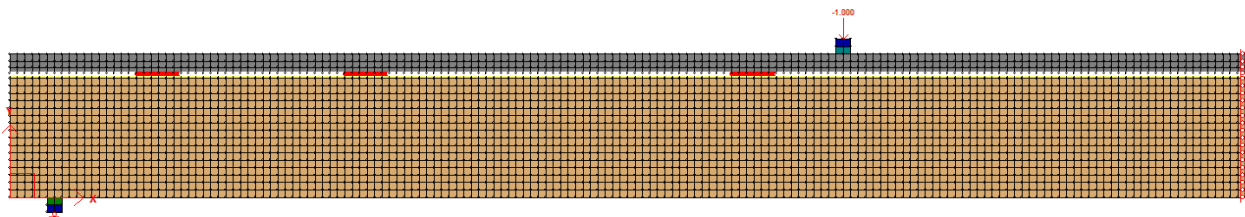
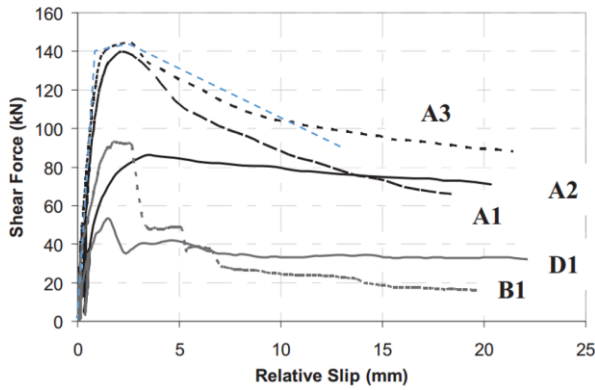
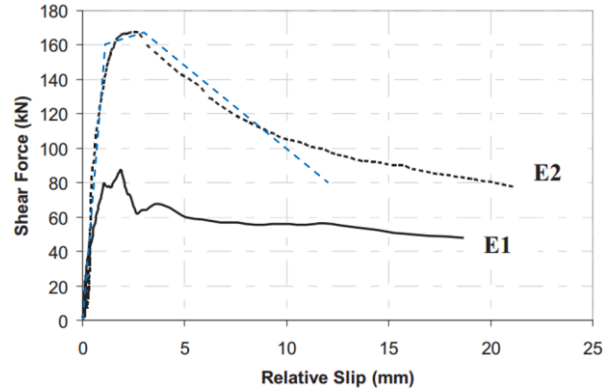


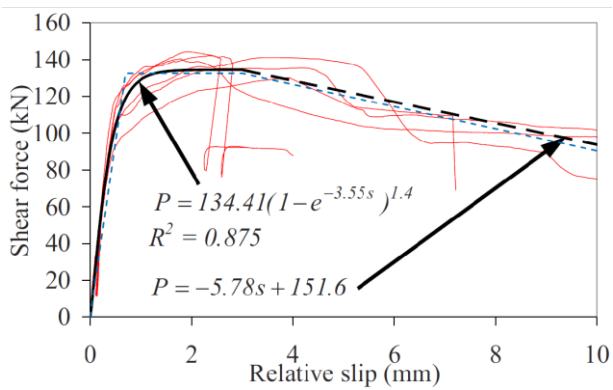
Figure 5-15 FE model for specimens A1 and A2



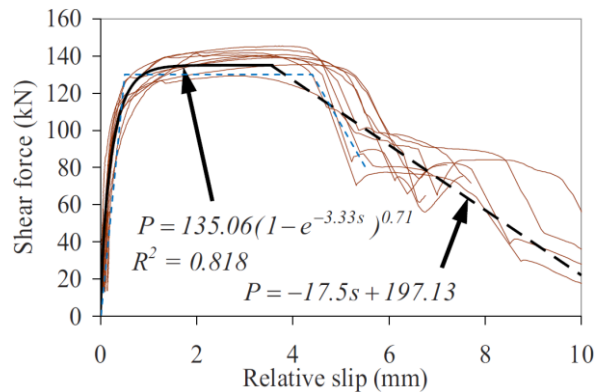
(a) R150



(b) T



(c) R300



(d) P

Figure 5-16 Load-slip curves (Yeoh, 2010)

A summary of the numerical results is presented in Table 5-6; the experimental load-deflection responses versus the predicted load-deflection responses are shown in Figure 5-17. In general, the experimental load-deflection curves and the failure loads were reasonably well predicted by VecTor2. Note that Specimen D1 was not loaded to complete destruction. Specimens B1, C1, C2, E1, and F1 experienced brittle tension failure while progressive tension failure was found in specimen G1. The failure modes of the rest of the specimens were not found in the literature. Some degree of post-peak strength recovery was observed in specimens B2 and F1 which was not properly captured by VecTor2.

The stiffness of specimens B1, B2, E1, and E2 were underpredicted by VecTor2. As a natural material, wood properties varies considerably. Consequently, the source of error could be solely

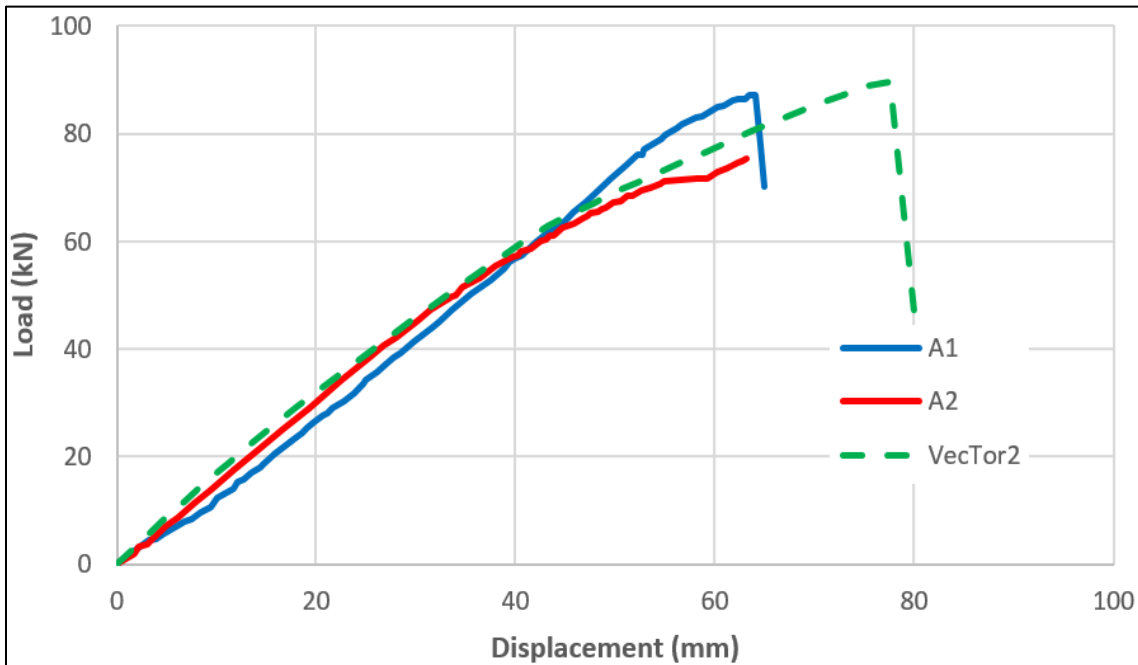
from the natural variability of modulus of elasticity of wood, which was assumed to be identical across all specimens.

It shall be pointed out that the predicted stiffness of Specimen F1 deviated from the experimental result at large loads. In this case, the spacing effect of the shear connectors could be ultimately responsible for the deviation. Shown in Figure 5-18 is the arrangement of the shear connectors of Specimen F1, and it is evident that the shear connectors were closely spaced near the support. Ceccotti et al. (2006) tested two push-out test specimens with variable spacing and found clear distinction between the corresponding load-slip curves. Depicted in Figure 5-19 are the specimen details together with the experimental results as reported by Cecotti et al. (2006).

Specimen G1, contrary to the brittle tension failure predicted by VecTor2, exhibited substantial post-peak displacement. No signs of connector failure were observed experimentally and the unusual plateau resulted from the progressive tension failure in the timber beam.

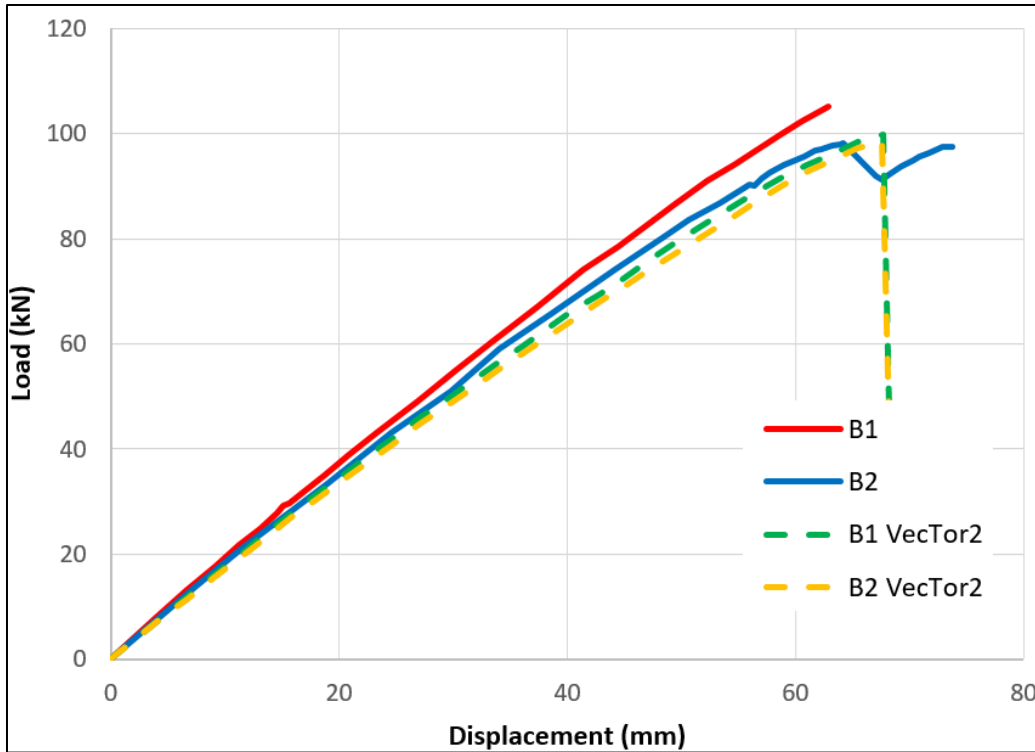
Table 5-6 Summary of results

Beam ID	Experimental		VecTor2		Comparison	
	Pu (kN)	Disp. (mm)	Pu (kN)	Disp. (mm)	Pu(exp.)/Pu(VT2)	Disp.(exp.)/Disp.(VT2)
A1	87.5	63.9	89.6	77.5	0.98	0.82
A2	75.1	63.0	89.6	77.5	0.84	0.81
B1	104.9	63.0	99.8	67.7	1.05	0.93
B2	98.1	63.6	98.4	67.6	1.00	0.94
C1	89.7	58.2	101.8	65.4	0.88	0.89
C2	109.7	66.8	101.8	65.4	1.08	1.02
E1	79.4	92.2	80.4	96.2	0.99	0.96
E2	55.9	66.4	79.0	96.9	0.71	0.69
F1	175.0	89.8	176.4	76.8	0.99	1.17
G1	201.1	69.2	199.2	67.6	1.01	1.02
Average					0.95	0.93
Stand. Deviation					0.11	0.13
Coeff. Variation					12%	14%

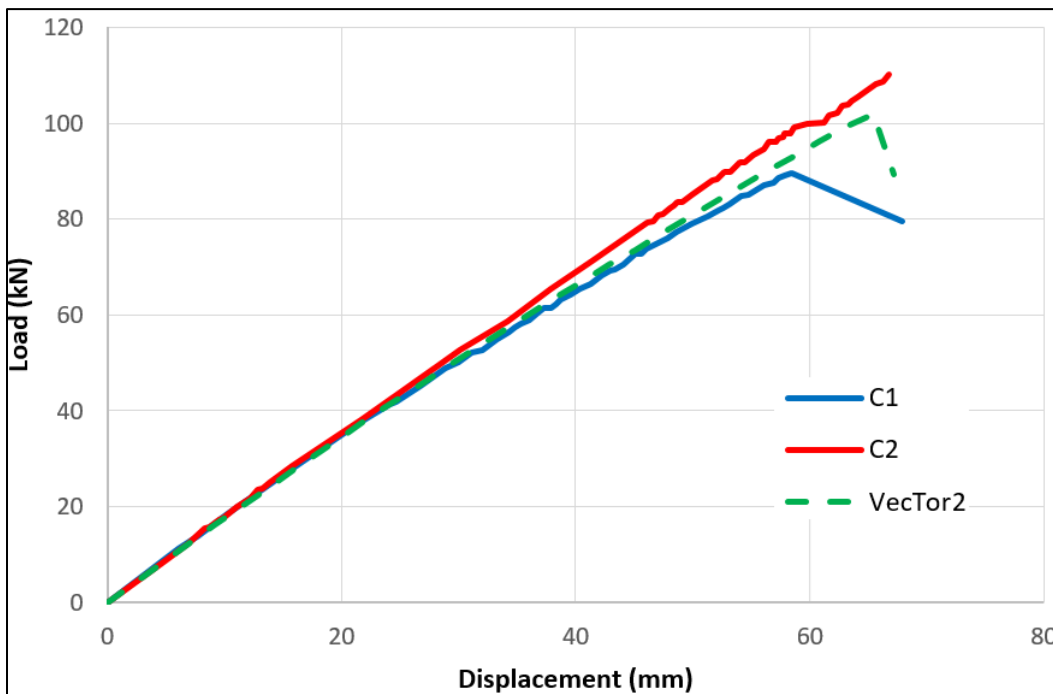


(a) Specimen A1 and A2

Figure 5-17 Load-deflection plots

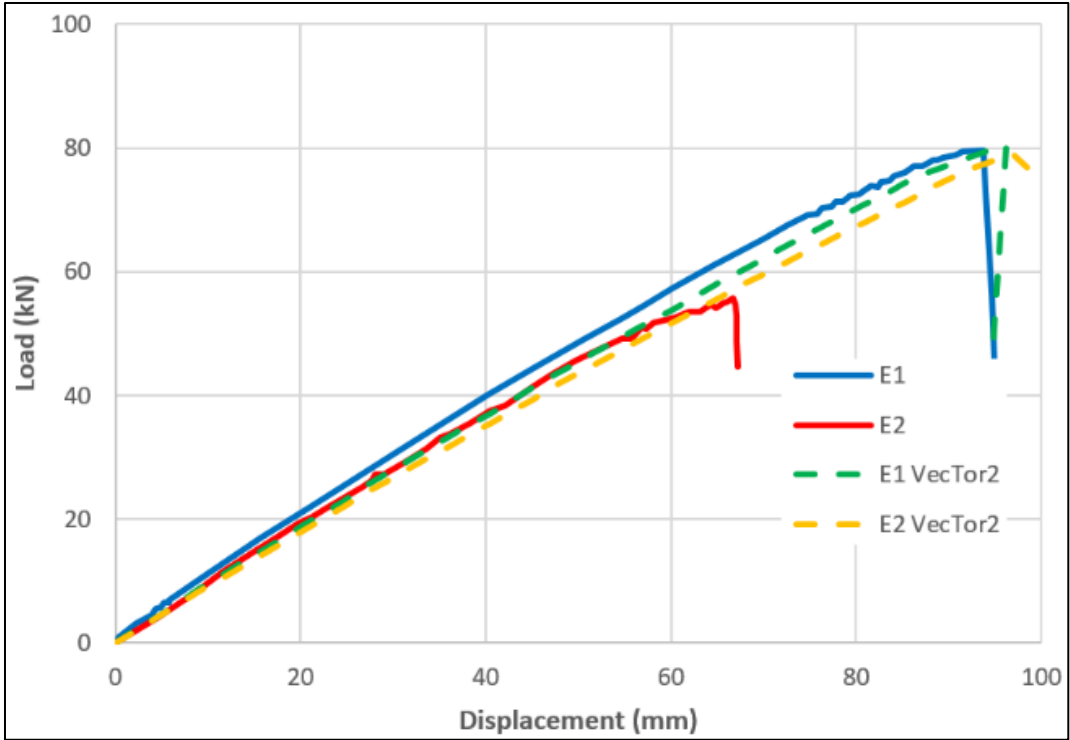


(b) Specimen B1 and B2

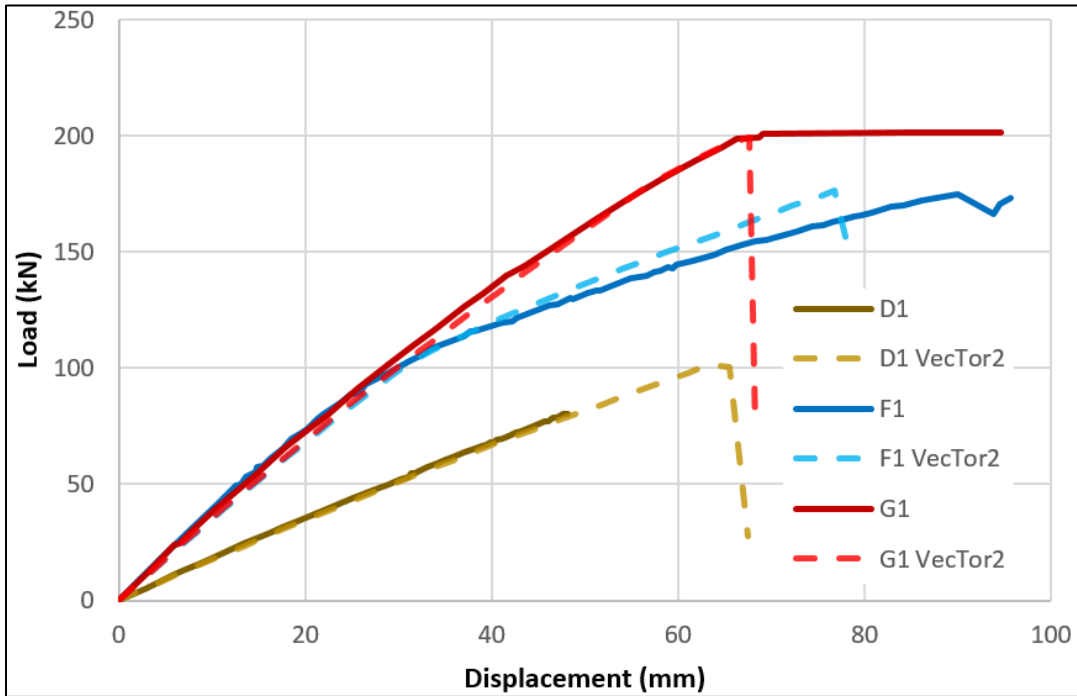


(c) Specimen C1 and C2

Figure 5-17 Load-deflection plots (continued)



(d) Specimen E1 and E2



(e) Specimen D1, F1, and G1

Figure 5-17 Load-deflection plots (continued)

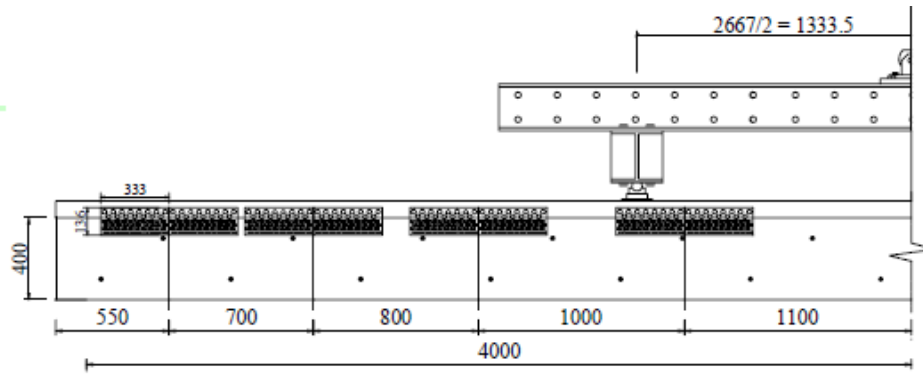


Figure 5-18 Arrangement of Specimen F1 (Yeoh, 2010)

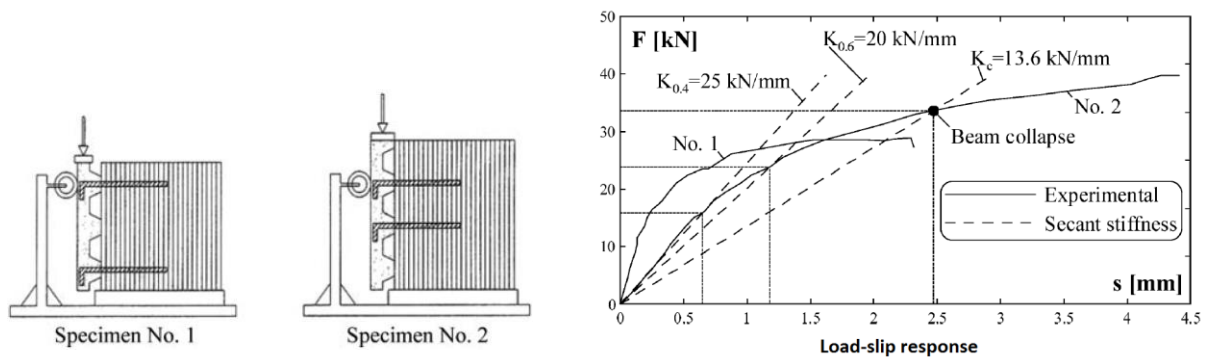


Figure 5-19 Specimen details and result (Cecotti et al., 2006)

5.4.3 Deam et al. (2008)

Another series of specimens tested at the University of Canterbury was selected for the verification studies. A summary of the four full-scale specimens is given in Table 5-7. The distinguishing characteristics of this series is that Specimens CS3 and CS4 were prestressed with low relaxation 7-wire stranded tendons.

Table 5-7 Characteristics of specimens

Specimen ID	No. of LVL Beams	Connection System	Concrete Weight	Prestressing Tendon
CS1	1	24 notches with screws	Normal	None
CS2	1	End bearing bolted saddles	Light	None
CS3	2	48 notches with screws	Normal	Straight
CS4	2	24 lag screws	Normal	Draped

No analysis was performed for Specimen CS2 since there was no push-out test performed for the novel connection system. While it is theoretically possible to model the draped tendon profile in Specimen CS4, it is currently impractical to do so because the current version of auto-meshing functionality of VecTor2 is not applicable to timber-concrete composite structures. In order to capture the draped tendon profile, a series of nodes must be created in line with the tendon profile and the bounded elements must be either triangular or quadrilateral. As such, Specimen CS4 was also excluded from the analysis.

Shown in Figure 5-20 are the cross sections of specimens CS1 and CS3. The specimens were all subjected to four-point bending as depicted in Figure 5-21. The modulus of elasticity (MOE) of timber was measured to be 12100 MPa while the modulus of rupture (MOR) was 42 MPa as per the manufacturer's design guideline. The mean cylinder compressive strength and Young's modulus of concrete were measured to be 37.9 MPa and 30100 MPa.

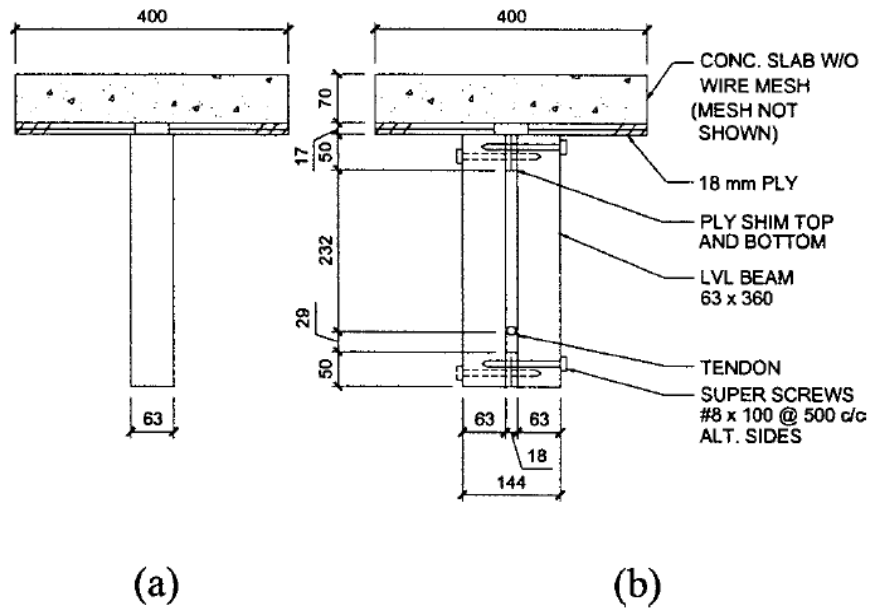


Figure 5-20 Cross sections of (a) CS1 and (b) CS3 (Deam et al., 2008)

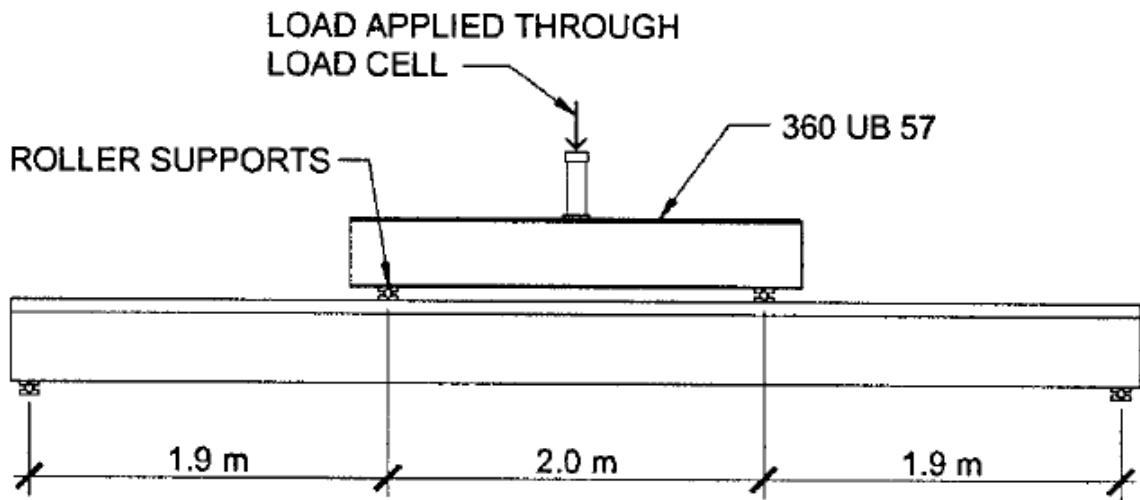


Figure 5-21 Test setup (Deam et al., 2008)

The plan view of the connector layout of Specimen CS3 is shown in Figure 5-22. The connector spacing for Specimen CS1 was similar to that for Specimen CS3. It should be pointed out that the push-out test specimens were constructed with timber of 105 mm thickness, whereas 63 mm thick timber beam was used in the full-scale specimens. Consequently, the load-slip curve needs to be adjusted to reflect the change in notch thickness, which, in this case, is dictated by

the thickness of timber. A simple linear adjustment was made to the load-slip curve based on the ratio of notch thickness. That is, the stiffness and strength of the shear connectors were scaled down linearly by a factor of 0.6 ($0.6 = 63/105$). This adjustment, while it may not be accurate, represents a reasonable estimate. The adopted and the adjusted load-slip relationships for the shear connectors are presented in Figure 5-23.

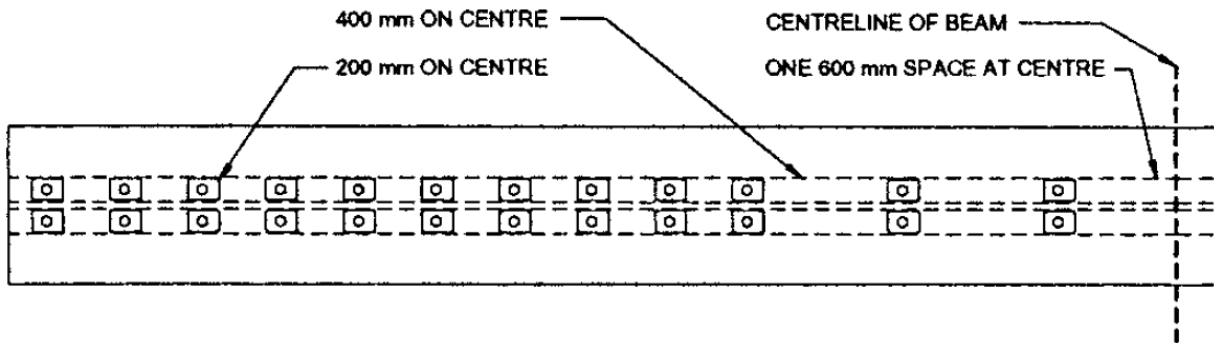


Figure 5-22 Connector layout for Specimen CS3 (Deam et al., 2008)

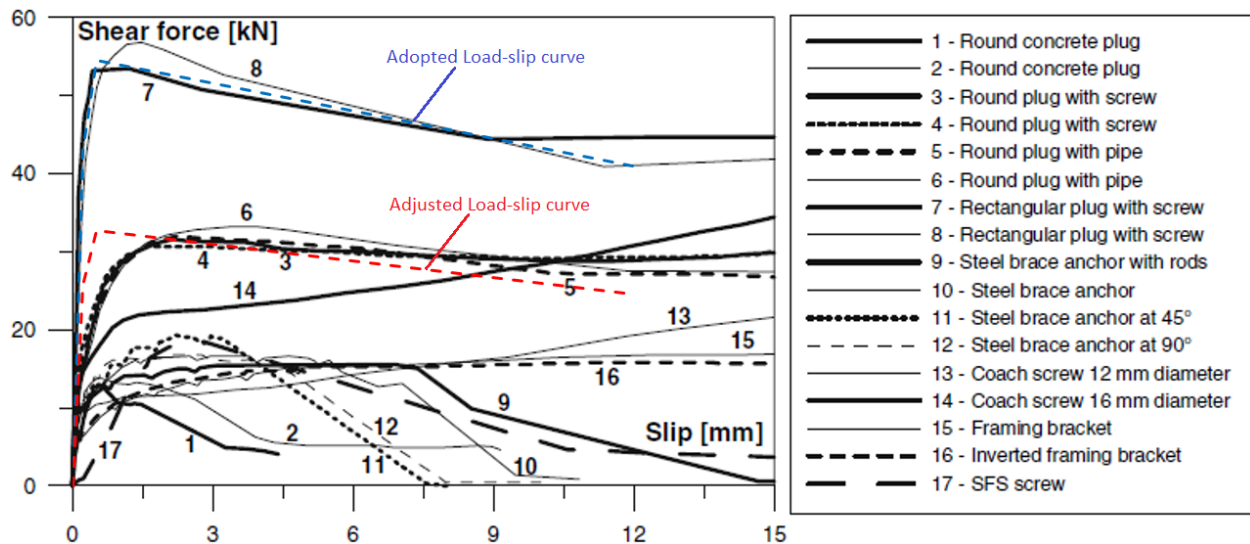


Figure 5-23 Adopted and adjusted load-slip curve (Deam et al., 2008)

Shown in Figure 5-24 is the FE model created for Specimen CS3. The locations and the lengths of the contacts were consistent with the actual specimen. Contact elements were used to reflect the bonding condition between the tendon and the timber beam as presented in Figure 5-25. Since the tendon was not grouted, the built-in contact element specifically for unbonded bars or tendons was applied between the two ends.

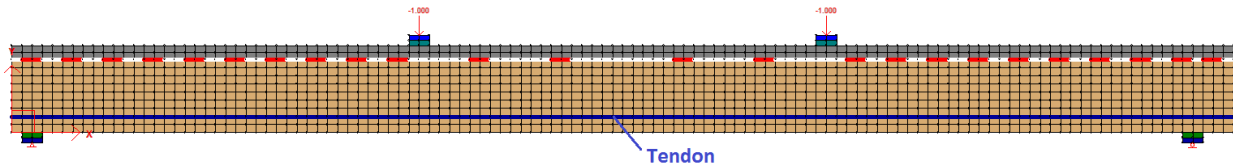


Figure 5-24 FE model for Specimen CS3

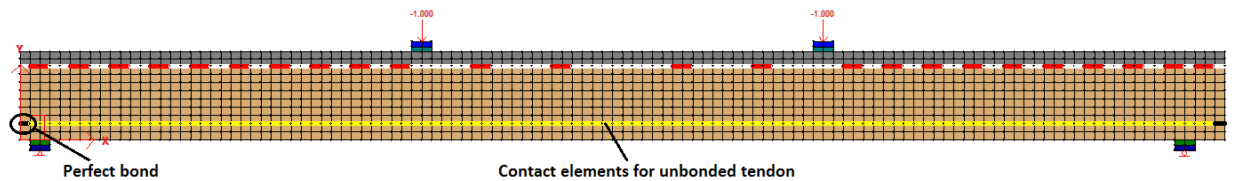


Figure 5-25 Definition of bond between tendon and timber

Shown in Figure 5-26 are the experimental load-deflection response versus the predicted load-deflection responses. For Specimen CS1, yielding of the shear connectors was overpredicted while the post-yielding stiffness was underpredicted. The accuracy of the predicted response may have been improved if the load-slip curve corresponding to the actual notch size was available. Nevertheless, the overall load-deflection response was captured with sufficient accuracy.

The final collapse of Specimen CS1 was caused as by rupturing of the timber beam in the constant moment region. The corresponding tensile stress at failure load was around 60 MPa which was about 43 % higher than the value prescribed by the manufacturer's specification.

Specimen CS3 was not loaded to complete destruction to avoid the potential danger of tendon failure. As can be observed, the added tendon had negligible influence on the global stiffness.

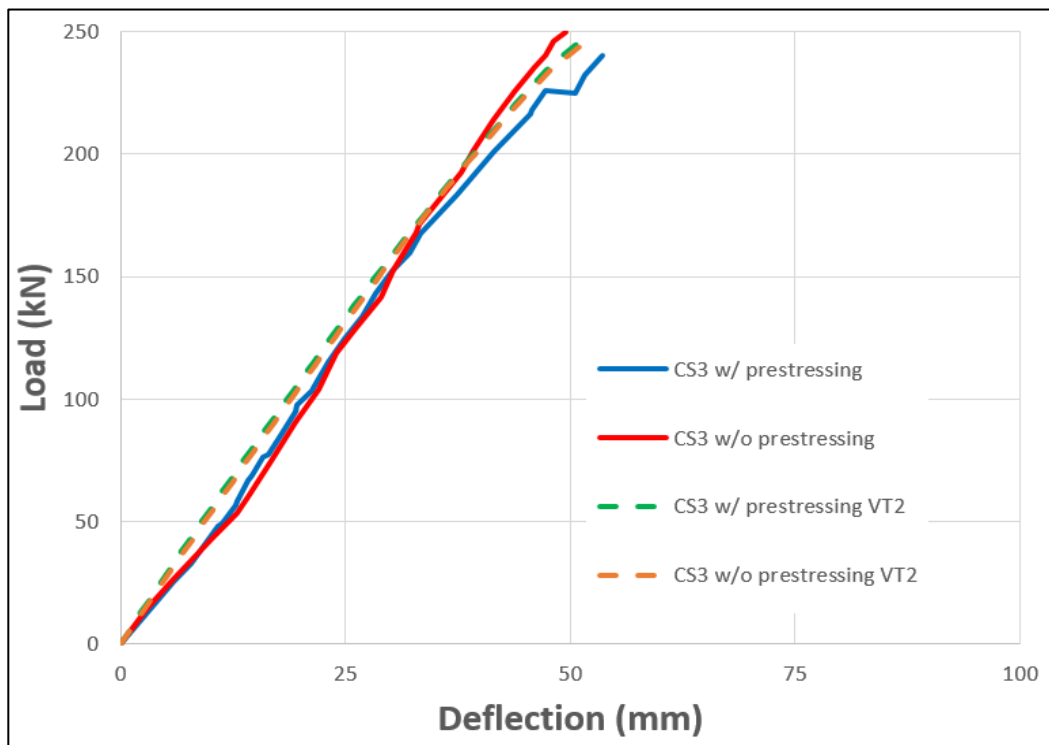
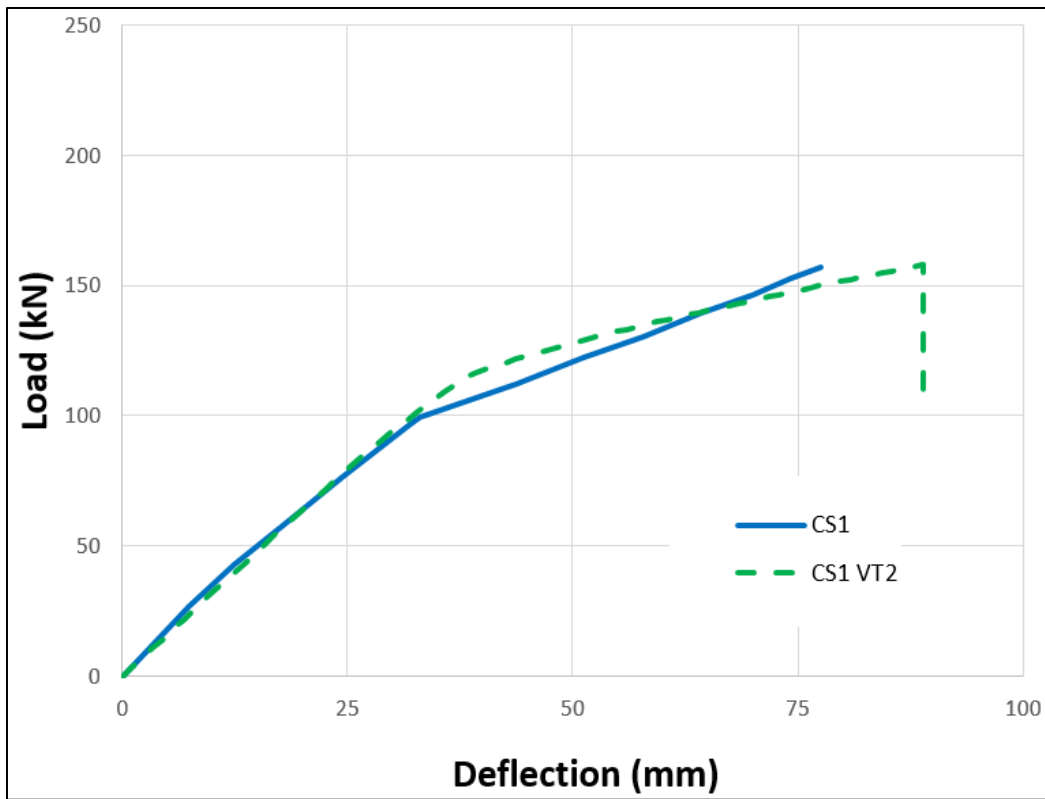


Figure 5-26 Load-deflection plots for Specimen CS1 and CS3

5.4.4 Gerber (2016)

Eighteen timber-concrete composite panels were tested at the University of British Columbia. These panels, unlike typical TCC beams, had uniform thickness over the depth. Nevertheless, the observed load-deflection behaviour of this series agreed fairly well with that of the TCC beams investigated previously.

All the specimens were modelled with the same approach described in the previous three experiment series (Section 5.4.1 through Section 5.4.3). Therefore, exhaustive modelling details are omitted for this series. A summary of the specimen characteristics and the timber specifications is given in Table 5-8 and Table 5-9, respectively. Additional details regarding configuration of shear connectors and layout of shear connectors can be found in the original literature. All specimens were loaded as per the experimental setup presented in Figure 5-27.

Table 5-8 Specimen characteristics

Series	Material	No. Specimens	Specimen Thickness (mm)	Specimen Length (mm)	Depth Concrete (mm)	Depth timber (mm)	Depth Interlayer (mm)
S1	LSL	2	610	6096	70	89	NA
S2	LVL	2	610	6096	70	89	NA
S3	CLT	2	600	6000	70	99	NA
S4	LSL	2	610	6096	70	89	25
S5	LVL	2	610	6096	70	89	NA
S6	LSL	2	610	6096	70	89	NA
S7	LVL	2	610	6096	70	89	NA
S8	CLT	2	600	6000	70	99	NA
S9	LVL	2	610	6096	70	89	25

Table 5-9 Timber specification

Material	Tensile Strength (MPa)	Young's Modulus (MPa)
LSL	33.3	10685
LVL	37.6	13790
CLT	11.8	9500

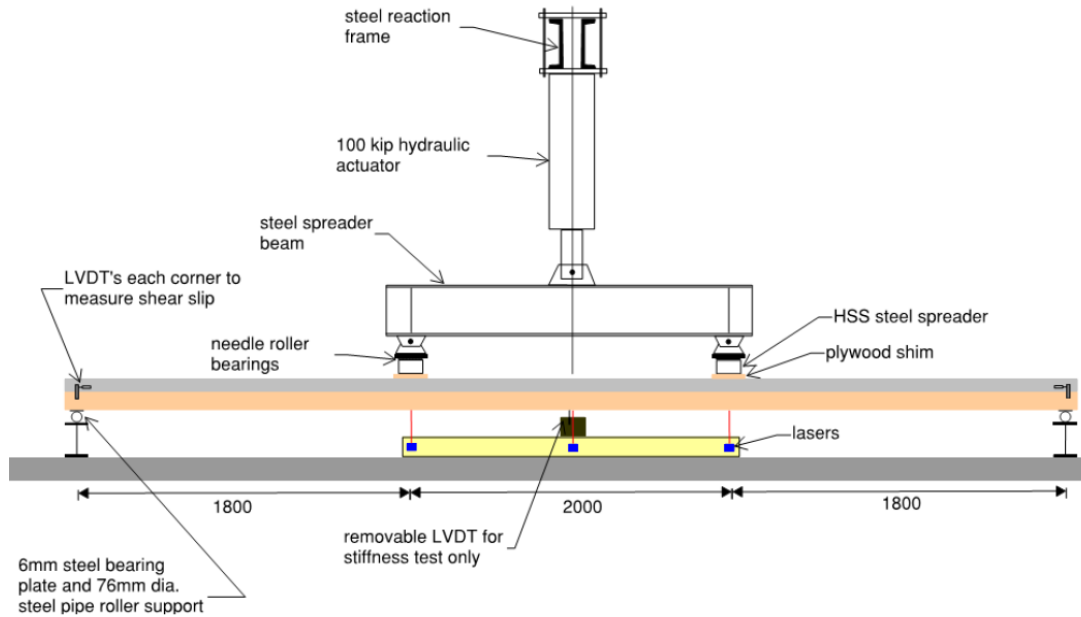


Figure 5-27 Experimental setup for Gerber Specimen

Particular attention was given to the modelling details of the four panels constructed with cross-laminated timber (CLT). Typically, CLT consists of an odd number of layers of timber boards stacked together in alternating directions; the direction with one extra layer of timber board is hereafter referred to as the primary direction whereas the orthogonal direction is denoted as the secondary direction. The intent of CLT is to have an improved stiffness in the secondary direction at a cost of a reduced stiffness in the primary direction. Consequently, it may be inappropriate to model CLT as a whole; the alternating layers must be reflected in the corresponding FE model.

Shown in Figure 5-28 is the FE model created for Series 2 with the sandwiched layer highlighted in yellow. The Young's modulus parallel to the grain was interchanged with the Young's modulus perpendicular to grain. While the sandwiched layer alone has a considerably reduced strength in the primary direction, one must not neglect the influence of the outer layers, which can act as confinement to the sandwiched layer. Currently it is impossible to quantify the influence of the clamping force exerted on the sandwiched layer. Therefore, all other mechanical properties were assumed to remain unchanged.

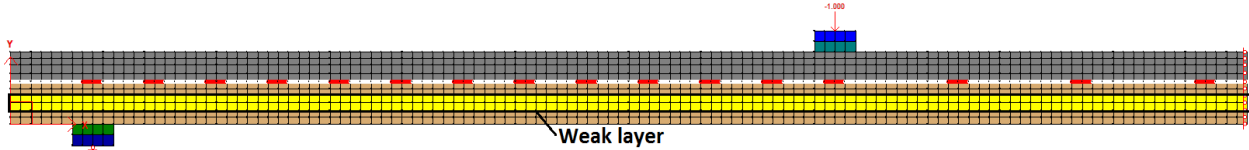
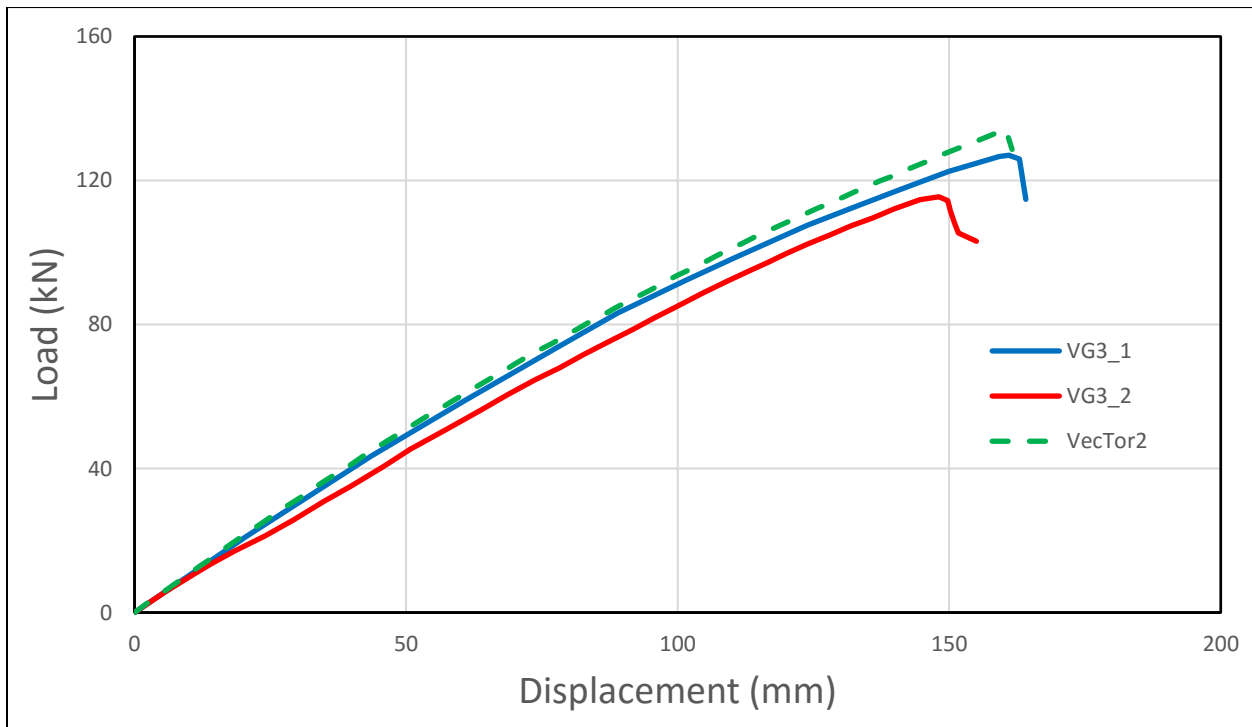


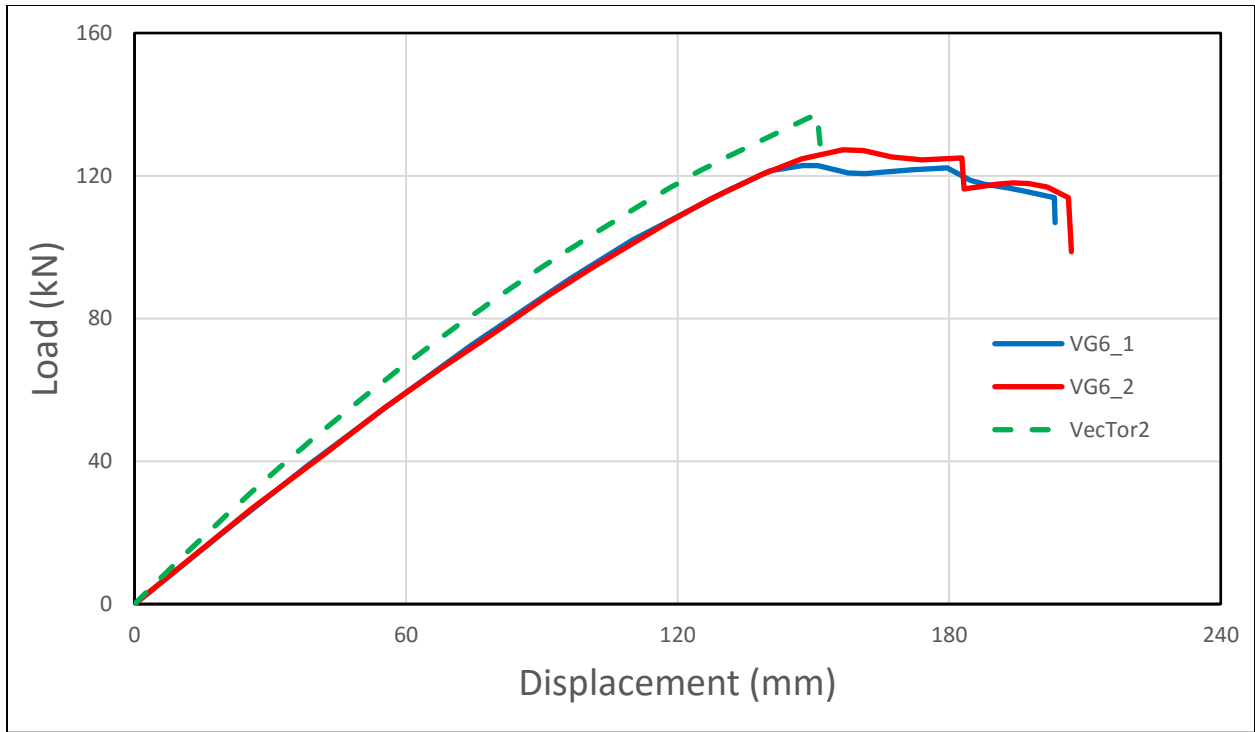
Figure 5-28 FE model for Series 2

The experimental load-deflection responses versus the predicted load-deflection responses are shown in Figure 5-29. In general, the predicted stiffness agrees reasonably well with the experimental results. The worst predicted case was Series 2 in which the stiffness was over-predicted by a margin of 15%. Such a discrepancy was likely caused by the inconsistency between the actual modulus of elasticity and the mean modulus of elasticity as suggested by the manufacturer.

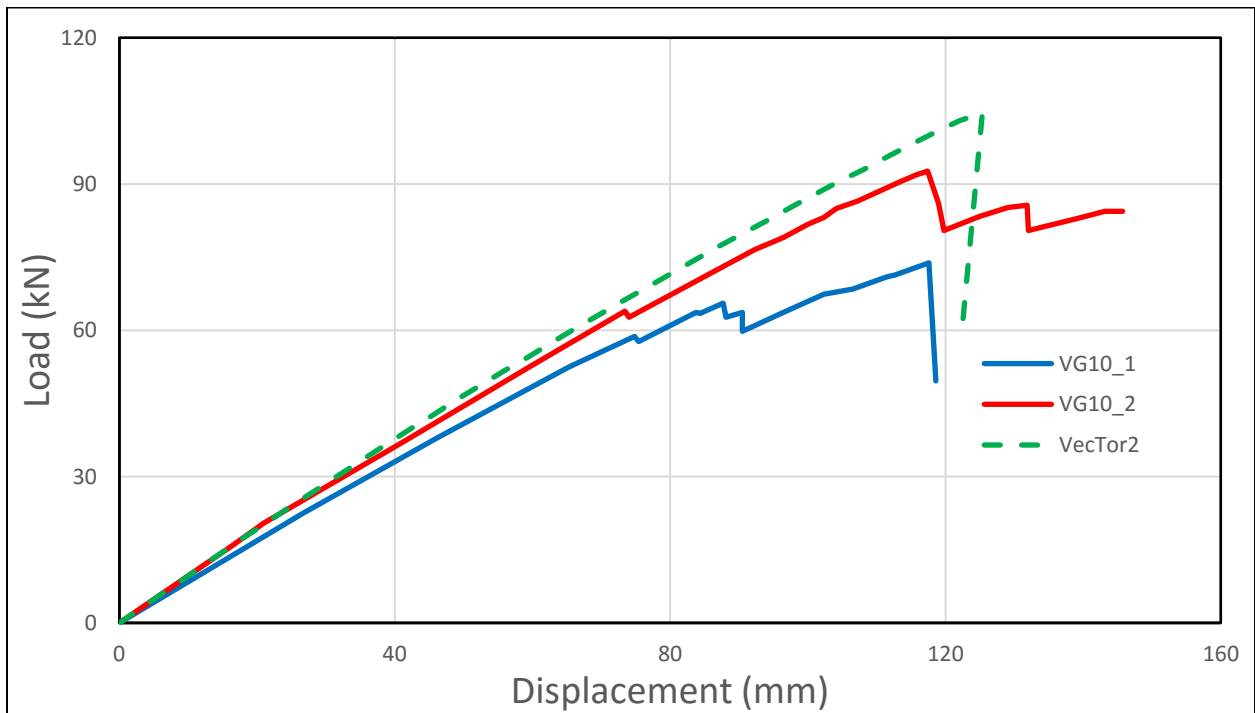


(a) Specimen S1

Figure 5-29 Load-deflection plots

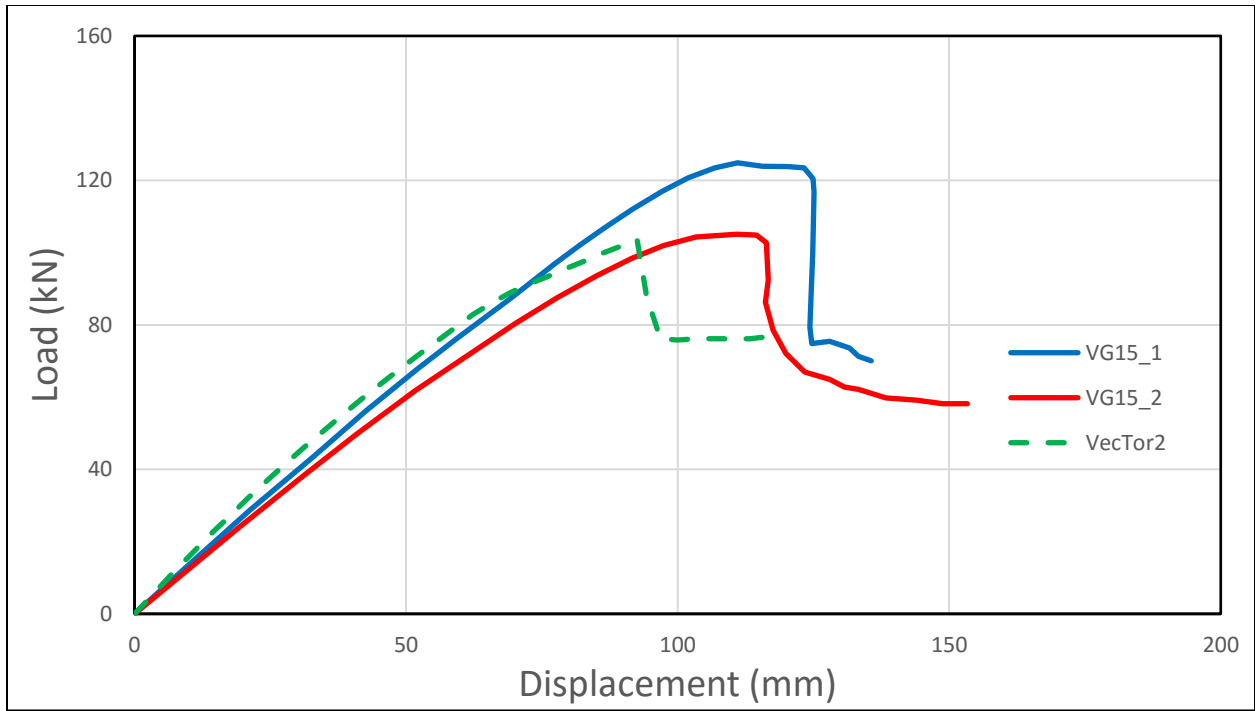


(b) Specimen S2

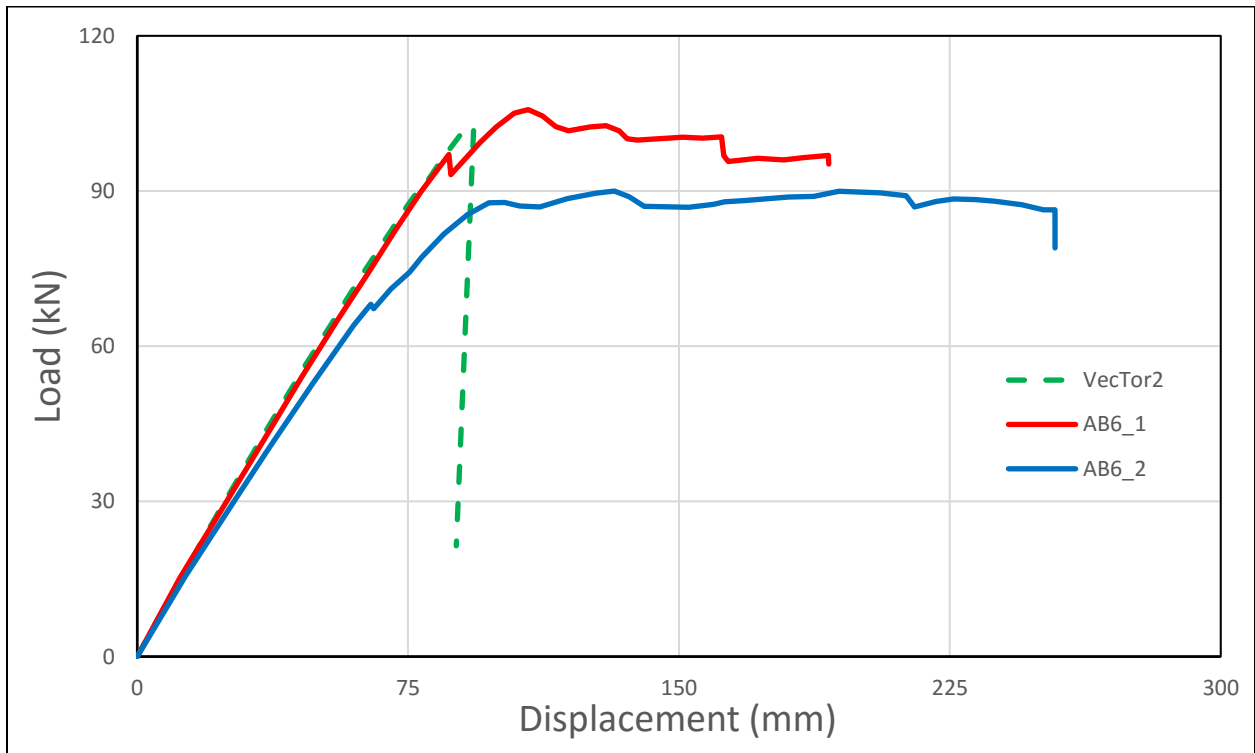


(c) Specimen S3

Figure 5-29 Load-deflection plots (continued)

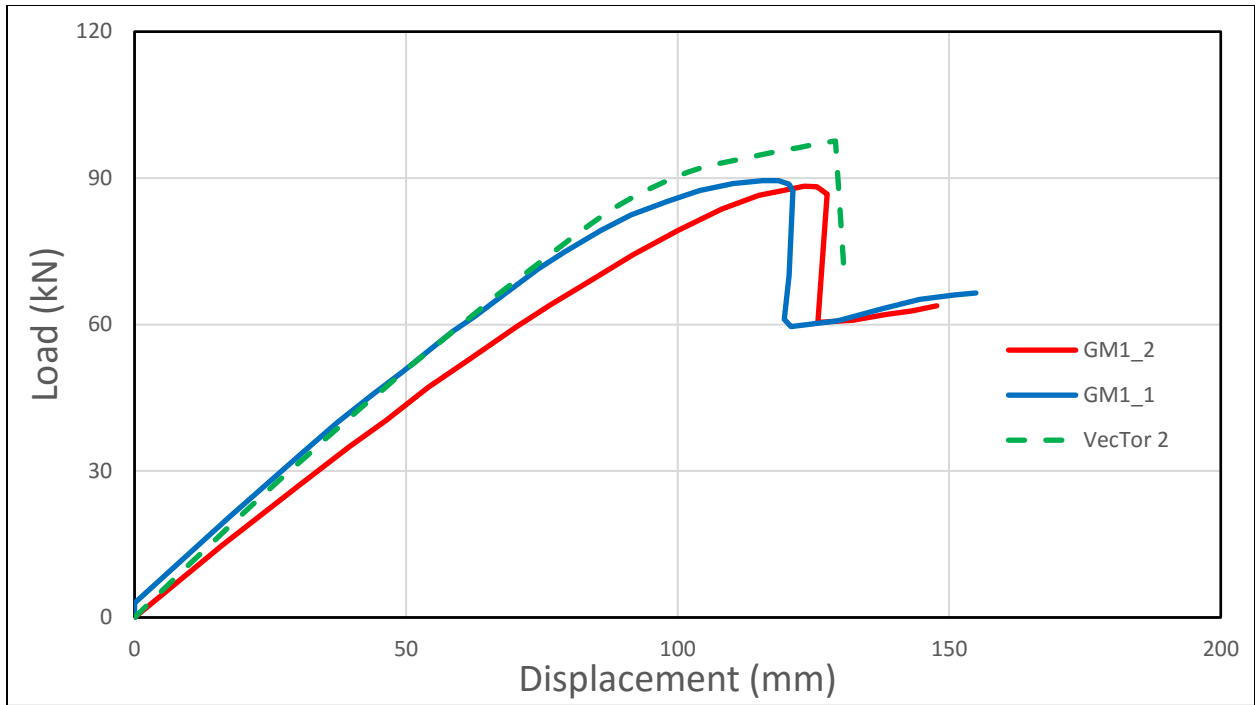


(d) Specimen S4

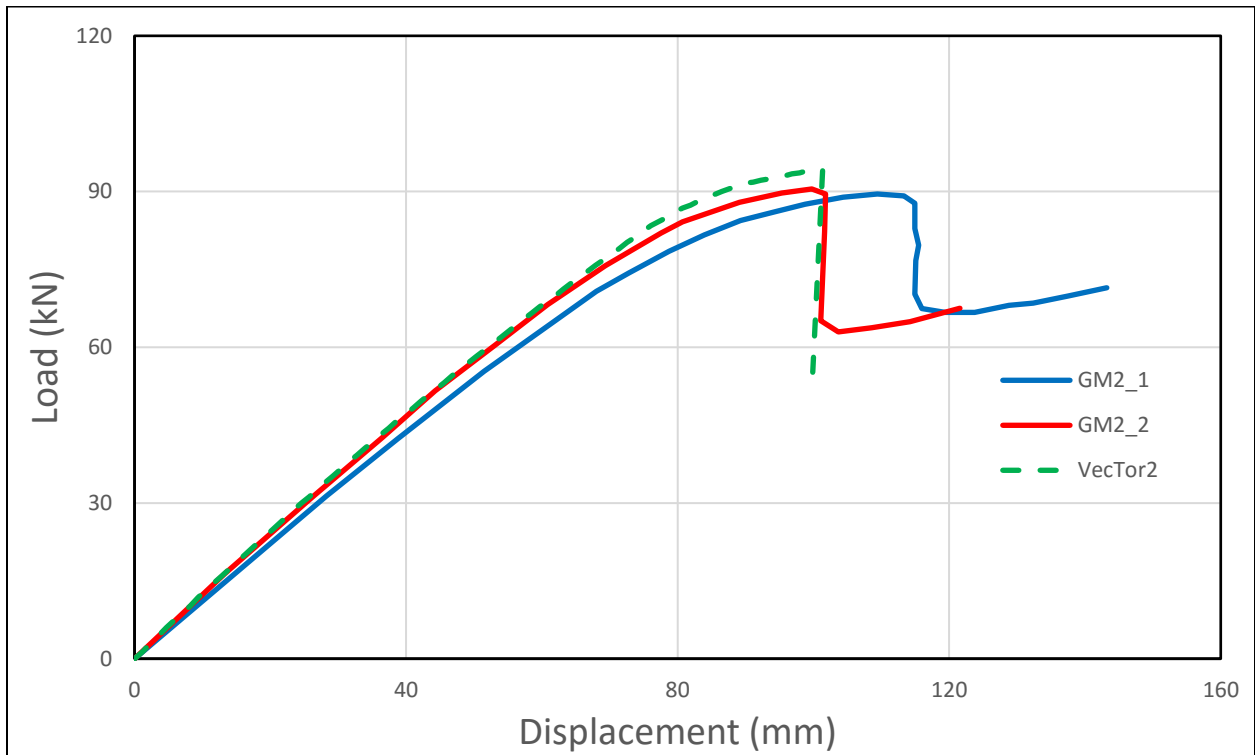


(e) Specimen S5

Figure 5-29 Load-deflection plots (continued)

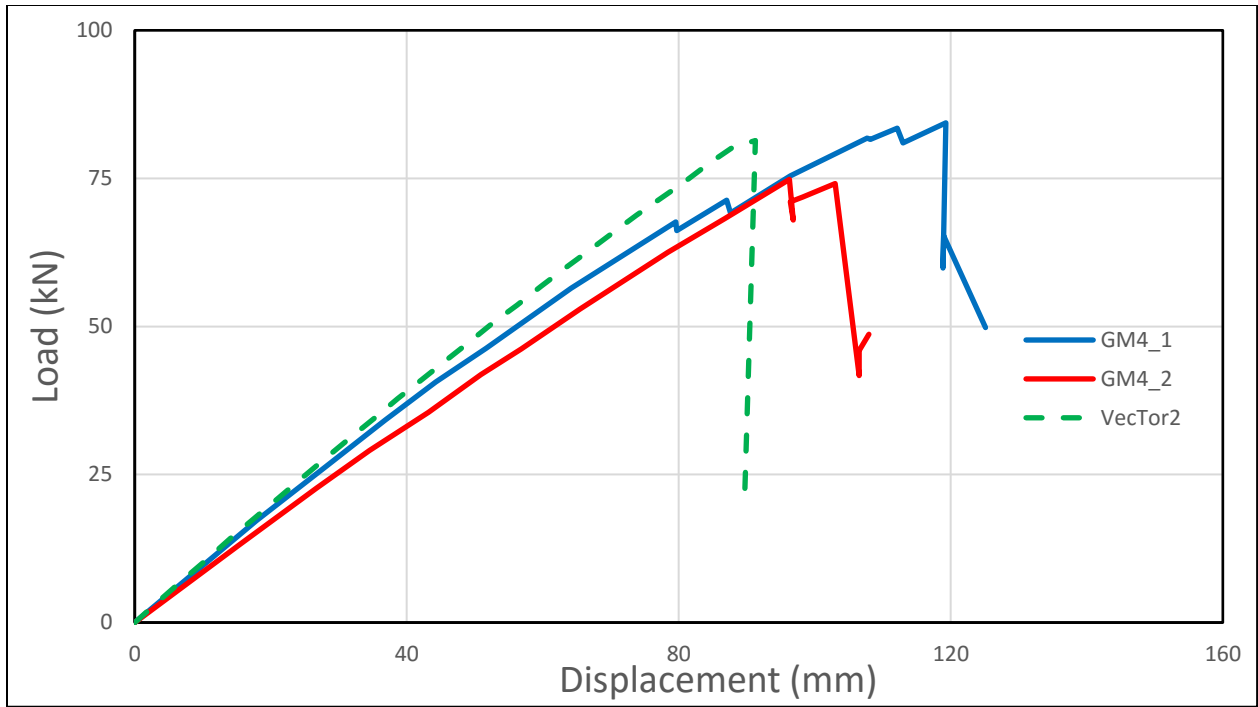


(f) Specimen S6

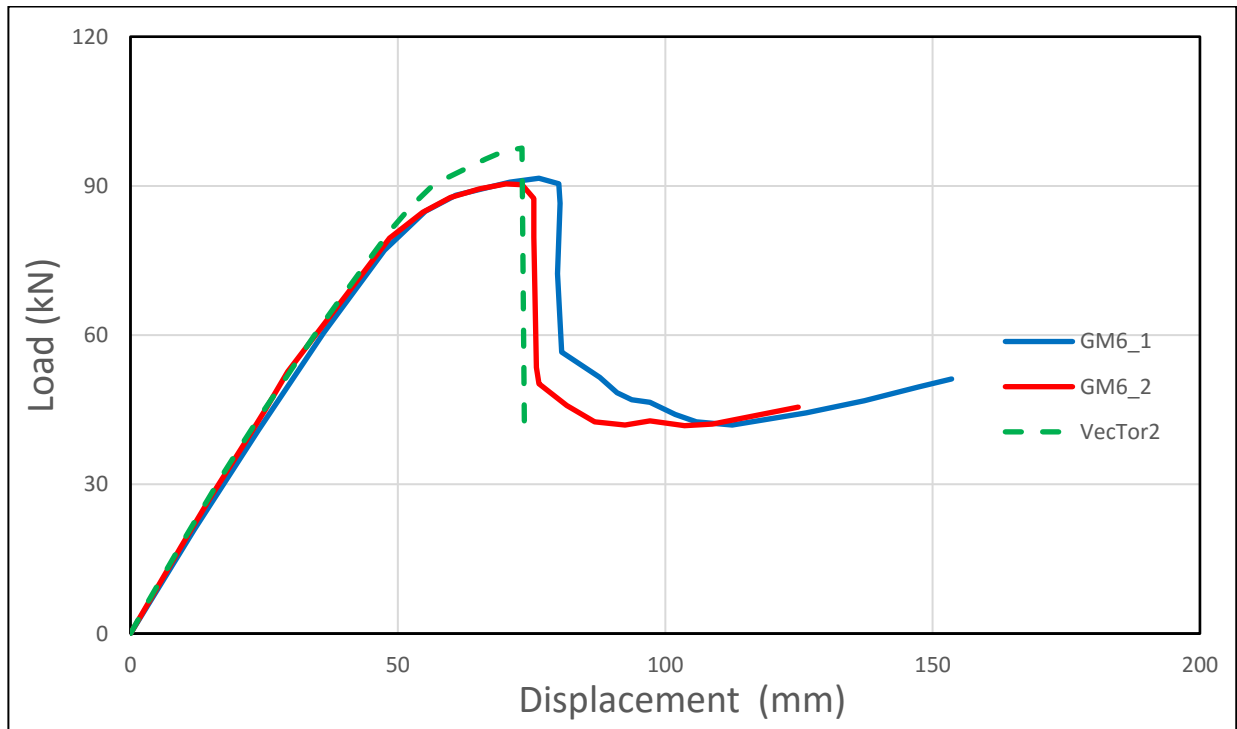


(g) Specimen S7

Figure 5-29 Load-deflection plots (continued)



(h) Specimen S8



(i) Specimen S9

Figure 5-29 Load-deflection plots (continued)

While the initial stiffness of the CLT specimens was well predicted by VecTor2, the stiffness at large loads was overpredicted by 9% on average. This may be attributed to the weaker sandwiched layer. According to the literature, it is common practice by the industry to use timber boards of lower grade as the inner layers of CLT. Rolling shear failure, a common type of failure found in CLT, may also contribute to the deviation in stiffness. As a result of the non-uniform distribution of glue strength, this type of failure typically occurs at locations where the shear stress demand exceeds the local glue strength. At the onset of rolling shear failure, the applied shear stress must be redistributed to the adjacent glue, causing a reduction in the global stiffness. Moreover, since the specimens were loaded under displacement control, the stress redistribution also gave rise to a series of sudden drops in force observed in the global load-deflection curves as highlighted in Figure 5-30. Ultimately, rolling shear failure is characterized as a local type failure; as long as the stress can find a way to redistribute, the global ultimate failure will not be triggered.

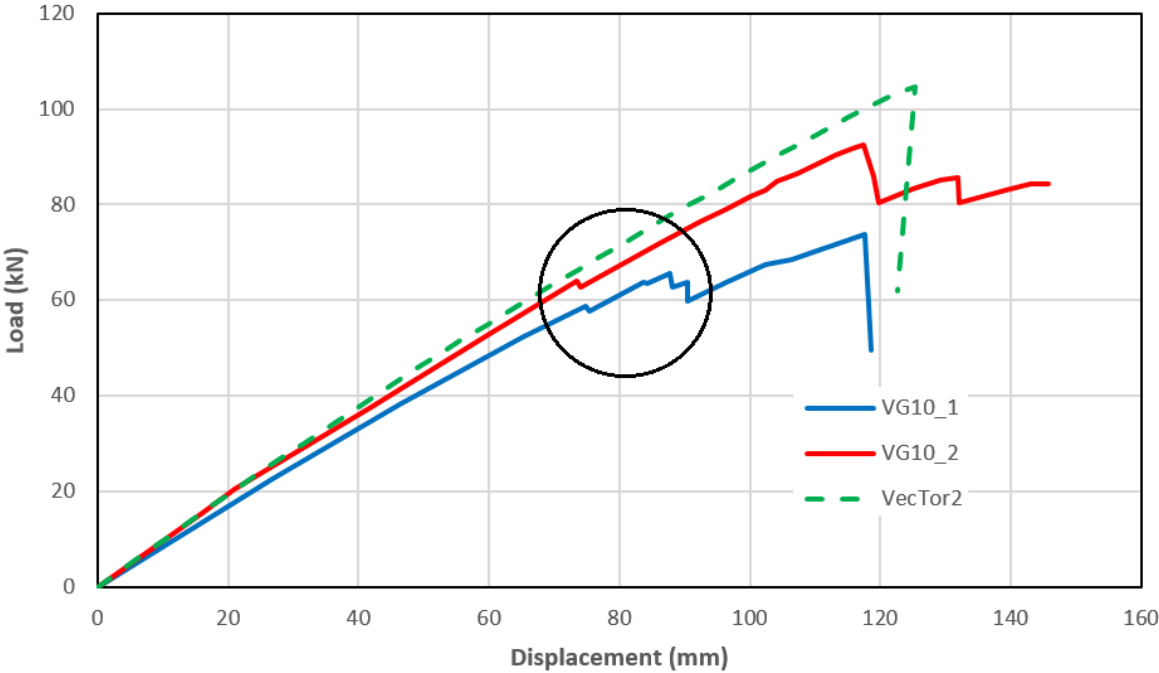


Figure 5-30 Close-up of sudden force drops

Modelling of local rolling shear failure in VecTor2 is theoretically possible yet practically impossible. It involves stochastic analysis which requires knowledge of the normal distribution

and the space variation of the glue strength. As such, perfect bonding was assumed in the FE models created and the overprediction was within a tolerable range.

Similar to Specimen G1 tested by Yeoh (2010), a substantial amount of post-peak displacement was found in Series 5. No convincing explanation was provided in the literature. While the reason for the plateau remains unknown, it is likely caused by yielding of shear connectors combined with progressive tension failure of the timber panel. Nevertheless, the load-deflection response was well captured up to the peak.

5.4.5 Other Experiment Series

Two other experiment series used for the verification studies were carried out by van der Linden (1999) and Lukaszewska (2009). van der Linden (1999) proposed an analytical model, commonly referred to as the “Frozen Shear Model”, based on the results obtained from 30 typical timber-concrete composite beams. Lukaszewska (2009) investigated the performance of connectors for prefabricated timber-concrete beams subjected to short- and long-term bending.

The specimens were modelled in the same fashion described previously, and reasonably good agreement was found in all specimens. As such, the remaining two series are not discussed in detail. Only the experimental setups and the numerical corroboration results are given in this section to further demonstrate VecTor2’s ability to reproduce the global load-deflection responses. Note that the true tensile strengths of the specimens were not estimated progressively, as previously done; instead, large values were assumed in all FE models.

5.4.5.1 van der Linden (1999)

van der Linden (1999) tested twenty timber-concrete composite beams, which had no interlayers separating the timber and the concrete components. Presented in Figure 5-31 and 5-32 were the specimen setup and the details of the shear connectors, respectively. The experimental results were published for eight of the twenty specimens; the experimental results were compared to the VecTor2 results in this section, as demonstrated in Figure 5-33. As per van der Linden (1999),

cracking of concrete was found to occur first underneath the loading jacks, with more cracks appearing along the span as the applied load increased. VecTor2 was able to predict the cracking load and locations accurately. Take Specimen N+S 7 as an example, VecTor2 predicted the first cracking underneath the loading jack at the applied load of 14.1 kN per jack, as shown in Figure 5-34; more cracks were predicted to occur and the crack pattern prediction at 30 kN per jack, as shown in Figure 5-35.

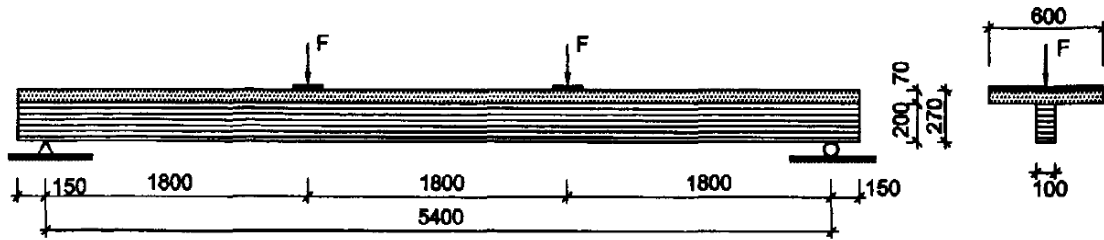


Figure 5-31 Experimental setup (van der Linden, 1999)

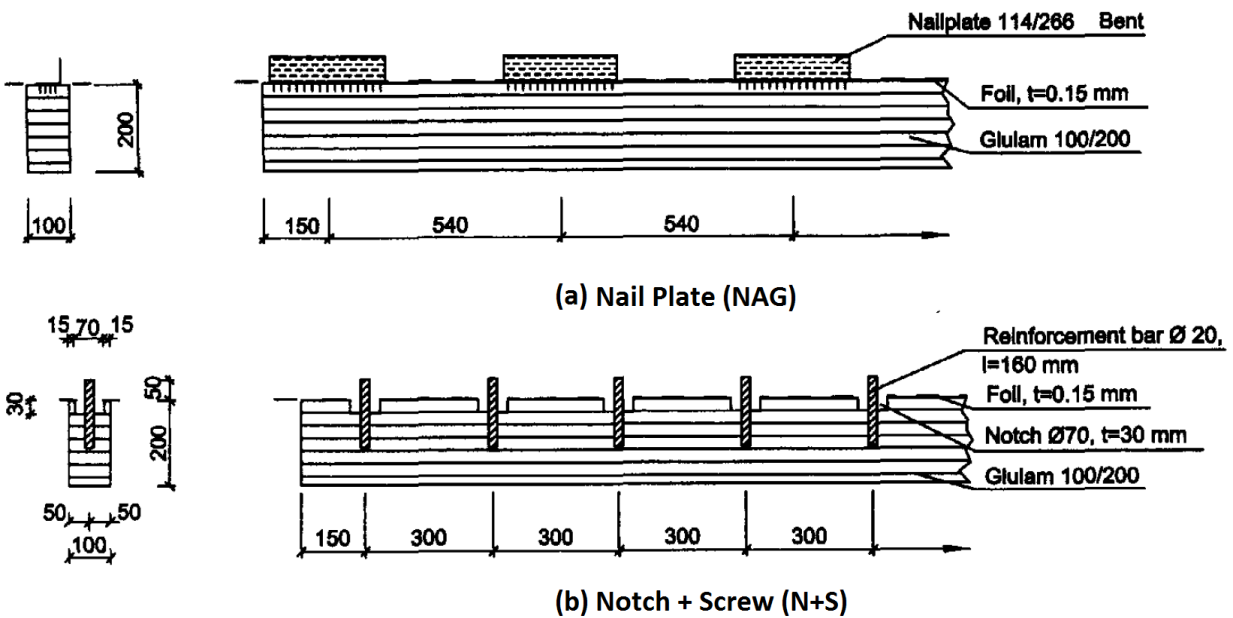
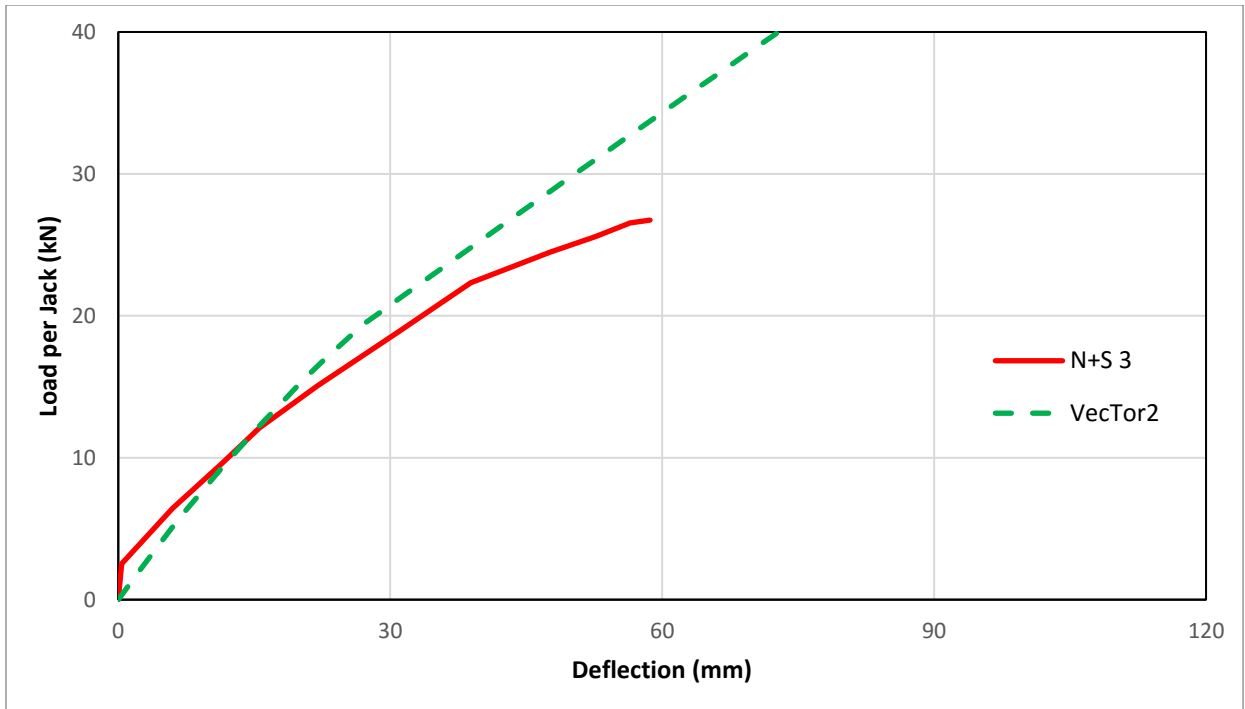
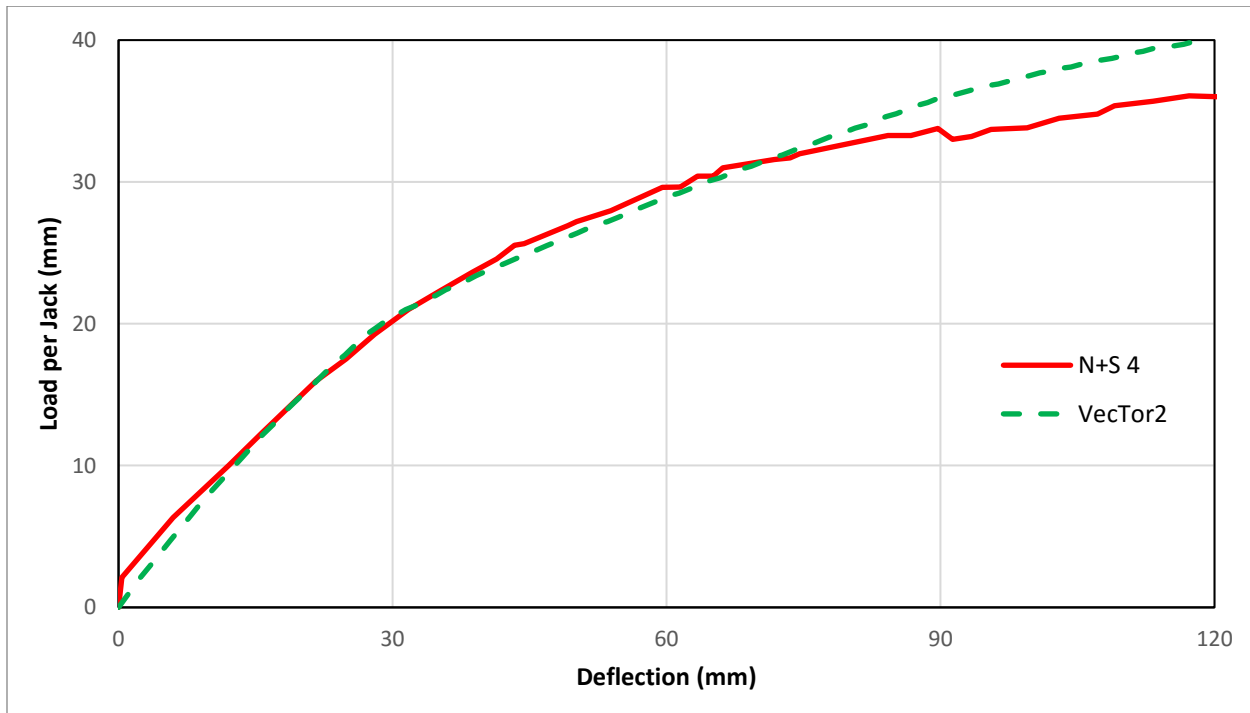


Figure 5-32 Connector Types (van der Linden, 1999)

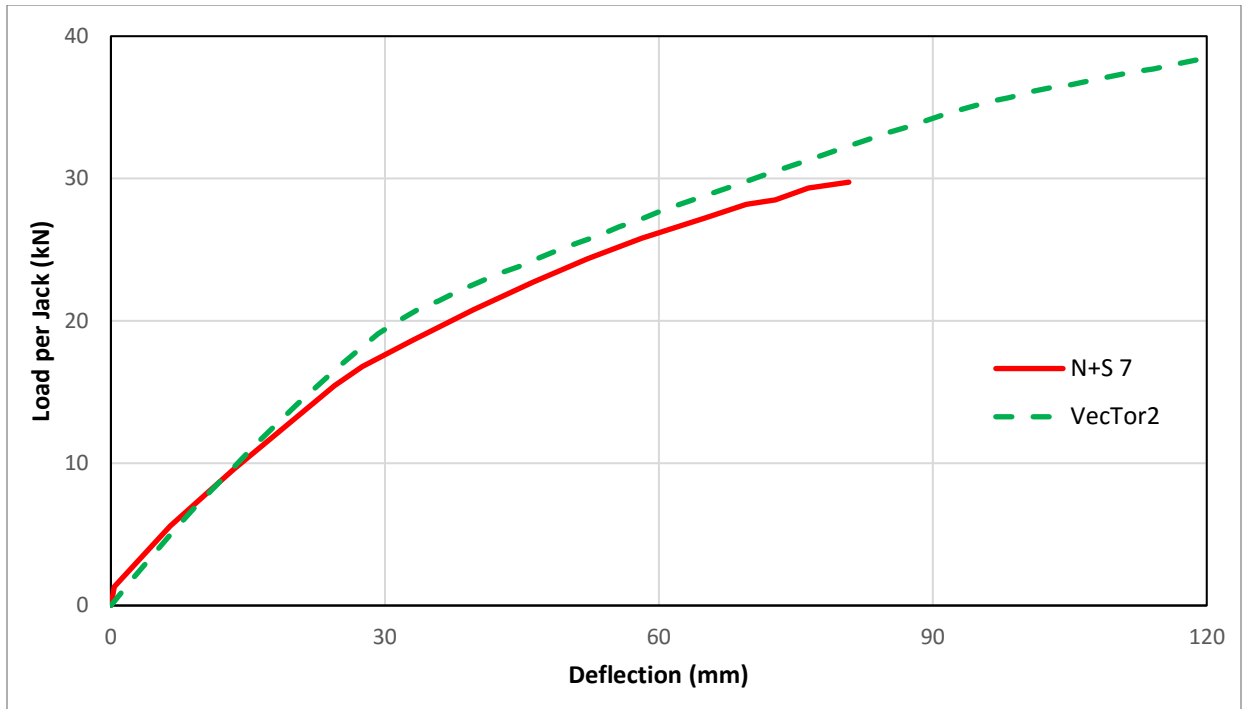


(a) N+S 3

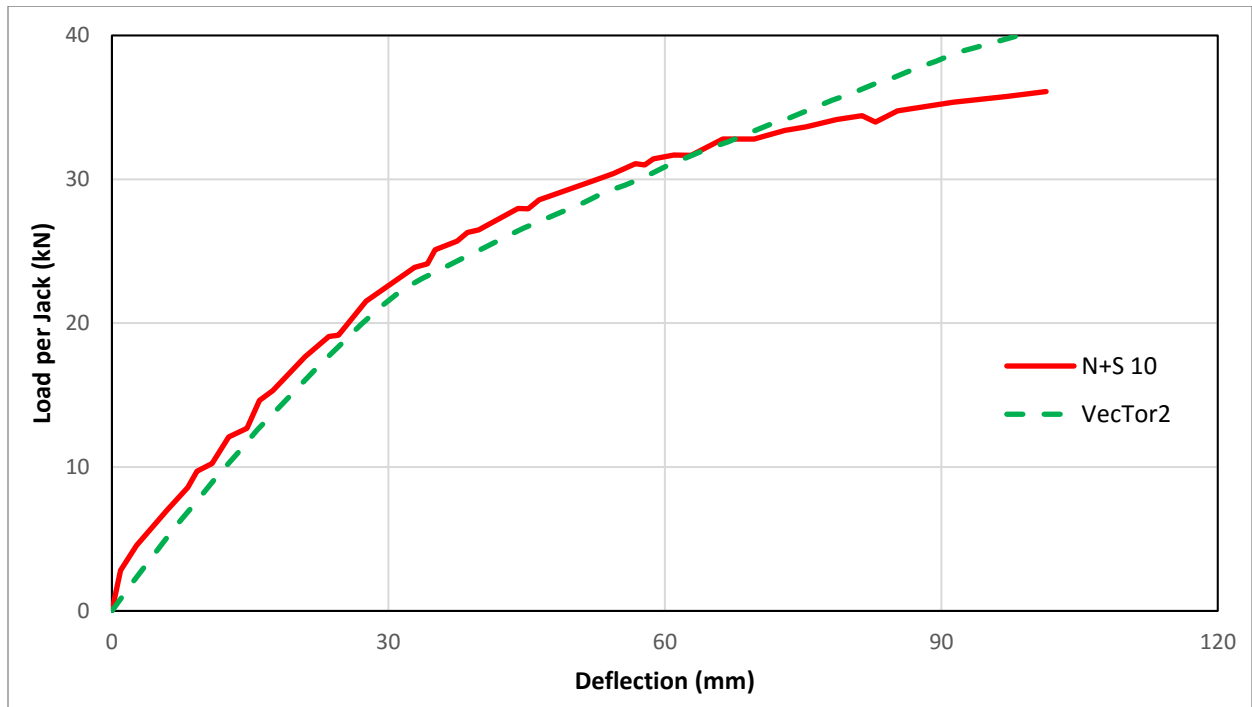


(b) N+S 4

Figure 5-33 Load-deflection response

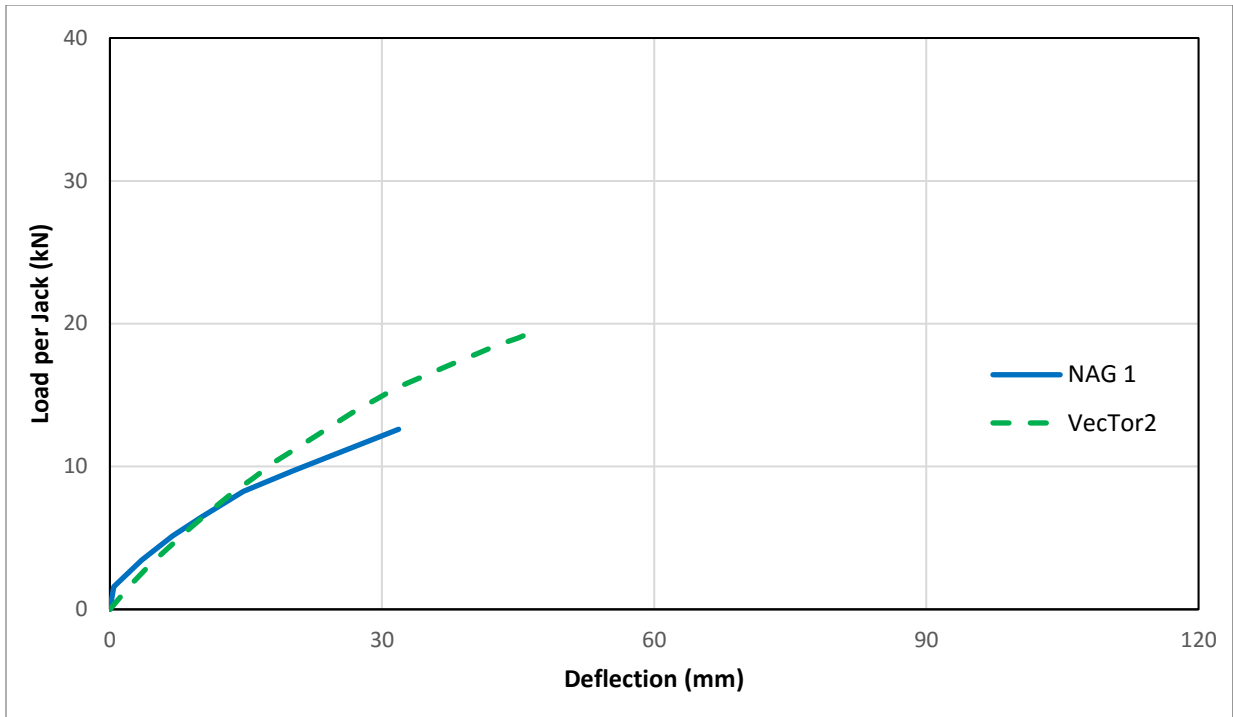


(c) N+S 7

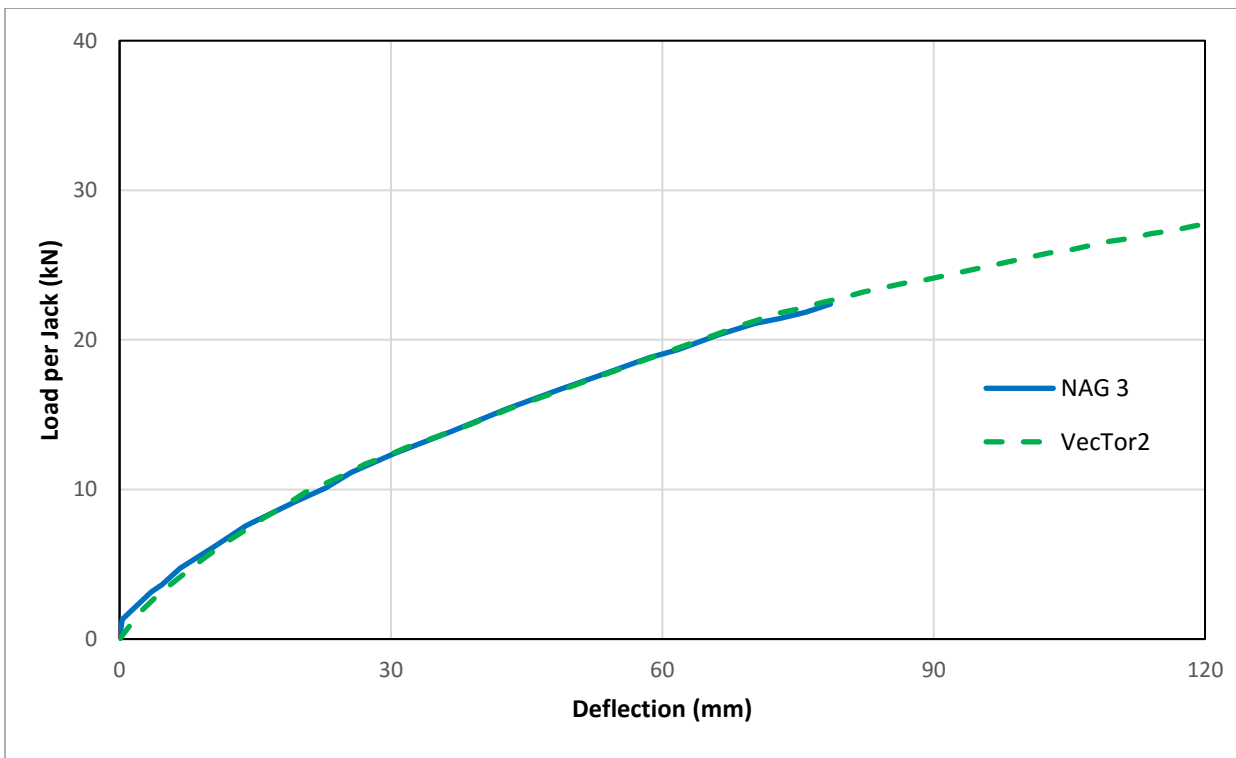


(d) N+S 10

Figure 5-33 Load-deflection response (continued)

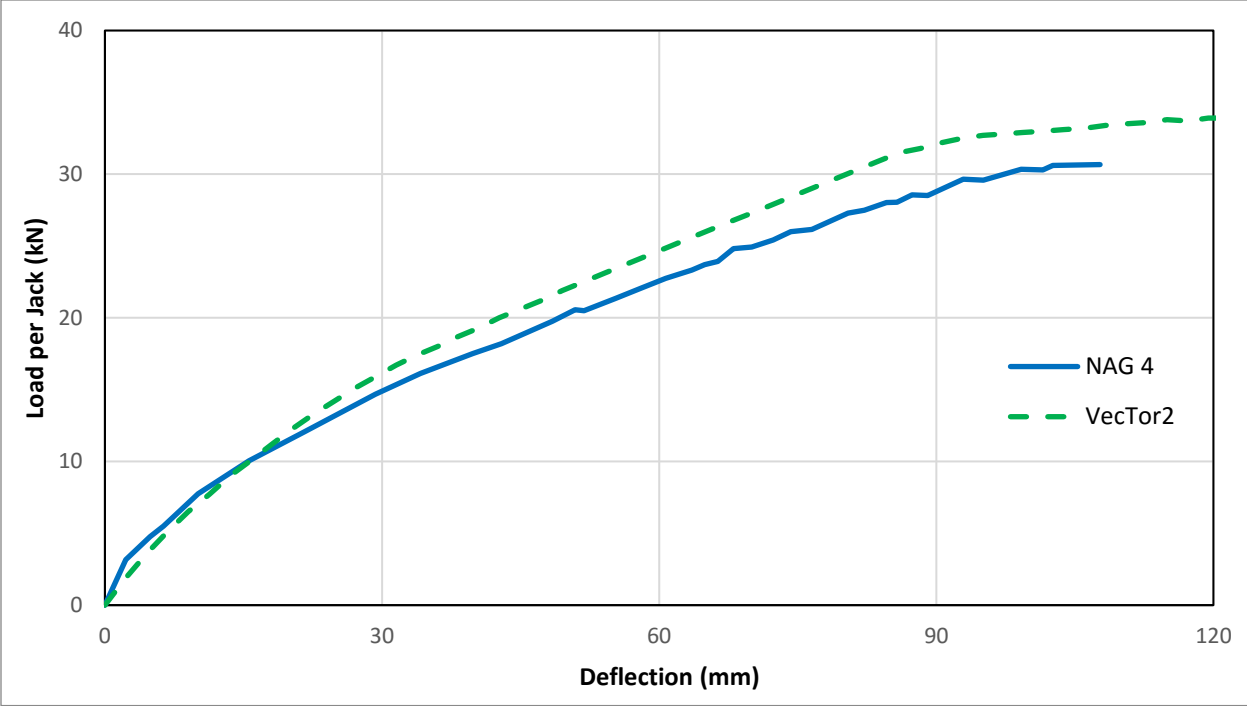


(e) NAG 1

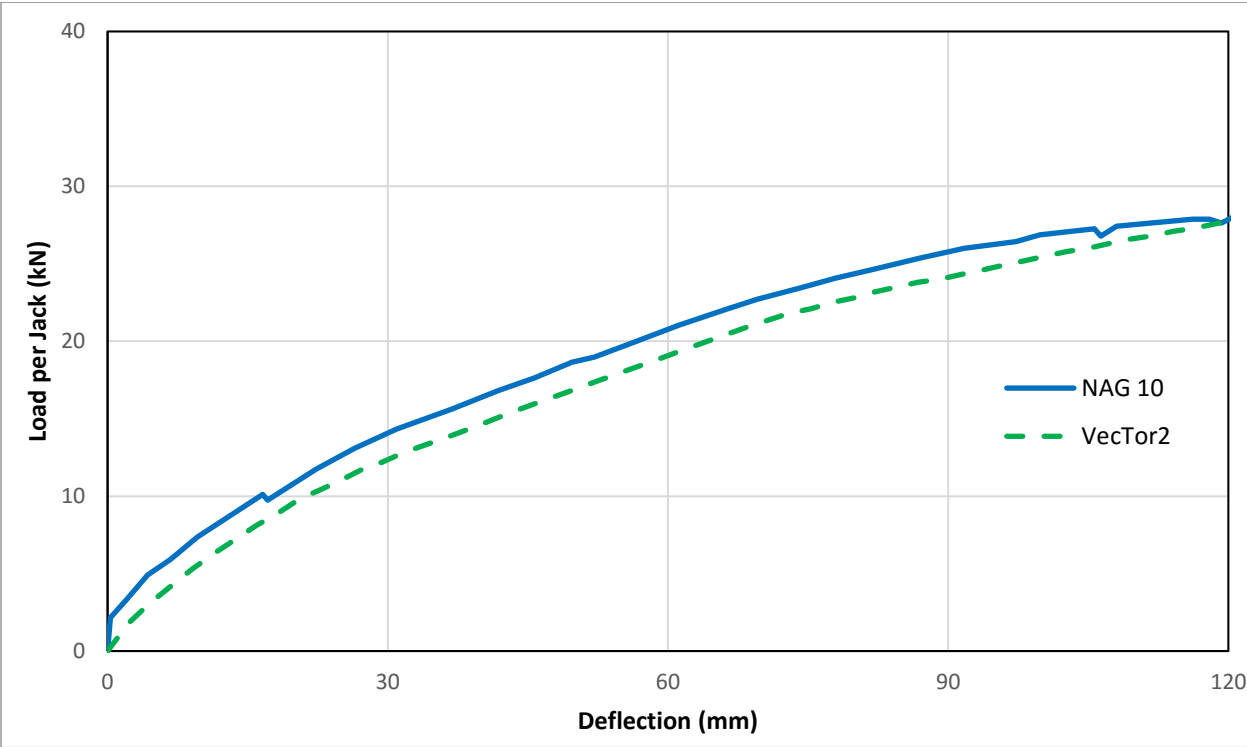


(f) NAG 3

Figure 5-33 Load-deflection response (continued)



(g) NAG 4



(h) NAG 10

Figure 5-33 Load-deflection response (continued)

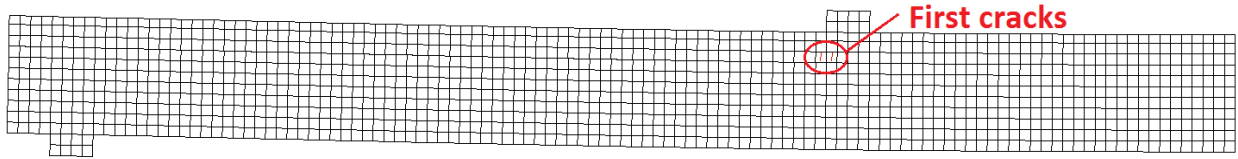


Figure 5-34 Crack pattern at 14 kN per jack

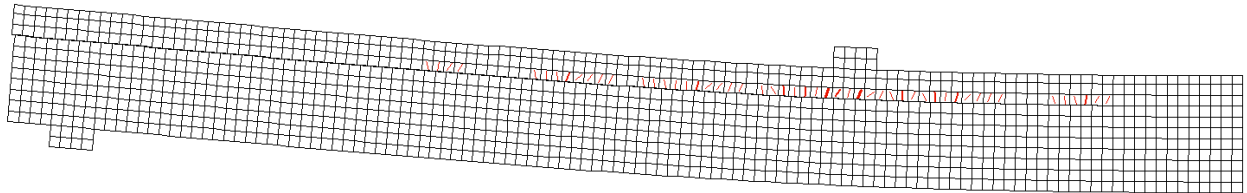


Figure 5-35 Crack pattern at 30 kN per jack

5.4.5.2 Lukaszewska (2009)

Lukaszewska (2009) tested five prefabricated specimens with identical cross sections and two types of shear connectors, as depicted in Figure 5-36 and Figure 5-37, respectively. The specimens were set up as demonstrated in Figure 5-38. The numerical load-deflection predictions, along with the experimental results, are presented in Figure 5-39.

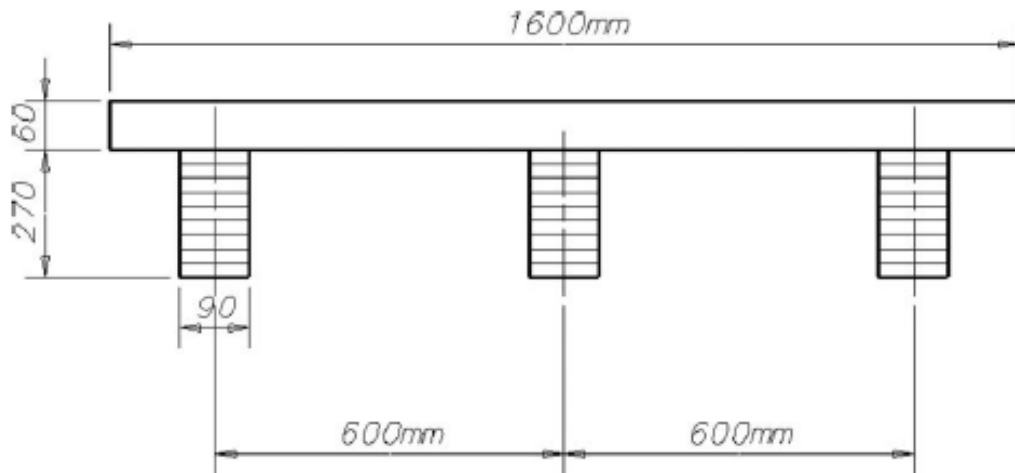


Figure 5-36 Specimen cross section (Lukaszewska, 2009)

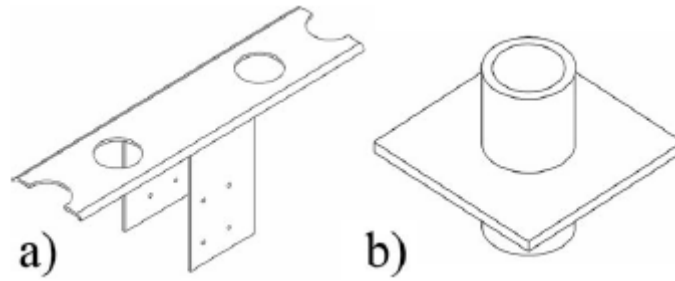


Figure 5-37 Connector types (a) SP+N; (b) SST + S (Lukaszewska, 2009)

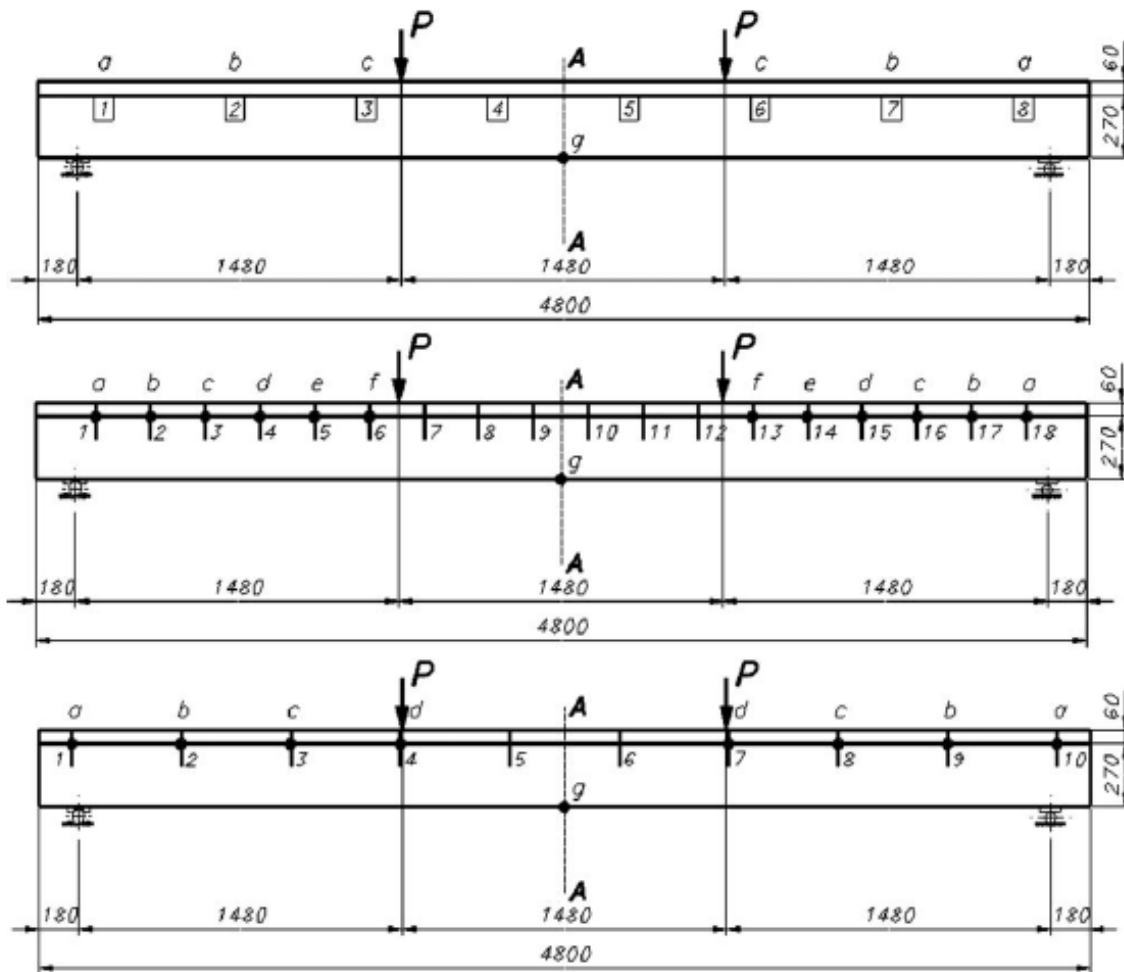
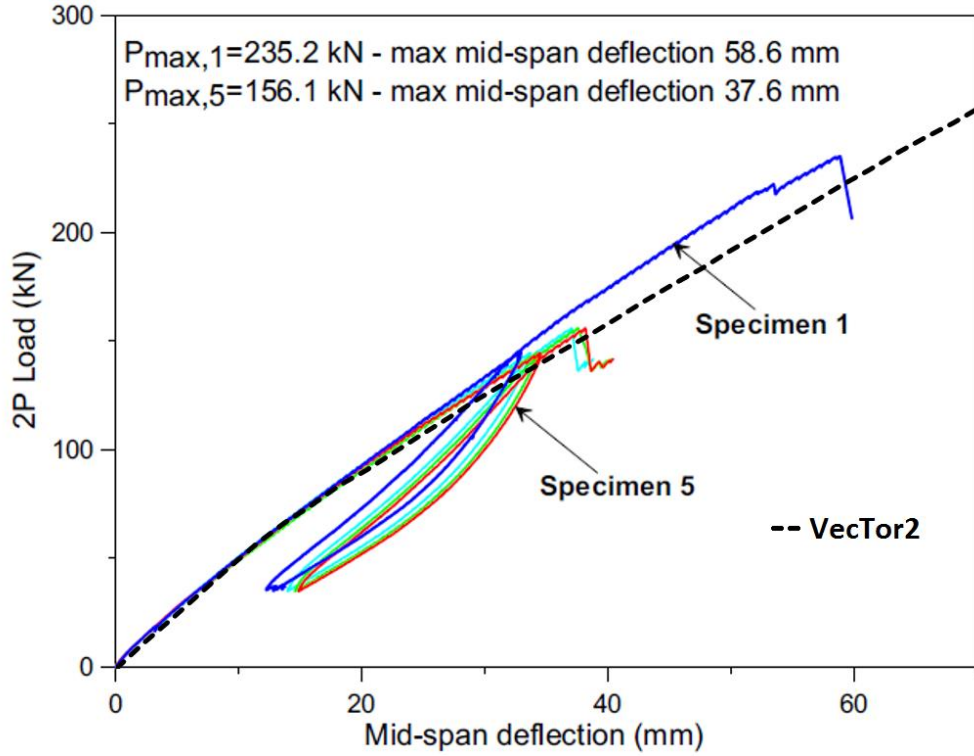
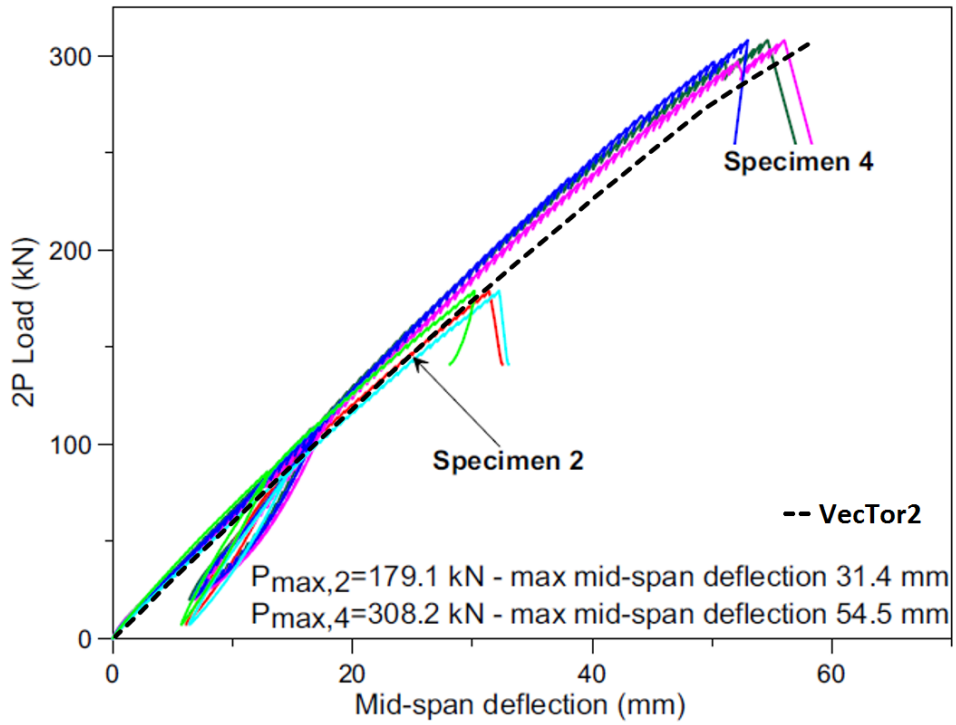


Figure 5-38 Connector Layout (a) Top: Specimen 1 and 5 (SP + N); (b) Middle: Specimen 2 and 4 (SST + S); (c) Bottom: Specimen 3 (SST + S) (Lukaszewska, 2009)

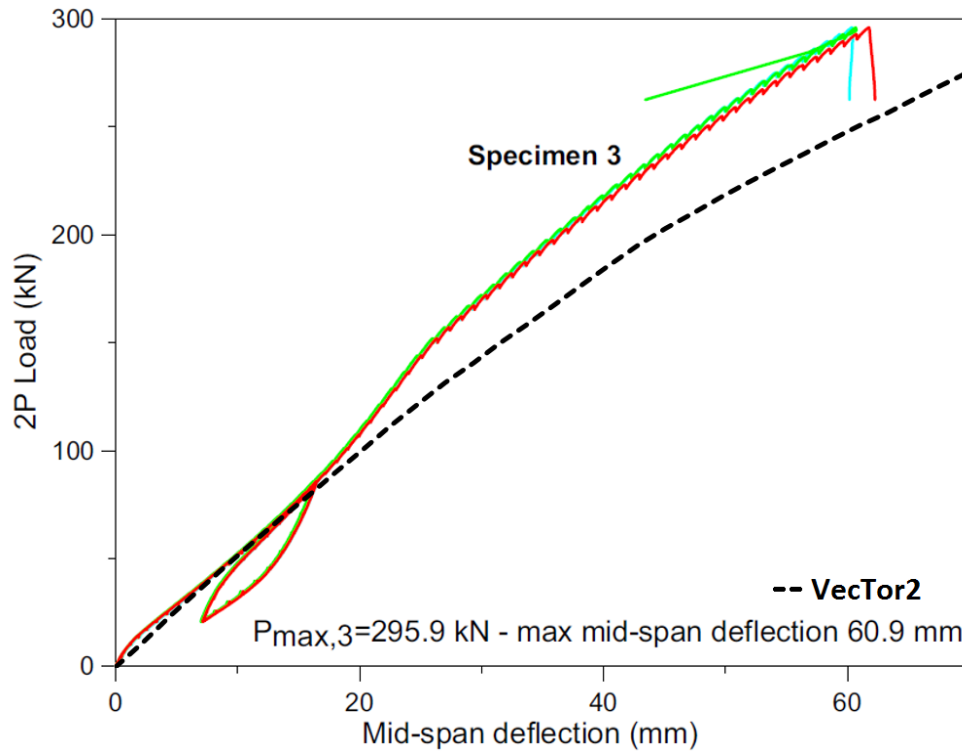


(a) Specimen 1 and 5



(b) Specimen 2 and 4

Figure 5-39 Load-deflection response (Lukaszewska, 2009)



(c) Specimen 3

Figure 5-39 Load-deflection response continued (Lukaszewska, 2009)

5.5 Sensitivity Analysis

5.5.1 Mesh Sensitivity

The precision of a FE analysis is normally heavily dependent on the mesh size. In order to obtain stable analysis result, the mesh size must be sufficiently fine. The mesh size of an FE model is considered to be adequate if further refinement of the mesh size yields no significant changes to the analysis results.

Figure 5-40 presents the FE two models created both for Specimen CS1 tested by Deam et al. (2010). Identical input parameters were used in each model. The model with the finer mesh had a grid size of 25 mm by 25 mm which was 3 times finer than that of the model with a “coarse mesh”. While the finer mesh is much more demanding in computation effort, the predicted load-deflection responses are practically identical, as depicted in Figure 5-41. The model with a finer

mesh did terminate earlier as a result of higher average stress within the critical element. Nevertheless, the model with a “coarse mesh” can be considered as adequately meshed.

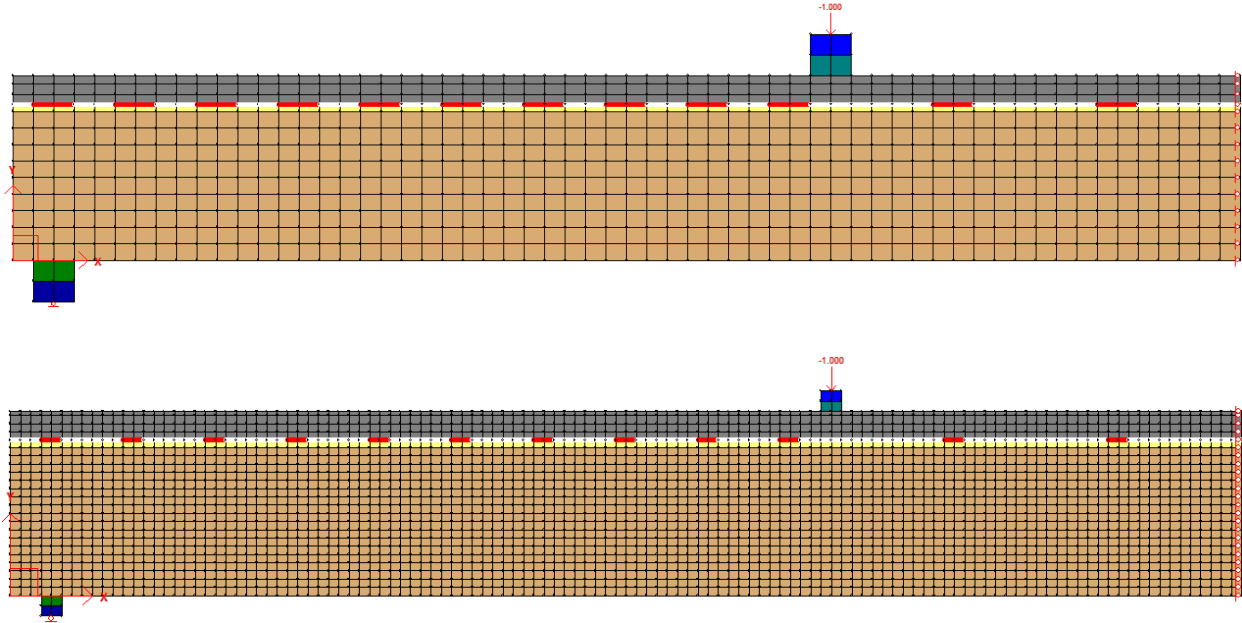


Figure 5-40 FE models with different mesh size

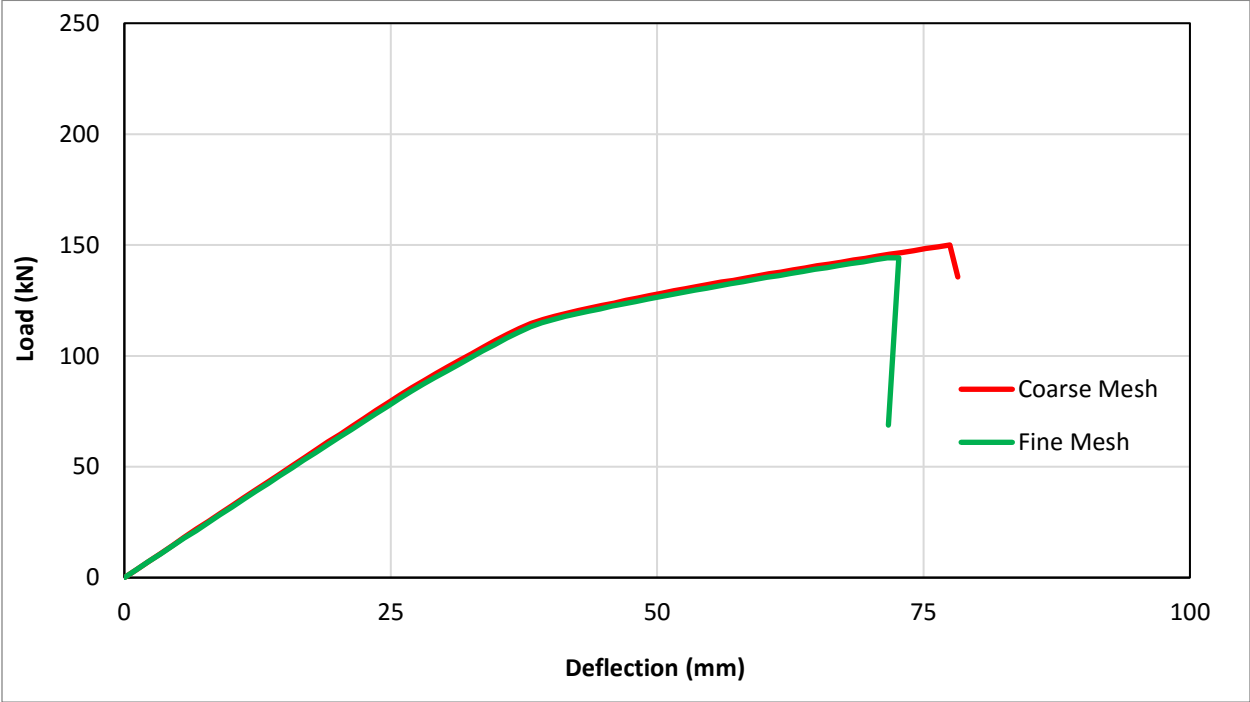


Figure 5-41 Comparison of predicted load-deflection responses of different mesh size

5.5.2 Material Sensitivity

Since nonlinear material constitutive models were adopted in VecTor2, it is important to examine the contribution of the nonlinear models to the global nonlinearity of the composite system. To do this, the material responses were set to linear-elastic models such that the shear connectors were the only source of nonlinearity of the global system.

Figure 5-42 compares the numerical results of Specimen CS1 (Deam 2010), with linear and nonlinear material models. While the linear material models yielded a slightly stiffer result, the difference was rather negligible. A similar comparison was performed for Specimen S7 which was discussed in Section 5.4.4 (Gerber 2016); the results are presented in Figure 5-43. This time, the linear material models yielded a noticeably stiffer load-deflection response than that of the nonlinear material models. The major distinction between the two specimens was the specimen configuration. The concrete slab of Specimen S7 had a depth of 70 mm and a total depth of 159 mm, while Specimen CS1 had the same depth of concrete slab but the total depth of the specimen was 448 mm.

Therefore, for a TCC beam of typical configuration where the depth of concrete slab is relatively thin to the total depth of the specimen, the global load-deflection response is generally not sensitive to the material nonlinearity. However, for a TCC beam with a higher percentage of concrete depth with respect to the total depth, inclusion of the nonlinear material models may yield more accurate results.

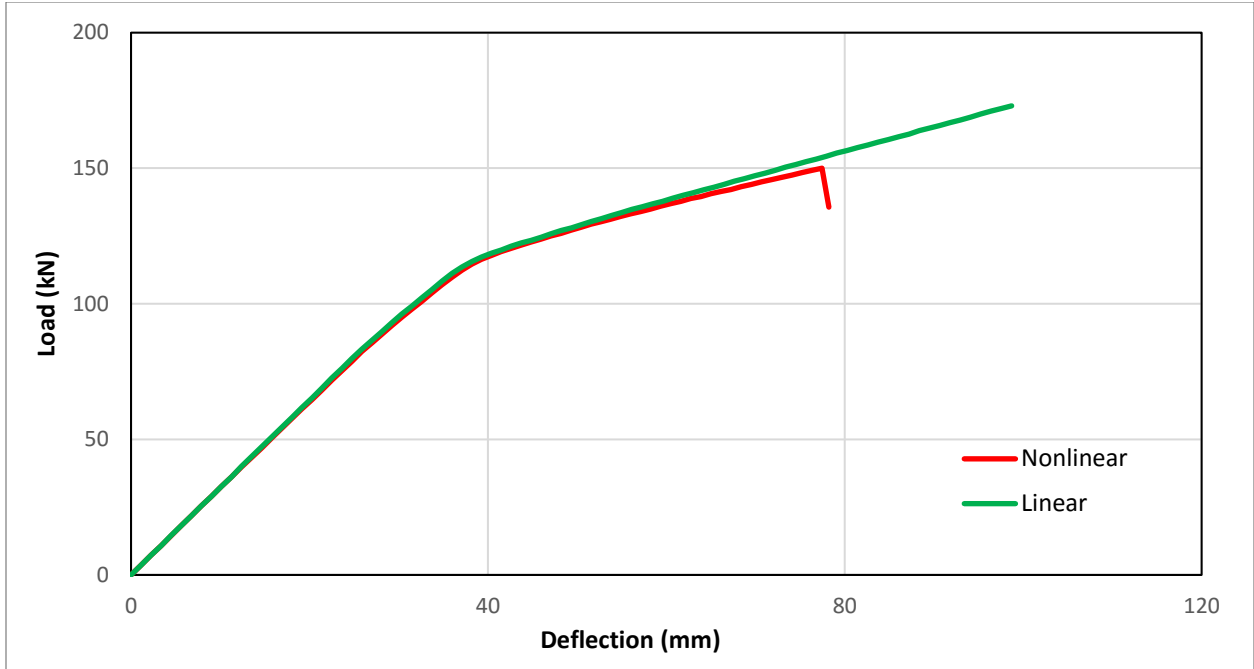


Figure 5-42 Load-deflection responses of Specimen CS1 with linear and nonlinear material constitutive models

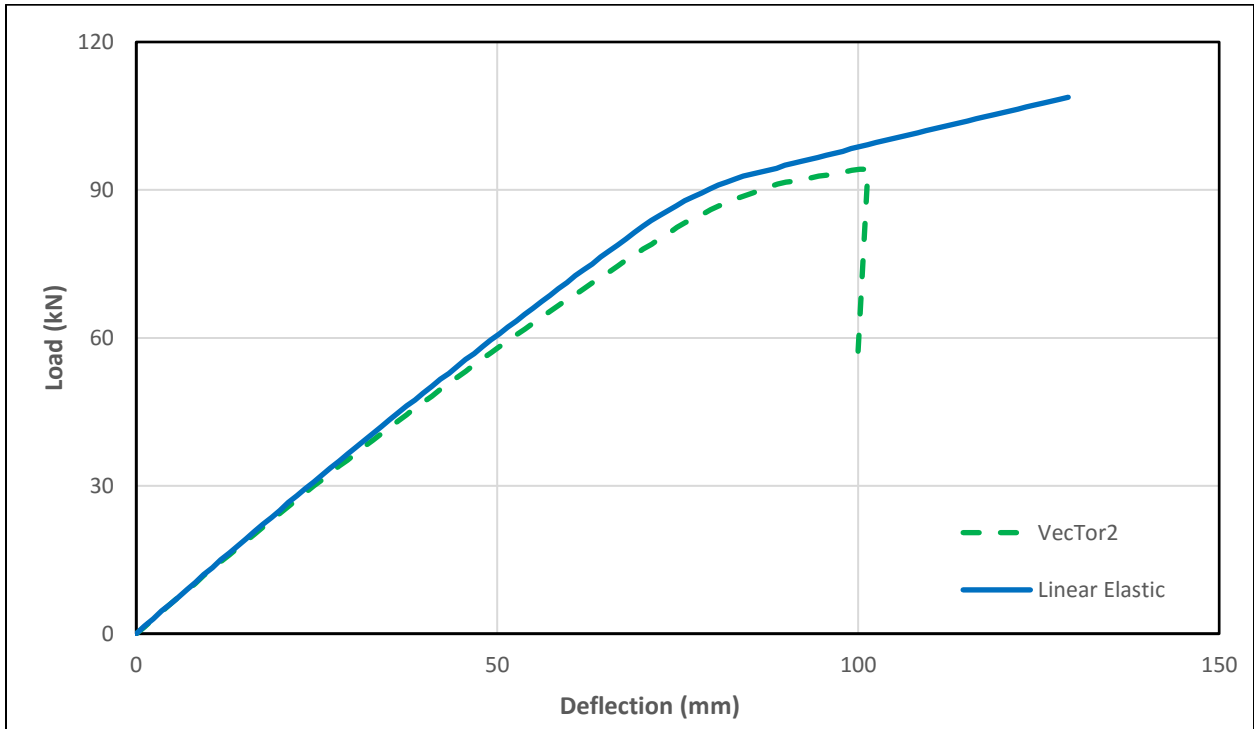


Figure 5-43 Load-deflection responses of Specimen S7 with linear and nonlinear material constitutive models

5.6 Conclusions

After careful examination of VecTor2's general applicability to various scenarios, the following conclusions can be drawn:

- The assumptions and simplifications made in Section 5.3.2 are appropriate in flexure-critical conditions.
- The total-load, secant-stiffness approach is found to be a viable approach for nonlinear finite element modelling of plain timber, or timber composite such as timber-FRP or timber-concrete composite.
- Currently, VecTor2 is capable of analysing flexure-critical timber-concrete composite beams subjected to short-term monotonic loadings. The load-deflection response of CLT specimens can be predicted with reasonable accuracy using the FE model presented in Figure 5-29.
- The true tensile strength, as determined from the failure loads of the beam specimens examined, is generally 30% to 50% higher than the mean suggested by the manufacturers.
- The performance of timber-concrete composite is largely dictated by the load-slip relationship of shear connectors. As illustrated by Yeoh (2010), the degree of composite action can be close to 100% if the shear connectors are sufficiently stiff. What is also observed is that the load-deflection remains fairly linear up to failure. The implication of this observation is that high degree of composite action is achieved at a cost of reduced global ductility.
- Shear connectors may be modelled using the smeared or discrete contact elements, depending on the connection type and the layout of shear connectors. For shear connectors with constant spacing or shear connectors that are installed continuously along the span such as the metal plate connectors, the smeared contact elements may be a better option, whereas, the discrete contact element is most suitable for connectors without uniform spacing.
- Size matters. The size of shear connectors in full-scale specimens should be consistent with that tested in the push-out test. As demonstrated in Deam et al. (2010), the accuracy

of the analysis is compromised when the size of shear connectors of push-out test specimens do not match with that of the full-scale bending specimens.

- The spacing effect should be taken into consideration in push-out tests. As demonstrated in Figure 5-19, the load-slip relationship can vary considerably as a function of spacing.
- Generally, the load-deflection response is well predicted by VecTor2 if the ultimate failure is caused by either the timber beam rupturing due to high tensile stress in the wood fibre, or by crushing of concrete. However, crushing of concrete is a less common type of failure for TCC specimens.
- Although cracking of concrete was predicted by VecTor2 for all the specimens investigated in this thesis, it was not experimentally observed in the TCC specimens with an interlayer acting as a permanent formwork for the concrete slab. However, van der Linden (1999) tested twenty TCC specimens without such interlayers and found visible cracks, which first occurred directly underneath the loading jacks. As the applied load continued to increase, more cracks were found along the span of the specimens. This suggests that the presence of interlayer may have confined or cushioned the bottom concrete from cracking.

Chapter 6 Conclusions and Recommendations

6.1 Conclusions

The goal of this thesis was to investigate VecTor2's potential capability to model timber-concrete composite (TCC) structures subjected to short-term loadings. Along the process, the following tasks were performed:

1. Implementation of appropriate wood constitutive model to describe the nonlinear behaviour of wood.
2. Verification of the wood constitutive models by modelling plain and reinforced timber beams subjected to short-term monotonic flexure.
3. Modelling of TCC beams subjected to short-term monotonic flexure, with variations in test setups, specimen configurations, materials, and types of shear connectors.

With the results obtained from numerical simulations, it is confirmed that VecTor2 can model TCC structures with sufficient accuracy. The generic FE models presented in Figure 5-1 and Figure 5-2 are found to be accurate and versatile, as they can be easily created and modified to deal with different case scenarios.

However, the successful modelling results are limited to flexure-critical situations, where the ultimate failure of TCC specimens is governed by brittle tension failure of timber in the bottom face. Incomplete information on the material properties of the beam tested prevents confirmation of the ability to model other failure modes.

Lastly, past experimental work on TCC has focused primarily on the development of shear connectors, and the TCC performance subjected to short- and long-term monotonic loadings. Hence, the numerical corroborations performed in this study are limited to short-term monotonic loadings; VecTor2's capability to perform dynamic analysis of TCC structures is uncertain.

6.2 Recommendations

While a wide range of further investigation is possible, some aspects closely related to the scope of work of this thesis are recommended for future work, as follows:

- VecTor2 development:

The current pre-processor of VecTor2, FormWorks, is not able to auto-mesh a TCC beam. As such, a step-by-step guideline is provided in Appendix B to explain the process to manually create a TCC model in FormWorks. In order to simplify the model creation process for TCC structures, work is required to update the FormWorks auto-meshing source code.

The post-processor, Augustus, does not read and display any results related to the bond-slip elements. Work needs to be devoted to expand the program's capability in this regard, and ultimately to make the program more user-friendly for practical use.

- Experimental work:

Future work must be undertaken to investigate the dynamic response of TCC. In the case of monotonic loadings, the concrete component is of little concern as it primarily resists compression, and the compression rarely surpasses the concrete's compressive strength. However, the concrete slab may become an issue under dynamic loading.

The global load-deflection response of any TCC system is heavily dependent on yielding of shear connectors. In general, shear connectors need to be sufficiently stiff to achieve a high degree of composite action, yet sufficiently ductile to contribute to the global ductility of a TCC system. The use of concrete notch shear connectors investigated by Yeoh (2010) enabled a high degree of composite action up to collapse, at the cost of reduced softening of the global load-deflection response. From the experimental investigation conducted by Gentile (2000), as discussed in Chapter 4, it is concluded that FRP reinforcement can be an effective measure to enhance the post-peak response of wood in tension. Therefore, it may be worthwhile to incorporate both FRP reinforcement and shear connectors of high stiffness within a TCC system, with each serving its own purpose.

References

1. Azzi VD., Tsai SW. (1965). Anisotropic strength of composites. *Exp Mech*; 5–9: 283–9
2. Bakoss, S.L., Greenland, A. and Crews, K.I. (1999). Bridge deck and industrial heavy-duty flooring system based on laminated veneer lumber beams reinforced with carbon fibre composites. *Proceedings of the 8th International Conference on Structural Faults and Repair*, London, UK, July 13- 15, 1999.
3. Bazan, I.M.M. (1980). *Ultimate bending strength of timber beams* (Doctoral dissertation). Nova Scotia Tech. College. Halifax, N.S. 269p.
4. Bentz, E. (2010). *Augustus: Post processor for VecTor2* (version 5.6.5). Copyright 1996-2010 E. Bentz.
5. Bodig, J., Jayne, B. A. (1982). *Mechanics of wood and wood composites*. Van Nostrand-Reinhold Co, Inc., New York.
6. Ceccotti, A., Fragiaco, M., and Giordano, S. (2006). Long-term and collapse tests on a timber-concrete composite beam with glued-in connection. *Materials and Structures, Special Volume on Timber*, in press.
7. Deam, B., Fragiaco, M., and Gross, L. (2008). Experimental behaviour of prestressed LVL-Concrete Composite Beams. *J. Struct. Eng.* 134(5): 801-809
8. Dorey, A.B. and Cheng, J.J.R. (1996). The behaviour of GFRP glued laminated timber beams. *Proceedings in Advanced Composite Materials in Bridges and Structures, ACMBS II*, M.M. El-Badry, Editor. Montreal, Quebec, Canada, pp. 787- 794.
9. de Ruvo, A., Carlsson, L., Fellers C. (1980). The biaxial strength of paper. *Tappi* 63(5):133–136
10. Hernandez, R., Davalos, J.F., Sonti, S.S., Kim, Y. and Moody, R.C. (1997). Strength and stiffness of reinforced yellow-poplar glued laminated beams. *Res. Pap. FPL-RP- 554*. Madison, Wisconsin, U.S. Department. of Agriculture, Forest Service, Forest Products Laboratory.

11. Fragiacom, M. (2005). A finite element model for long-term analysis of timber-concrete composite beams. *Structural Engineering and Mechanics*, 22(2), pp. 173-189.
12. Fragiacom, M. (2012). Experimental behaviour of a full-scale timber-concrete composite floor with mechanical connectors. *Materials and Structures*, 45(11): 1717-1735.
13. Frangi, A., and Fontana, M. (2003). Elasto-plastic model for timber-concrete composite beams with ductile connection. *Structural Engineering International* 13 (1): 47-57.
14. Dias, A. M. P. G. (2005). Mechanical behaviour of timber-concrete joints (Doctoral dissertation). University of Coimbra, Coimbra, Portugal.
15. Gentile, C. (2000). Flexural strengthening of timber bridge beams using FRP (MAsc dissertation). University of Manitoba.
16. Gerber, A. (2016). Timber-concrete composite connectors in flat-plate engineered wood products (MAsc dissertation). University of British Columbia.
17. Glos, P. (1978). Berichte zur Zuverlaessigkeitstheorie der Bauwerke: Zur Bestimmung des Festigkeitsverhaltens von Brettschichtholz bei Druckbeanspruchung aus Werkstoff- und Einwirkungskenngroessen. (Reliability theory for timber structures: determination of compression strength behaviour of glulam components from interaction of material properties). Heft 34/1978. Laboratorium fuer den Konstruktiven Ingenieurbau. Technische Universitaet Muenchen. 335p.
18. Hankinson, R.L. (1921). Investigation of crushing strength of spruce at varying angles of grain. Air Service Information Circular No. 259, U.S. Air Service.
19. Hashin, Z. (1980). Failure criteria for unidirectional fiber composites. *Journal of Applied Mechanics*, 47:329-33.
20. Hoffman O. (1967). The brittle strength of orthotropic materials. *J. Compos. Mater.* 200-6. 2-1.
21. Holmberg, S., Persson, K., and Petersson, H. (1998). Nonlinear mechanical behaviour and analysis of wood and fibre materials. *Computers and Structures* 72. 459-480.
22. Jones RM. (1975). *Mechanics of composite materials*. first ed. Tokyo: McGraw Hill Kogakusha.

23. Kasal, B., Leichti, R.J. (2005). State of the art in multiaxial phenomenological failure criteria for wood members. *Prog Struct Mat Eng* 7:3–13
24. Lau, W. (2000). Strength model and finite element analysis of wood beam-columns in truss applications (Doctoral dissertation). University of British Columbia.
25. Lukaszewska, E. (2009). Development of prefabricated timber-concrete composite floors (Doctoral dissertation). Luleå tekniska universitet.
26. Malhotra, S.K. and Mazur, S.J. (1970). Buckling strength of solid timber columns. *Trans Eng. Inst. of Canada, Published in the Eng. J.* 13(A-4): I-VII.
27. Neely, S. T. (1898). Relation of compression-endwise to breaking load of beam. *Progress in Timber Physics. USDA Division of Forest Circular No. 18:* 13- 17.
28. Norris C.B. (1950). Strength of orthotropic materials subjected to combined stress. Report No. 18126, US. Department of Agriculture, Forest Products Laboratory, Madison, WI.
29. Persaud, R., Symons, D. (2006). Design and testing of a composite timber and concrete floor system. *The Structural Engineer*, 21, pp. 22-30.
30. van der Put TACM. (2005). The tensor polynomial failure criterion for wood. Delft Wood Science Foundation, Delft.
31. Vecchio, F., and Collins, M. (1986). The modified compression field theory for reinforced concrete elements subjected to shear. *ACI Journal*, 83(2), March-April 1986, pp. 219- 231.
32. Vecchio, F. (1990). Reinforced concrete membrane element formulation. *ASCE Journal of Structural Engineering*, Vol. 116, No. 3, pp.730-750
33. Vecchio, F. (2000). Disturbed stress field model for reinforced concrete: formulation. *ASCE Journal of Structural Engineering*, 126(9), September 2000, pp. 1071-1077.
34. Wong, P., Trommels, H., Vecchio, F. (2013). *VecTor2 and FormWorks Manual*.
35. Yeoh, D. (2010). Behaviour and design of timber-concrete composite floor system (Doctoral dissertation). University of Canterbury.
36. Ylinen, A. (1956). A method of determining the buckling stress and the required cross-sectional area for centrally loaded straight columns in elastic and inelastic range. *IABSA Publications*. 16:529-549.

37. Zhang, C., Gauvreau, P. (2015). Timber-concrete composite systems with ductile connections. *Journal of Structural Engineering*, 141(7).

Appendix Modelling Guideline

This section serves as a step-by-step guideline which aims to explain the VecTor2 modelling process for timber-concrete composite beams subjected to short-term monotonic loadings. All models are created with the program FormWorks (Wong et al., 2013), a pre-processor developed specifically for VecTor2. The current auto-meshing functionality of FormWorks is not compatible with timber-concrete composite structures; as such, all models must be manually created using the built-in manual-meshing function. A newer version of the auto-meshing function is currently under development, which will not only automate the model generation process, but also improve the overall computation efficiency.

Step 1 Defining Regions

The process to manually create a timber-concrete composite beam model in FormWorks can be tedious and time-consuming; patterns should always be exploited to simplify the process substantially. In order to utilize such patterns, a TCC model should be first broken down into multiples regions. Nodes and elements can then be added in batches following the specific patterns associated with each region as defined.

The model created for Specimen CS1 tested by Deam et al. (2008) is used as a comprehensive example. More details regarding the experimental setup can be found in Section 5.4.3 of this thesis. Shown in Figure 1 is an example of how regions were defined for Specimen CS1. In this case, the regions were defined entirely based on the original experimental setup, with each region representing a particular material type (i.e. Region 2 representing the timber beam and Region 3 representing the shear connectors). This example represents a simple yet feasible approach that finds a balance between the computation demand, and simplicity in model creation. All other specimens used for the validation studies in Chapter 5 were created following the same procedure.

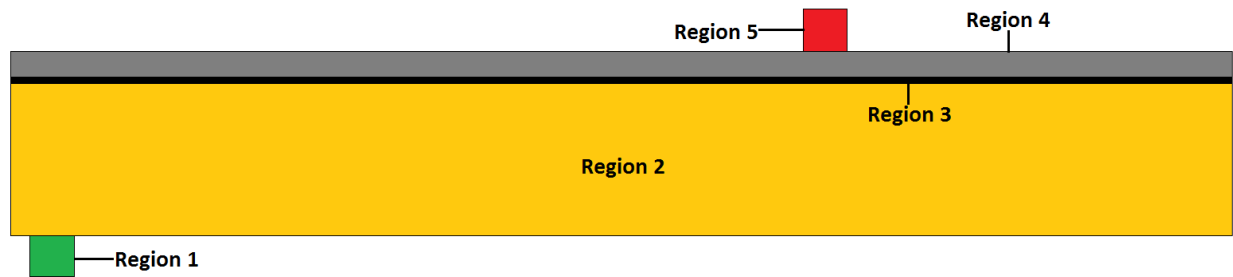


Figure 1 Region definition

Step 2 Adding Nodes

A timber-concrete composite beam model in FormWorks comprises a series of rectangular elements which are defined by the four corner nodes. All nodes are added using the “Create Nodes” dialog box as presented in Figure 2.

Specimen CS1 had a total span of 6 meters, and the timber beams supporting the concrete slab was 360 mm deep. Only half of the specimen was modelled due to symmetry. It was decided to use 50 mm by 40 mm rectangular elements for the timber component; this translates into a total of 540 rectangular elements for the timber component, with 60 elements in the horizontal direction and nine elements in the vertical direction. As such, there were 10 rows of nodes created for the timber component, with each row consisting of 61 horizontal nodes. Demonstrated in Figure 3 were the nodes added to the model for Region 1 and Region 2. Shown in Figure 4 is a close-up of Figure 3 in the bottom left corner. Notice that nodes 1 to 6 were created for Region 1, while nodes 8, 9 and 10 were the common nodes shared by both Region 1 and Region 2 (Figure 4). These three common nodes were excluded when adding nodes for Region 1; instead, they were added together with all other nodes in Region 2. Although this may interfere with the node pattern in Region 1, it preserved the integrity of the node pattern in Region 2. In this case, the amount of nodes in Region 2 was significantly greater than that in Region 1, and therefore the priority was given to Region 2. Similarly, the common nodes for Region 4 and Region 5 were assigned to Region 4.

As a requirement of the contact elements, nodes must be created in pairs with the same coordinates at each node location. As such, Region 3 consisted of nodes pairs, including the top row of nodes of Region 2, and the bottom row of nodes of Region 4. There were no common nodes, and therefore the node patterns of Region 2 and Region 4 were not interrupted.

Following the aforementioned rules, all nodes were added in 4 batches. Each batch of nodes corresponded to a specific region with the only exception being Region 3, where the node pairs were located. Further details of how nodes are manually added in FormWorks can be found in Section 10.4.3 of the VecTor2 and FormWorks Manual (Wong et al. 2013).

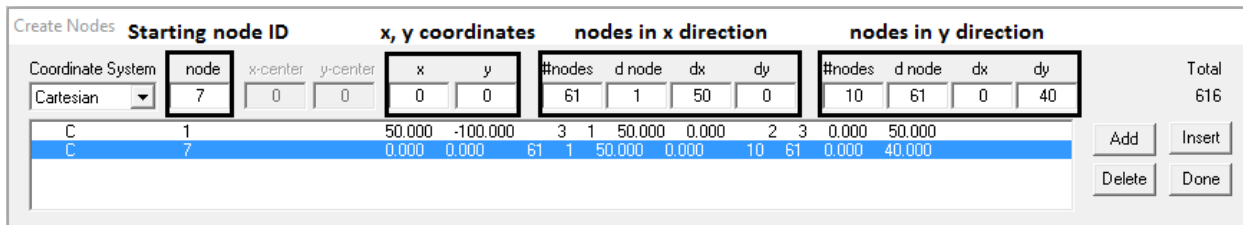


Figure 2 Create Nodes dialog box

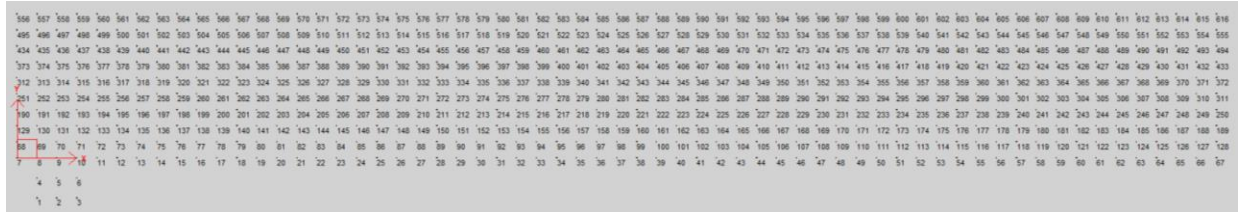


Figure 3 Nodes added for Region 1 and Region 2

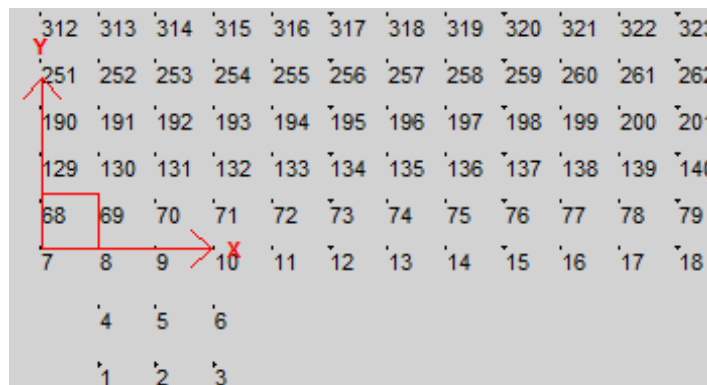


Figure 4 Close-up of Figure 3 (bottom left corner)

Step 3 Adding Elements

The rectangular membrane elements and the contact elements were added to the model using the “Create Rectangular Elements” dialog box as shown in Figure 5, and the “Create Interface Elements” dialog box shown in Figure 6, respectively. It should be pointed out that while the two dialog boxes look similar, the node conventions are different. For more detailed explanation of the node conventions and the required inputs for the dialog boxes, refer to Section 10.4.4 of the VecTor2 and FormWorks Manual (Wong et al. 2013). As the node pattern integrity was preserved for Regions 2, 3, and 4, elements in these regions were easily added, simply by following the specific node pattern for each region. For Region 1 and 5, elements were added in two stages because the node patterns were interrupted. Shown in Figure 7 was the model after all elements were added, with the rectangular membrane elements shown in white, and the contact elements shown in cyan.

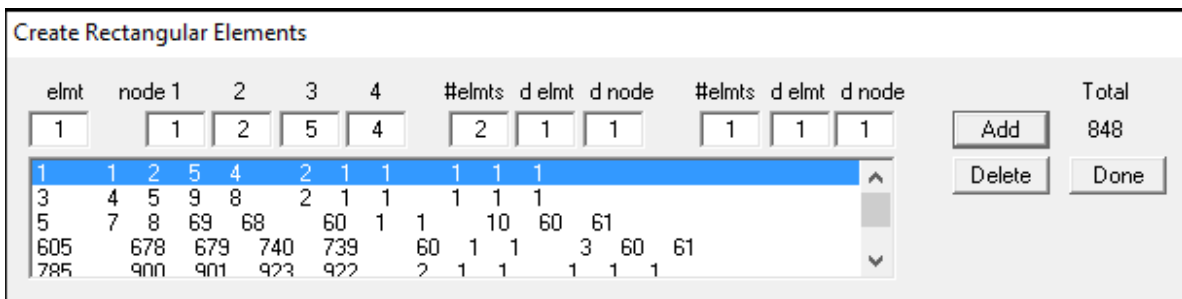


Figure 5 Create Rectangular Elements dialog box

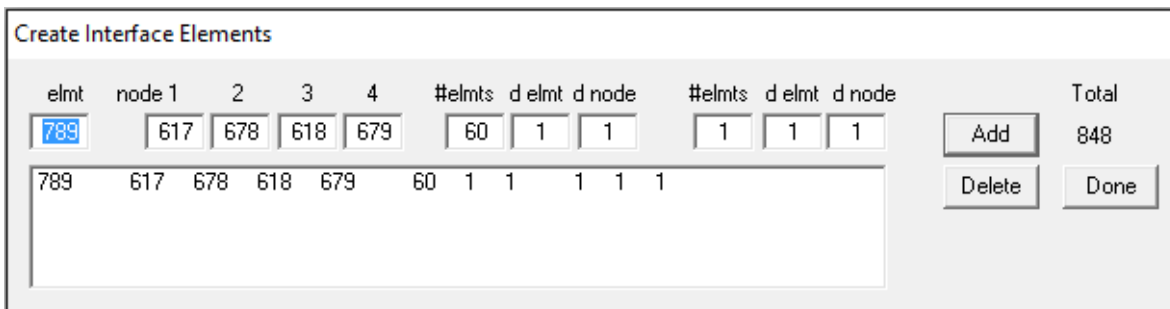


Figure 6 Create Interface Elements dialog box

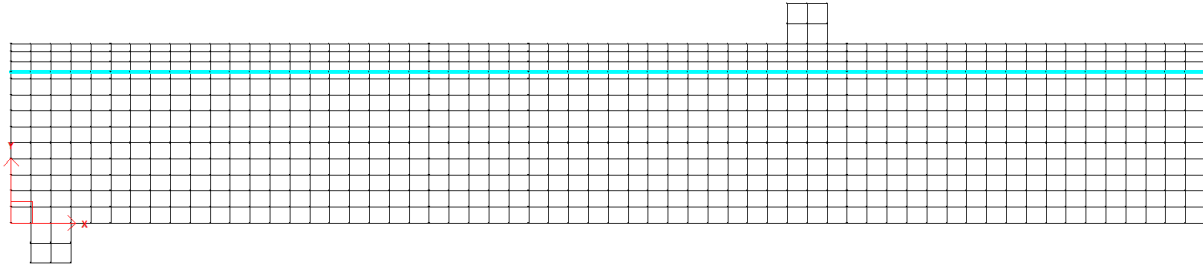


Figure 7 FE model with all elements added

Step 4 Defining Material Properties

Prior to assigning material types, the material and bond properties must be defined in advance. The material and bond property definition interface were presented previously as shown in Figure 5-3 through Figure 5-5. Refer to Section 5.3 for more details regarding the required material inputs.

Step 5 Assigning Material Types

After the material properties were defined, material types were then assigned to the designated elements using the “Assignment Material Types” dialog box depicted in Figure 8.

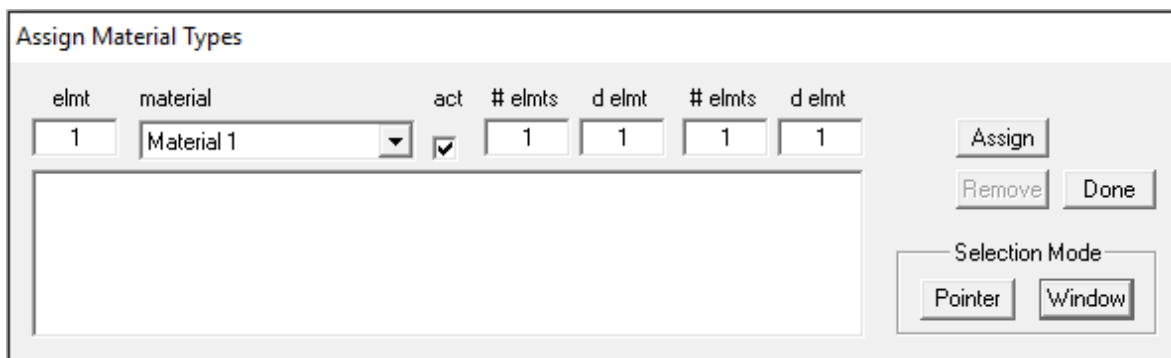


Figure 8 Assign Material Types dialog box

STEP 6 Adding Boundary Conditions

Since only half of Specimen CS1 was modelled, a series of vertical rollers were added to the nodes at mid-span; these rollers were introduced to enable the mid-span nodes to deflect freely in the vertical direction, yet fixed against any longitudinal movement. The specimen was also simply supported at the bearing plate and therefore a vertical roller was provided. It should be pointed out that since the model was horizontally restrained at mid-span, the bearing plate should not be pinned; doing so may cause local failure of the elements directly above the baseplate. However, when the specimen was modelled as a whole as presented in Figure 5-25, one of the bearing plates must be fixed against transverse movement, or the global stiffness matrix would not be strictly positive-definite, and a unique solution would not be possible.

Step 7 Adding Loads

Since Specimen CS1 was loaded in a displacement control loading protocol, a downward support displacement was applied to the top bearing plate. The completed FE model for Specimen CS1 is presented in Figure 9, and the model is now ready for analysis.

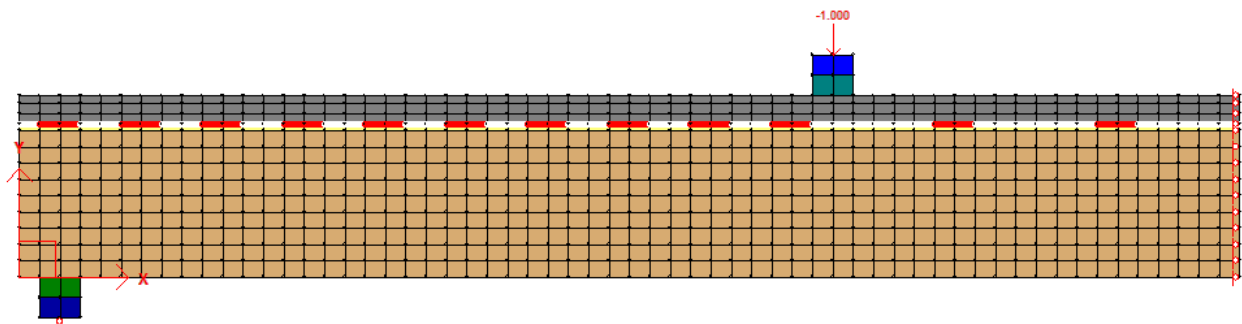


Figure 9 Completed FE model for Specimen CS1

Step 8 Interpreting Simulation Results

Augustus, a post-processor for VecTor2, can be used to retrieve the majority of the simulation results, such as the load-deflection response, and membrane elements' stress and strain. However, the simulation results with regards to the contact elements need to be extracted manually by accessing the text files where all the simulation results at a given load stage are stored.

To generate the load-deflection plot at mid-span, follow the procedures below:

1. Click the "Element Plot" button (Figure 10).
2. Move the cursor to the designated element, left click to select (Figure 10).
3. Click the "X Variable" button and select "Avg Y-Displacement" as x variable for the plot (Figure 11).
4. Click the "Y Variable" button and select "Avg Y Restraint Force" as y variable for the plot (Figure 12).
5. Click the "Produce Plot" button to generate the plot (Figure 13).

Notice that on the bottom left corner, a "Control Chart" is displayed, which corresponds to the load-deflection response at the loading jack. For three-point bending, the "Control Chart" corresponds to the mid-span deflection. In the case of Specimen CS1, the specimen was subjected to four-point bending and therefore the produced mid-span deflection plot deviated from the "Control Chart".

Obtaining the load-slip response is a manual process which is time consuming; the user will need to manually open each "A2E" file corresponding to a specific load stage through the Text Editor (Figure 14), locate the "Bond Element SLIPS & STRESSES" section and then record the slip information corresponding to a specific contact element (e.g. the contact element at the beam end).

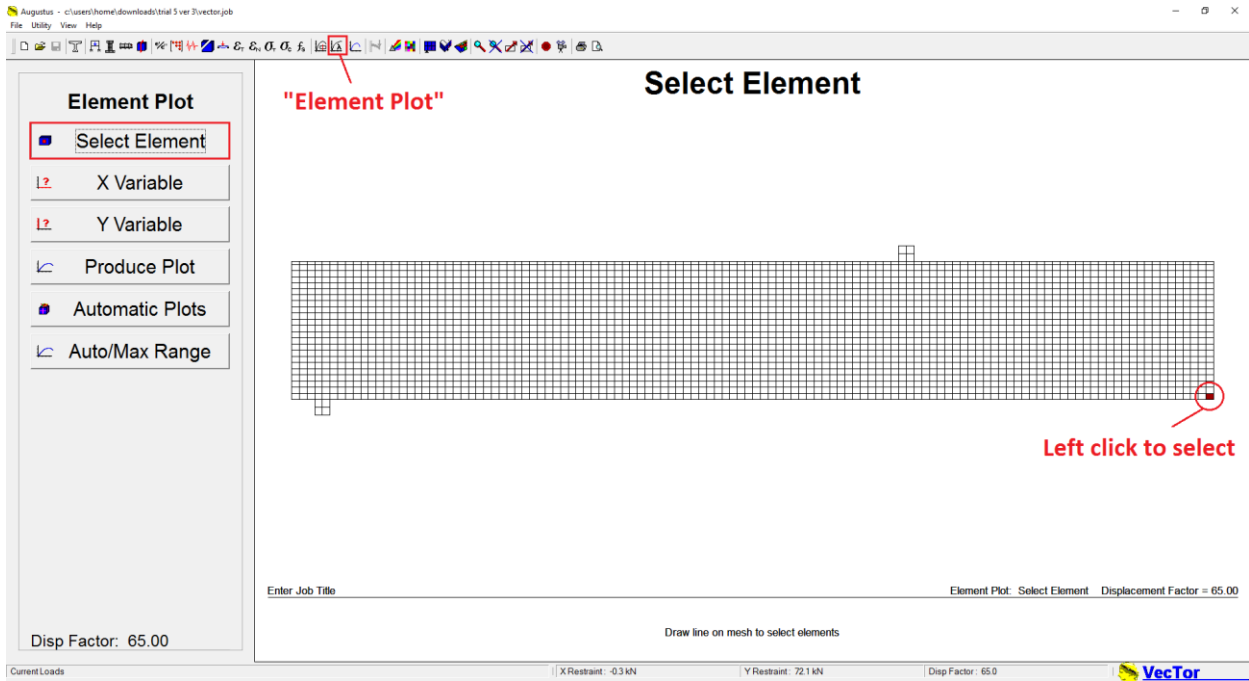


Figure 10 Select specific element

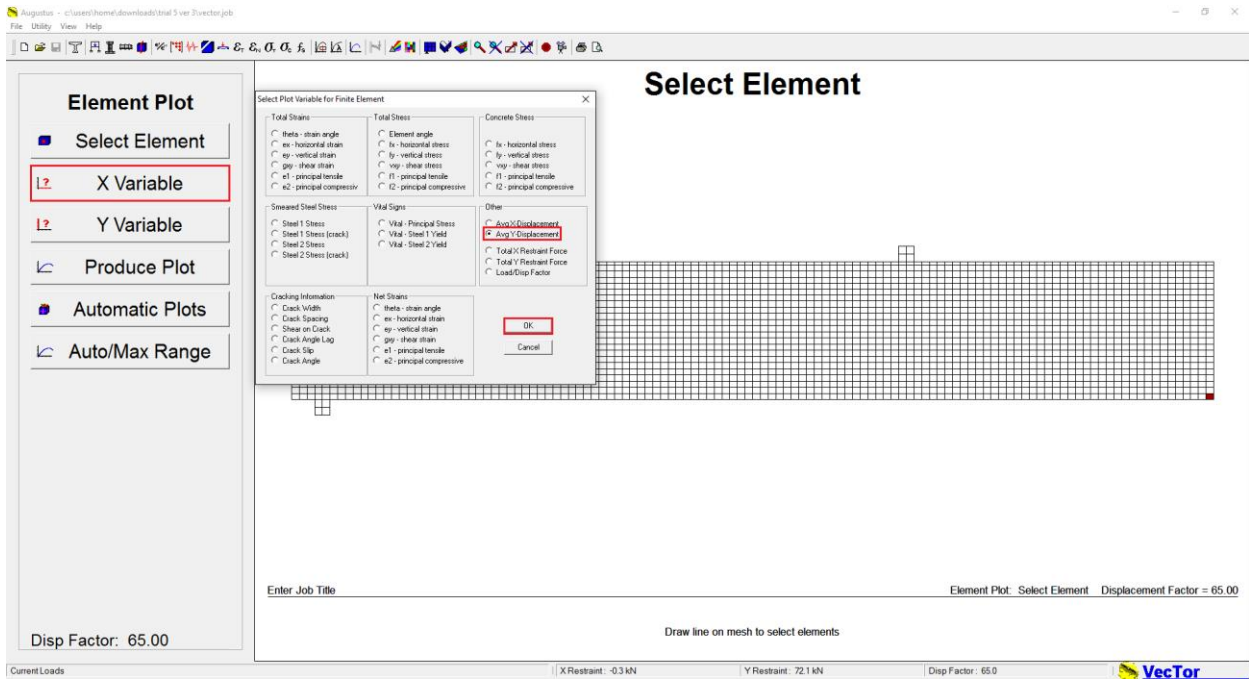


Figure 11 Specify X variable

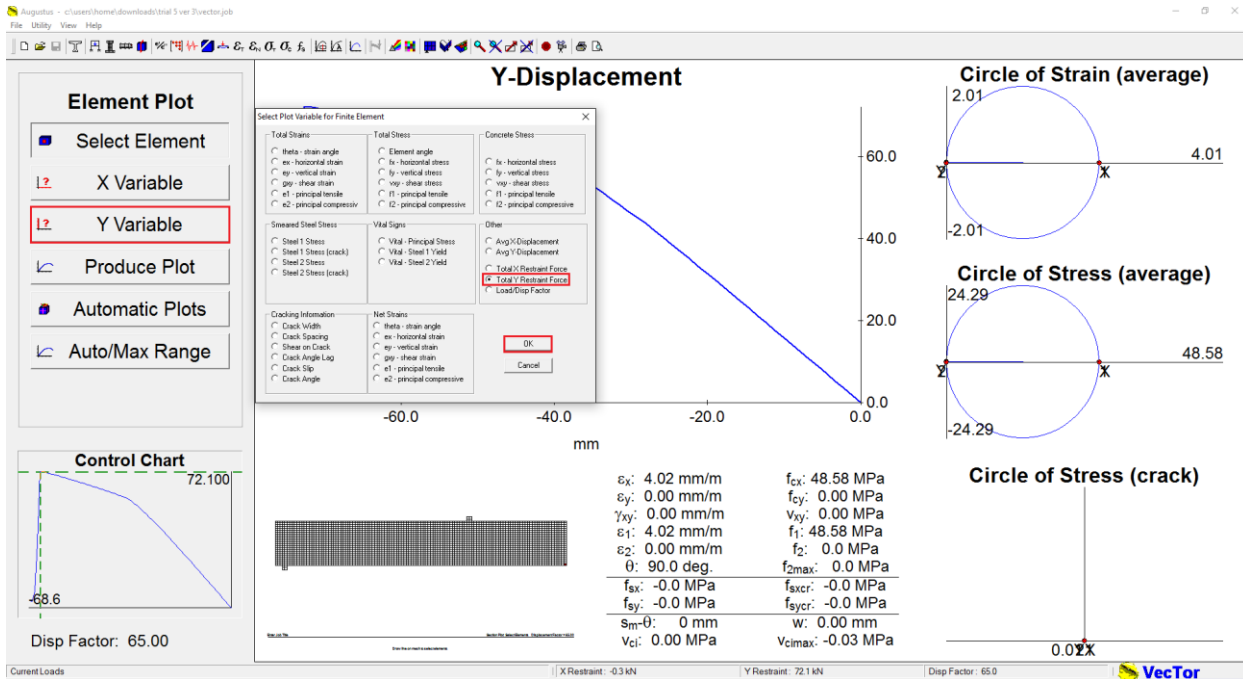


Figure 12 Specify Y variable

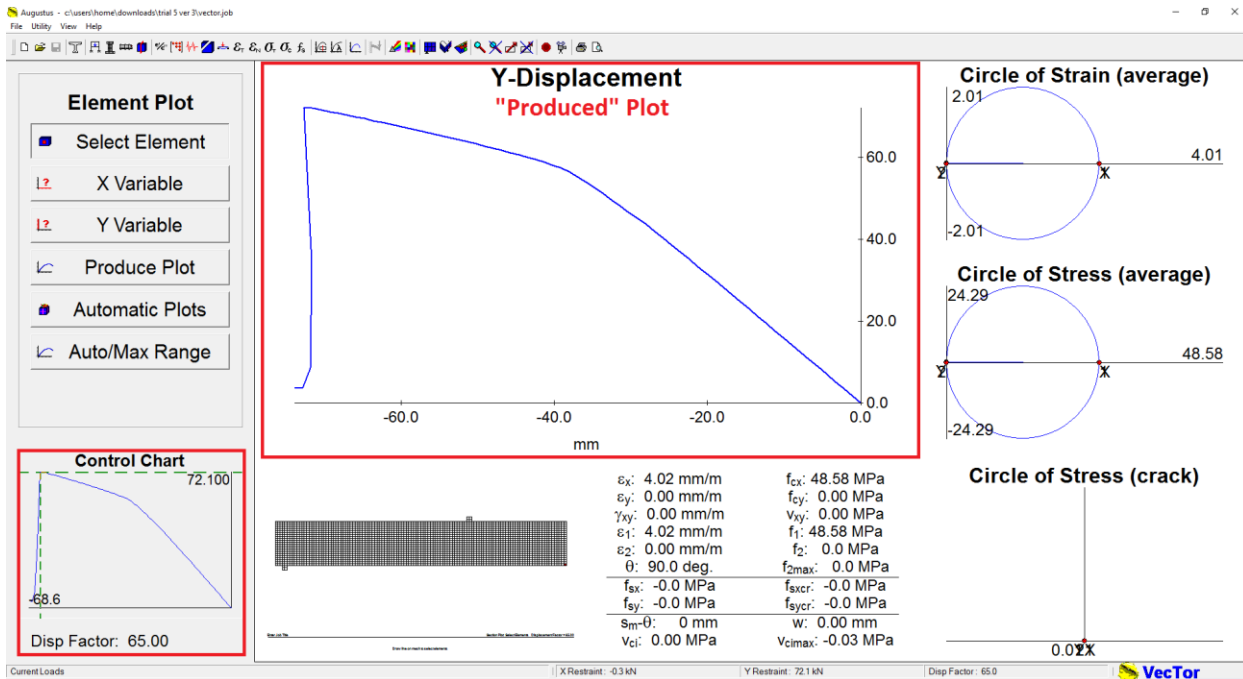


Figure 13 Generate plot

Load Stage

File Edit Format View Help

Contact Element ID

BOND ELEMENT SLIPS & STRESSES

ELMT	S/Sm	SLIP-1 (mm)	SLIP-2 (mm)	Fx-1 (MPa)	Fx-2 (MPa)	Fx-Avg (MPa)	Damage (0-1)
2769	23.50	-4.699	-4.695	-0.00	-0.00	-0.00	0.00
2770	23.47	-4.695	-4.682	-0.00	-0.00	-0.00	0.00
2771	23.41	-4.682	-4.649	-0.00	-0.00	-0.00	0.00
2772	23.25	-4.649	-4.632	-9.46	-9.46	-9.46	0.00
2773	23.34	-4.632	-4.668	-9.46	-9.46	-9.46	0.00
2774	23.59	-4.668	-4.718	-0.00	-0.00	-0.00	0.00
2775	23.73	-4.718	-4.747	-0.00	-0.00	-0.00	0.00
2776	23.81	-4.747	-4.763	-0.00	-0.00	-0.00	0.00
2777	23.84	-4.763	-4.767	-0.00	-0.00	-0.00	0.00
2778	23.84	-4.767	-4.759	-0.00	-0.00	-0.00	0.00
2779	23.79	-4.759	-4.728	-0.00	-0.00	-0.00	0.00
2780	23.64	-4.728	-4.709	-9.44	-9.45	-9.44	0.00
2781	23.71	-4.709	-4.742	-9.45	-9.44	-9.44	0.00
2782	23.93	-4.742	-4.787	-0.00	-0.00	-0.00	0.00
2783	24.05	-4.787	-4.809	-0.00	-0.00	-0.00	0.00
2784	24.09	-4.809	-4.818	-0.00	-0.00	-0.00	0.00
2785	24.09	-4.818	-4.814	-0.00	-0.00	-0.00	0.00
2786	24.07	-4.814	-4.796	-0.00	-0.00	-0.00	0.00
2787	23.98	-4.796	-4.755	-0.00	-0.00	-0.00	0.00
2788	23.77	-4.755	-4.726	-9.44	-9.44	-9.44	0.00
2789	23.74	-4.726	-4.748	-9.44	-9.44	-9.44	0.00
2790	23.91	-4.748	-4.782	-0.00	-0.00	-0.00	0.00
2791	23.97	-4.782	-4.794	-0.00	-0.00	-0.00	0.00
2792	23.97	-4.794	-4.791	-0.00	-0.00	-0.00	0.00
2793	23.96	-4.791	-4.777	-0.00	-0.00	-0.00	0.00
2794	23.88	-4.777	-4.747	-0.00	-0.00	-0.00	0.00
2795	23.73	-4.747	-4.693	-0.00	-0.00	-0.00	0.00
2796	23.46	-4.693	-4.652	-9.45	-9.46	-9.46	0.00
2797	23.32	-4.652	-4.664	-9.46	-9.46	-9.46	0.00
2798	23.44	-4.664	-4.688	-0.00	-0.00	-0.00	0.00
2799	23.45	-4.688	-4.689	-0.00	-0.00	-0.00	0.00
2800	23.45	-4.689	-4.676	-0.00	-0.00	-0.00	0.00
2801	23.38	-4.676	-4.650	-0.00	-0.00	-0.00	0.00
2802	23.25	-4.650	-4.610	-0.00	-0.00	-0.00	0.00
2803	23.05	-4.610	-4.544	-0.00	-0.00	-0.00	0.00
2804	22.72	-4.544	-4.492	-9.48	-9.50	-9.49	0.00
2805	22.48	-4.492	-4.496	-9.50	-9.50	-9.50	0.00
2806	22.55	-4.496	-4.510	-0.00	-0.00	-0.00	0.00
2807	22.55	-4.510	-4.503	-0.00	-0.00	-0.00	0.00
2808	22.51	-4.503	-4.480	-0.00	-0.00	-0.00	0.00
2809	22.40	-4.480	-4.445	-0.00	-0.00	-0.00	0.00
2810	22.23	-4.445	-4.395	-0.00	-0.00	-0.00	0.00
2811	21.98	-4.395	-4.319	-0.00	-0.00	-0.00	0.00

Ln 17473, Col 56

Figure 14 Retrieve the contact element results